

Unterschrift des Betreuers



TECHNISCHE
UNIVERSITÄT
WIEN

Diplomarbeit

Characterizing Simplified Models for Heavy Higgs Decays to Supersymmetric Particles

Ausgeführt am
Atominstut
der Technischen Universität Wien

unter der Anleitung von

Univ.-Doz. Dr. techn. Dipl.-Ing. Claudia-Elisabeth Wulz
und
Dr. Suchita Kulkarni

durch
Lukas Lechner, BSc
Leystraße 157/1/17
1020 Wien

Wien, am 25. Oktober 2017

Unterschrift des Studenten

Abstract

The search for heavy Higgs bosons is an important step to probe the parameter space of the Minimal Supersymmetric Standard Model. This work defines simplified models for heavy Higgs bosons decaying to supersymmetric particles by using the `SModelS` framework. In doing so, a new method to characterize simplified models for SUSY resonances using `SModelS` is proposed. To evaluate the viable parameter space, limits from the dark matter relic density, the Higgs and the flavor sector, as well as limits from LEP and LHC searches for supersymmetry are applied to the pre-collected data sample from the ATLAS pMSSM analysis. Using this sample, the parameter space resulting in maximal signal at the LHC is defined. The predicted cross sections are computed for 14 TeV center-of-mass energy to determine the sensitivity of the High-Luminosity LHC. Detailed studies of the heavy Higgs production, its decay and the resulting signatures are performed for the full 19-dimensional pMSSM parameter space. As a result, a reinterpretation of current mono- X analyses ($X = h, W, Z$) for resonant heavy Higgs searches with higgsino- or bino-like LSPs, as well as a future displaced-vertex analysis with wino-like LSPs are proposed.

Kurzfassung

Ein wichtiger Schritt in der systematischen Analyse des Parameterraums des Minimal Supersymmetrischen Standardmodells ist die Suche nach schweren Higgs Bosonen. Diese Arbeit definiert vereinfachte Modelle für den Zerfall schwerer Higgs Bosonen in supersymmetrische Teilchen unter der Verwendung von `SModelS`. Weiters wird eine neue Methode zur Verwendung des Programms für resonante SUSY Analysen gezeigt. Der Datensatz des verfügbaren Parameterraums berücksichtigt aktuelle Grenzen der Dunklen Materie Dichte zum Zeitpunkt des Ausfrierens, Grenzen im Higgs- und Flavor-Sektor, sowie LEP und LHC Analysen für Supersymmetrie. Um die Sensitivität des High-Luminosity LHC, mit 3 ab^{-1} integrierter Luminosität, zu bestimmen werden die Wechselwirkungsquerschnitte für eine Schwerpunktsenergie von 14 TeV berechnet. Die detaillierte Studie der schweren Higgs Boson Produktion und dessen Zerfall berücksichtigt den gesamten 19-dimensionalen pMSSM Parameterraum. Dadurch wird der Bereich mit best-möglichem Signal am LHC ermittelt. Aufgrund des Ergebnisses dieser Arbeit wird eine Neuinterpretation heutiger mono- X Analysen ($X = h, W, Z$) für resonante schwere Higgs Boson Produktionen mit higgsino- oder bino-ähnlichen LSPs, sowie eine zukünftige Analyse für verschobene Vertices mit wino-ähnlichen LSPs empfohlen.

Publications and Talks

This work was presented in the following talks and is published in the following scientific journal.

Publications

- Ursula Laa, Lukas Lechner and Suchita Kulkarni
Characterizing Simplified Models for Heavy Higgs Decays to Supersymmetric Particles
Journal, submitted on
ArXiv

Presentations

- Lukas Lechner, Ursula Laa and Suchita Kulkarni
Simplified Models of Heavy Higgs Bosons Decaying to Supersymmetric Particles
SPG/OePG Joint Annual Meeting 2017, August 24th, Geneva/Switzerland

Acknowledgements

Contents

Abstract	I
Publications and Talks	III
Acknowledgements	IV
1 Introduction	1
2 The Standard Model of Particle Physics	3
2.1 The Standard Model Particle Content	3
2.2 Electroweak Symmetry Breaking	5
2.3 Issues within the Standard Model	5
2.3.1 The Hierarchy Problem	6
2.3.2 Gauge Coupling Unification	7
2.3.3 Dark Matter	7
3 Supersymmetry	8
3.1 The Minimal Supersymmetric Standard Model	8
3.2 Phenomenological Minimal Supersymmetric Standard Model	9
3.2.1 The pMSSM Particle Content	10
3.2.2 Heavy Higgs Couplings	13
3.2.3 Heavy Higgs Decays	15
3.2.4 Higgs Boson Production Processes	16
3.3 Soft Symmetry Breaking in MSSM	19
3.4 Standard Model Issues within Supersymmetry	19
3.4.1 Hierarchy Problem in SUSY	20
3.4.2 Gauge Coupling Unification in SUSY	20
3.4.3 Dark Matter Candidates	21
4 Analysis Setup	22
4.1 Simplified Model Spectra	22
4.2 The SModelS Framework	23
4.2.1 The SModelS Notation	25
4.2.2 Compression of Elements within SModelS	25
4.2.3 The SModelS Database	26
4.2.4 The SModelS Output	27
4.3 Additional Frameworks	28
4.3.1 SuperIso	28
4.3.2 HiggsBounds	28
4.3.3 HiggsSignals	29
4.3.4 SusHi	30
4.4 The ATLAS pMSSM Dataset	30
4.4.1 Study of the Excluded Parameter Space	33

5	Results	38
5.1	Heavy Higgs Decays with Mono- X Signature	40
5.1.1	Study of the Parameter Dependence	43
5.1.2	Study of the Production Process	45
5.2	Invisible Heavy Higgs Decays	45
5.3	Heavy Higgs Decays with Dijet and Dilepton Signature	48
5.4	Long-Cascade Decays	48
5.5	Constraints from LHC Direct SUSY Searches	51
5.6	Complementarity with Direct Heavy Higgs Searches	51
5.7	Results for Wino-like LSPs	55
6	Conclusion	56
A	Detailed Calculations	58
A.1	The Diagonalization of the Chargino Mass Matrix	58
A.2	The Calculation of Gluon Fusion Processes	60
A.3	Minimizing the Superpotential	65
B	Additional Results	67
B.1	Heavy Higgs Production with Mono- X Signature	68
B.1.1	Study of the Parameter Dependence	69
B.1.2	Study of the Production Process	70
B.2	Heavy Higgs Decays with Dijet and Dilepton Signature	71
	List of Figures	72
	List of Tables	74
	Bibliography	75

1 Introduction

The discovery of the Higgs boson at the Large Hadron Collider (LHC) has been a remarkable success for the Standard Model (SM) of Particle Physics. While this discovery has brought a new era in this direction, there is no final word on whether the observed Higgs boson is a part of an extended sector. The main focus of the LHC is now the search for physics beyond the Standard Model (BSM), where the searches for heavy Higgs forms an important avenue.

Extended Higgs sectors appear in a variety of BSM scenarios. At the LHC, the searches for heavy Higgs bosons are primarily carried out in SM final states. However, within BSM scenarios, Higgs decays to new particles are possible. If the branching ratio to BSM particles is large, the Higgs searches in SM final states are no longer effective.

Among the theoretical scenarios featuring an extended Higgs sector, supersymmetry (SUSY) is a well motivated candidate. To successfully make predictions within the supersymmetric SM extension, their parameter space can be reduced to 19 free parameters in the phenomenological Minimal Supersymmetric Standard Model (pMSSM). While searches for direct production of SUSY particles are extensively carried out at the LHC, it is also possible that the supersymmetric heavy neutral Higgs decays to SUSY particles, with the Feynman-like diagram for the simplified model of this process given in fig. 1.0.1. This opens another possibility to search for an extended Higgs sector and thus, probe the pMSSM parameter space.

It has been previously shown that MSSM Higgs can in general have a large branching ratio to SUSY particles [1], and correspondingly result in a large signal cross section at the LHC [2, 3]. Despite these early encouraging studies, a complete classification of supersymmetric Higgs to SUSY final states and associate signatures at the colliders remains to be done.

This work aims to systematically classify pMSSM neutral heavy Higgs decays to SUSY final states in a realistic parameter space of the phenomenological Minimal Supersymmetric Standard Model. The study differs from the previous attempts in a few ways. First and foremost, it is allowed for squarks and sleptons to also to be light, as the work uses a full scan of the parameter space. Thus, not only the electroweak sector can be light, as has been focused on so far. Secondly, a systematic and complete survey of possible pMSSM Higgs decay modes is performed. Finally, the differences with respect to traditional LHC direct BSM searches are discussed and suggestions for future avenues for searching for heavy Higgs bosons in SUSY final state are made.

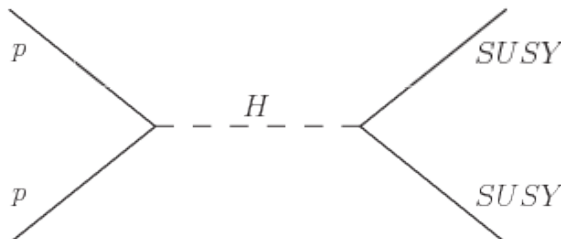


Figure 1.0.1: Simplified model for a pMSSM neutral heavy Higgs H production in proton-proton collisions with a decay to supersymmetric particles. The figure was created using Jaxodraw-2.1 [4].

In doing so, the production mechanisms of heavy Higgs bosons at the LHC and their parameter dependence are studied in detail using the `SusHi` framework. The viable parameter space is evaluated in applying current constraints on the dataset. Limits on the light and heavy Higgs sector are checked using `HiggsSignals` and `HiggsBounds`, respectively. Since the branching ratios of e.g. B -meson decays and the anomalous magnetic moment of the muon are sensitive to contributions from supersymmetric particles, limits in the flavor sector are applied using `SuperIso`.

The `SModelS` framework is adopted to evaluate the LHC signatures from Higgs decaying to supersymmetric particles and define the parameter space for maximal signal. A detailed study of the production mechanism of heavy Higgs bosons and the underlying parameter dependence of the branching ratios to supersymmetric particles has been performed. Since the dataset of wino-like Lightest Supersymmetric Particles (LSPs) mostly contains long-lived sparticles and can thus not be handled by the current version of the `SModelS` framework, a study on the lifetime of the lightest chargino has been done to point out new ways of searching for supersymmetric particles in displaced vertex signatures of future LHC analyses. Furthermore, limits from LHC Run 1 searches and early studies from LHC Run 2 with 3.2 fb^{-1} integrated luminosity were studied to probe the impacts of direct LHC SUSY searches on this work.

This work is organized as follows:

- Section 2 gives a brief introduction into the Standard Model of Particle Physics. The main focus lies on the Higgs sector and how electroweak symmetry breaking is introduced into the SM. Furthermore, Standard Model issues are discussed, as supersymmetric models can give a solution to its shortcomings.
- As supersymmetry is the main focus of this work, the phenomenological Minimal Supersymmetric Standard Model (pMSSM) is discussed in section 3, where an introduction to its particle content and the derivation of the SUSY particle masses is given. The focus lies on the heavy Higgs boson, its production mechanisms, coupling to (supersymmetric) particles and the decay to SUSY. Furthermore, the process of soft symmetry breaking and how supersymmetry introduces a solution to the previously mentioned SM shortcomings are highlighted.
- A detailed discussion about the codes used in this work, with a special focus on the `SModelS` framework, is given in section 4. Furthermore, the analysis set-up, the pre-collected ATLAS pMSSM dataset of the full parameter scan and the applied constraints are discussed. The results for a study of the excluded parameter space is given in this section.
- The results of the systematic heavy Higgs decay analysis are given in section 5. Besides the most dominant and most frequent occurring signatures from heavy Higgs decays, a detailed study of the mono- X topology is performed. Furthermore, the underlying production process and the branching ratios to SUSY particles are discussed. A study on the lifetime of SUSY particles highlights the possibility of displaced vertex analyses on heavy Higgs searches.
- Section 6 will summarize the work and give the proposals for current and future analyses at the LHC.
- Detailed calculations performed within the scope of this work are given in appendix A. Here, the diagonalization of the chargino mass matrix, the computation of the production cross section of heavy Higgs bosons in gluon fusion processes and the minimization of the superpotential is shown. Appendix B gives additional plots to the results of this work.

2 The Standard Model of Particle Physics

The Standard Model (SM) of Particle Physics [5, 6] is a theoretical model of the building blocks of our visible universe. Since most theories of new physics are an extension of the SM, this section gives a brief introduction to its content. As the Higgs boson plays a crucial role in this work, the process of electroweak symmetry breaking within the SM is discussed. Furthermore, the shortcomings of the SM are highlighted.

2.1 The Standard Model Particle Content

The SM is based on quantum field theory and is described by the local gauge group $SU(3)_C \otimes SU(2)_L \otimes U(1)_Y$, for the strong ($SU(3)_C$) and the electroweak force ($SU(2)_L \otimes U(1)_Y$), where the latter breaks into the weak and the electromagnetic interaction at low energies. It describes all known elementary particles and their fundamental interactions, except the gravitational interaction, which is not quantized yet. Its particle content, given in table 2.1.1, is classified according to their spin, mass and quantum numbers and consists of fermions (spin- $\frac{1}{2}$), which are again separated into quarks and leptons, gauge bosons (spin-1) and a scalar particle, the Higgs boson (spin-0).

Quarks carry a color charge and are therefore the only fermions interacting with the strong force. They build bounded colorless states containing either two or three (anti-)quarks, the mesons and baryons, respectively. Due to this confinement, no free quarks are observable. Mesons are confined states consisting of a quark and an anti-quark (e.g. pions), whereas three-quark states, the baryons, contain a quark of each color (e.g. protons). In addition to the strong force, they participate in the electromagnetic and the weak interaction.

Neutrinos, the neutral leptons, are considered as massless within the SM¹ and interact only via the weak force. The electron, muon and tau, are leptons carrying an electric charge and thus undergo the electromagnetic interaction. In addition they participate as every fermion to the weak force.

Fermions are organized in three generations with identical quantum numbers, but increasing mass. For all fermions, an anti-particle exists, having the same mass, but opposite electric and color charge.

Gauge bosons are the mediator particles for fundamental forces, associated with the local gauge groups within the SM. The electromagnetic force, mediated through massless photons, interacts with charged particles among an infinite range. For $SU(n)$ symmetry groups, there are $n^2 - 1$ generators, leading to 8 gluons as the mediator particles of the strong force. Even though they are massless, they carry a color charge, limiting the range of the strong force to about 10^{-15} m. The propagator of the weak interaction, the W and Z bosons, acquire mass due to electroweak symmetry breaking [6], which thus limits the range of the weak force to about 10^{-18} m. In the process of symmetry breaking, the Higgs field plays a crucial role, where the interaction with

¹Neutrino masses have been experimentally confirmed by neutrino oscillation experiments [7–9], but are not included in the SM.

this field also gives mass to charged leptons and quarks. The Higgs boson, the excitation of this field, is the only scalar (spin-0) elementary particle in the SM.

Since the heavier particles are unstable, the visible universe mainly consists of up- and down quarks, electrons, neutrinos² and photons.

FERMIONS						
Quarks						
Particle	Symbol	Spin	Charge [e]	Mass [MeV] [11]	Generation	Interaction
up quark	u	$\frac{1}{2}$	$\frac{2}{3}$	$2.2^{+0.6}_{-0.4}$	1 st gen.	electromagn., weak, strong
down quark	d	$\frac{1}{2}$	$-\frac{1}{3}$	$4.7^{+0.5}_{-0.4}$		
charm quark	c	$\frac{1}{2}$	$\frac{2}{3}$	1280 ± 30	2 nd gen.	
strange quark	s	$\frac{1}{2}$	$-\frac{1}{3}$	96^{+8}_{-4}		
top quark	t	$\frac{1}{2}$	$\frac{2}{3}$	173500 ± 1100 (pole)	3 rd gen.	
bottom quark	b	$\frac{1}{2}$	$-\frac{1}{3}$	4180^{+40}_{-30}		
Leptons						
Particle	Symbol	Spin	Charge [e]	Mass [MeV] [11]	Generation	Interaction
electron	e	$\frac{1}{2}$	-1	0.51	1 st gen.	electromagn., weak
electron-neutrino	ν_e	$\frac{1}{2}$	0	$< 2 \times 10^{-6}$		
muon	μ	$\frac{1}{2}$	-1	105.66	2 nd gen.	
muon-neutrino	ν_μ	$\frac{1}{2}$	0	$< 2 \times 10^{-6}$		
tau	τ	$\frac{1}{2}$	-1	1776.86 ± 0.12	3 rd gen.	
tau-neutrino	ν_τ	$\frac{1}{2}$	0	$< 2 \times 10^{-6}$		
BOSONS						
Gauge Bosons						
Particle	Symbol	Spin	Charge [e]	Mass [GeV] [11]	Interaction	Range [m]
photon	γ	1	$< 10^{-35}$	$< 10^{-27}$	electromagn.	∞
W boson	W	1	± 1	80.385 ± 0.015	weak	$\sim 10^{-18}$
Z boson	Z	1	0	91.1876 ± 0.0021	weak	$\sim 10^{-18}$
gluon	g	1	0	0	strong	$\sim 10^{-15}$
Scalar Bosons						
Particle	Symbol	Spin	Charge [e]	Mass [GeV] [11]		
Higgs boson	h	0	0	125.09 ± 0.24		

Table 2.1.1: The particle content of the Standard Model of Particle Physics including fermions (quarks and leptons), gauge bosons and the Higgs boson.

²Neutrinos have mass and therefore undergo a flavor oscillation process. Depending on the distance to the neutrino source and the neutrino energy, neutrino detectors are able to measure an almost equal fraction of each generation (neutrino flavor) [10].

2.2 Electroweak Symmetry Breaking

The SM unifies the electromagnetic and the weak fundamental force to the electroweak interaction associated with the non-abelian Glashow-Weinberg-Salam theory [12, 13], which is specified with the $SU(2)_L \otimes U(1)_Y$ gauge symmetry group. As referred before, this symmetry must be spontaneously broken at low energies. To achieve the symmetry breaking, a Lagrangian for a complex scalar field $\phi_h = \frac{1}{\sqrt{2}}(\phi + i\chi)$ is considered

$$\mathcal{L} = (\partial_\mu \phi_h)^* (\partial^\mu \phi_h) - V(\phi_h) \quad (2.2.1)$$

$$V(\phi_h) = \mu^2 \phi_h^* \phi_h + \lambda (\phi_h^* \phi_h)^2 \quad (2.2.2)$$

$$= \frac{\mu^2}{2} (\phi^2 + \chi^2) + \frac{\lambda}{4} (\phi^2 + \chi^2)^2 \quad (2.2.3)$$

where $V(\phi_h)$ is the Higgs potential [6, 14, 15], which is bound from below³ for $\lambda > 0$ [18]. Terms of the order of $(\phi_h^* \phi_h)^n$, with $n > 2$ are forbidden, as they produce infinite values of the calculated observables [19].

A minimal energy state can be found for the potential $V(\phi_h)$ being minimal. For $\mu^2 > 0$, the minimum is given for $\phi_h = 0$ and therefore a vanishing vacuum expectation value (vev) $\langle \phi_h \rangle = 0$. For the case of $\mu^2 < 0$, the potential appears to have minimum energy states at

$$V(\phi_h)_{\min} = \frac{\mu^2}{2} \nu^2 + \frac{\lambda}{4} \nu^4 = -\frac{\lambda}{4} \nu^4 < 0 \quad (2.2.4)$$

$$(\phi_h^* \phi_h)_{\min} = \frac{\nu^2}{2} \quad (2.2.5)$$

$$\nu^2 = \phi^2 + \chi^2 = -\frac{\mu^2}{\lambda} > 0 \quad (2.2.6)$$

with a vev value of $\nu \approx 246$ GeV [11]. The Lagrangian is invariant under local $U(1)$ transformations $\phi_h \rightarrow e^{i\alpha(x)} \phi_h$ and therefore has an infinite number of minimum energy states along the complex plane with a radius of ν [18]. Spontaneous symmetry breaking occurs by choosing the vacuum expectation value for the real component $\phi = \nu$ with a vanishing imaginary component $\chi = 0$ in vacuum. In fig. 2.2.1, the Higgs potential is given for a vanishing vev with $\mu^2 > 0$ (left) and for $\mu^2 < 0$ in the real plane of the scalar field (right).

This process is commonly referred to as the Higgs mechanism [20, 21] and predicts the existence of a neutral spin-0 boson, the Higgs boson, with a mass $m_h = \sqrt{2}|\mu|$. It is crucial, as it allows the mediator particles of the weak force, the W and Z bosons to have mass [6, 14, 15]. The Higgs boson, the last missing particle of the SM, has been discovered in proton-proton collisions at the CMS [22] and ATLAS [23] experiment of the LHC in 2012.

2.3 Issues within the Standard Model

The SM has been tested extensively by e.g. particle colliders or cosmological experiments, which are searching for deviations with unique precision at incredible high energies. It was able to succeed in almost every aspect so far, but it still leaves open questions. This section will introduce some of its problems. A possible solution for those issues is the introduction of supersymmetry, as described in section 3.4.

³A local minimum allows tunneling effects. Thus, only a global minimum of the Higgs potential leads to vacuum stability [16, 17].

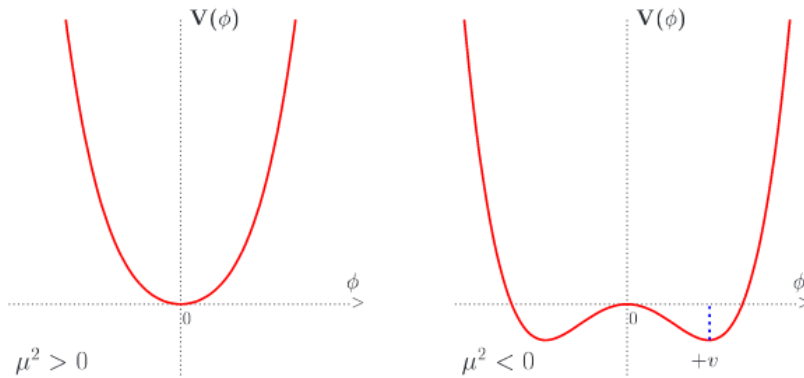


Figure 2.2.1: The Higgs potential $V(\phi_h)$ for a complex scalar field ϕ_h , $\lambda > 0$ and $\mu^2 > 0$ (left) or $\mu^2 < 0$ (right). Figure taken from Ref. [18].

2.3.1 The Hierarchy Problem

The hierarchy problem, or fine-tuning problem, arises due to the major discrepancy between the weak-scale, with the masses of the weak- and Higgs bosons of $m_{\text{weak}} \approx 10^2$ GeV, and the Planck-scale of $m_{\text{Planck}} \approx 10^{18}$ GeV. The latter is defined using universal physical constants and is the maximum energy up to where the Standard Model is considered as valid, since above that scale gravitational effects become important.

In quantum field theory, the Higgs boson mass is sensitive to quadratically divergent corrections proportional to the UV-cutoff energy Λ_{UV} of the SM, thus the Planck scale [24]. Those corrections especially arise from heavy 3rd generation fermions, e.g. the top quark, with one example given in fig. 2.3.1. It visualizes the Feynman diagram for an interaction of a virtual $t\bar{t}$ pair with the Higgs boson. The Higgs mass including corrections due to the top quark is given by

$$m_h^2 = m_0^2 + \frac{\lambda_t^2}{16\pi^2} \Lambda_{\text{UV}}^2 + \mathcal{O}(m_{\text{weak}}^2) \quad (2.3.1)$$

where m_0 is the bare Higgs mass and λ_t is the Yukawa coupling of the top quark [15]. A non-zero Higgs mass below the Planck-scale can only be the result of a precise (large) negative value for m_0^2 , canceling other corrections. Solutions to quadratical divergences typically involve the introduction of new particles or extra-dimensions. One possibility to avoid unnatural fine-tuning of a parameter is the introduction of a new symmetry, as it is done in supersymmetry.

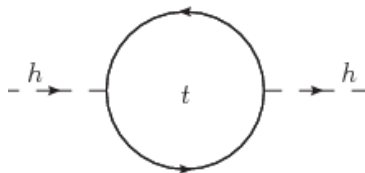


Figure 2.3.1: Feynman diagram for corrections to the Higgs mass due to heavy fermions as e.g. the top quark. The figure was created using Jaxodraw-2.1 [4].

2.3.2 Gauge Coupling Unification

Coupling constants arise naturally in quantum field theory and are dimensionless numbers⁴ determining the strength of an interaction in the Lagrangian of the SM. The energy dependence of the strength of the coupling parameters is commonly referred as running couplings [24] and can be described by renormalization group equations. While the strength of non-abelian symmetry groups, as the $SU(2)_L$ and $SU(3)_C$ symmetry with their couplings g_2 and g_3 , respectively, decreases at higher energies, the strength of abelian interactions, as e.g. $U(1)_Y$ with the coupling g_1 increases. The calculations of the energy dependence of coupling constants predict the gauge coupling strength at higher scales [25]. Fig. 2.3.2 shows the inverse couplings for the SM in dependence of the logarithm of the energy, where $\alpha_i = g_i^2/4\pi$. As seen, the values of the couplings are very similar at an energy scale of about $m_{\text{GUT}} \approx 10^{13}\text{-}10^{17}$ GeV. However, they do not exactly unify, which is expected and a requirement for a Grand Unified Theory (GUT). Therefore, many theories of BSM physics include GUT scale unification of the gauge couplings, which sets boundary conditions to the model and therefore strong constraints on their parameter space.

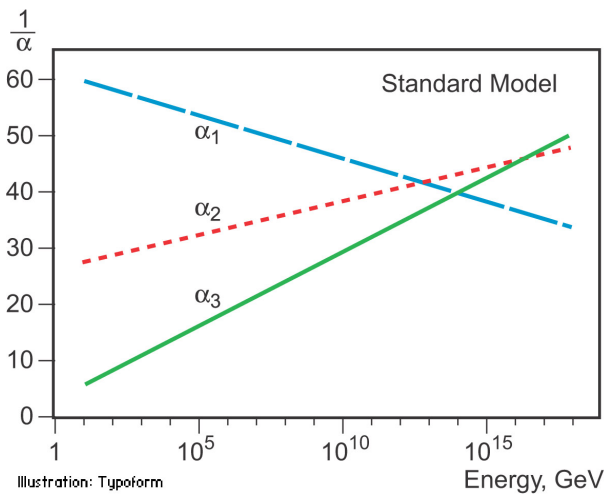


Figure 2.3.2: Energy-dependence of the gauge couplings in the Standard Model. Figure taken from Ref. [26].

2.3.3 Dark Matter

Even though the SM is the theory of all known elementary particles, it is only able to describe about 4.9% [27] of the energy density in the universe. Astrophysical experiments as e.g. the Planck satellite [28] revealed the existence of about five times more non-barionic matter than visible matter.

First evidence of dark matter (DM) was measured by Fritz Zwicky in 1933 [29], when he studied the velocity of galaxies in the Coma cluster in comparison to the gravitational force acting on them. His measurements unveiled the missing of a large amount of non-luminous matter, leading to the indication of dark matter. Since then, more and more effects of DM were uncovered. It plays a crucial role in e.g. the structure formation in the early universe [30], Baryonic Acoustic Oscillations (BAO) [31] and the anisotropies in the Cosmic Microwave Background (CMB) [27, 32, 33]. While some theories try to explain the effects of dark matter in modifying Newton's laws [34], another possibility is the introduction of a new particle not considered in the SM.

⁴Coupling constants are dimensionless for renormalizable theories.

3 Supersymmetry

One possibility of physics beyond the SM (BSM) was created as a conceptual idea in the early 70's. Since then, the idea of supersymmetry (SUSY) encourages theorists and experimentalists in high-energy physics to search for new particles. In this section, basic concepts of the Minimal Supersymmetric Standard Model (MSSM) and the phenomenological MSSM (pMSSM) are introduced. In addition, their particle content and the derivation of supersymmetric particle (sparticle) masses are given. As it is the focus of this work, the production, coupling and possible decays of MSSM Higgs bosons are discussed in detail. Furthermore, the conditions for soft symmetry breaking are derived. Calculations, performed in this section are given in appendix A.

3.1 The Minimal Supersymmetric Standard Model

MSSM is a non-trivial extension of the Poincaré group with the fermionic operator \mathcal{Q} converting bosonic states into fermionic ones and vice versa.

$$\begin{aligned} \mathcal{Q}|\text{boson}\rangle &= |\text{fermion}\rangle \\ \mathcal{Q}|\text{fermion}\rangle &= |\text{boson}\rangle \end{aligned} \tag{3.1.1}$$

Sparticles have, compared to their SM partners, equal quantum numbers, except the spin differs half-integrally⁵ [15, 35, 36]. The symmetry would imply an equal mass of a sparticle and its SM partner, however this is ruled out by experimental data. Therefore, supersymmetry must be a broken symmetry [35].

Standard Model Particles			Supersymmetric Particles		
Particle	Symbol	Spin	Sparticle	Symbol	Spin
quark	u, d, c, s, t, b	1/2	squark	$\tilde{u}, \tilde{d}, \tilde{c}, \tilde{s}, \tilde{t}, \tilde{b}$	0
lepton	$e, \nu_e, \mu, \nu_\mu, \tau, \nu_\tau$	1/2	slepton	$\tilde{e}, \tilde{\nu}_e, \tilde{\mu}, \tilde{\nu}_\mu, \tilde{\tau}, \tilde{\nu}_\tau$	0
gluon	g	1	gluino	\tilde{g}	1/2
photon	γ	1	bino	\tilde{B}	1/2
W, Z boson	W^\pm, Z	1	wino	\tilde{W}	1/2
Higgs boson	h	0	higgsino	\tilde{h}	1/2
			Higgs boson	h, H, A, H^\pm	0

Table 3.1.1: Standard Model particles and their superpartners. In addition, MSSM contains the neutral and charged heavy Higgs bosons H, A and H^\pm [35].

⁵In $N = 1$ MSSM, the superpartner of SM fermions, the sfermions, are spin-0 scalar particles [15, 35, 36].

Due to soft symmetry breaking (SSB) (see section 3.3), sparticles with same electric charge mix. Therefore, electroweak gauginos and higgsinos (electroweakinos) are mixed states called neutralinos $\tilde{\chi}^0$ and charginos $\tilde{\chi}^\pm$ (see section 3.2.1). They arise as a mixture of the superpartners of the SM states of the electroweak force and the SM Higgs boson. Their pure states are classified as binos, winos and higgsinos. In addition, squarks and sleptons can be separated into right- and left-handed components [15, 35]. Only left-handed sneutrinos are included in MSSM, as there is no right-handed superpartner in the SM (see table 3.1.2). As gluinos are the only colored fermions in MSSM, they have no mixing partners.

In general, superpartners of fermions are named with the prefix ‘s’ (for ‘scalar’) and the partners of bosons are attached with the ending ‘ino’. All sparticles are labeled with a tilde.

Squarks		Sleptons		Gauginos/Electroweakinos	
Sparticle	Symbol	Sparticle	Symbol	Sparticle	Symbol
(left, right) selectron	$\tilde{e}_{L,R}$	(left, right) up squark	$\tilde{u}_{L,R}$	lightest neutralino	$\tilde{\chi}_1^0$
(left, right) smuon	$\tilde{\mu}_{L,R}$	(left, right) down squark	$\tilde{d}_{L,R}$	next-to-lightest neutralino	$\tilde{\chi}_2^0$
(left, right) stau	$\tilde{\tau}_{L,R}$	(left, right) charm squark	$\tilde{c}_{L,R}$	next-to-heaviest neutralino	$\tilde{\chi}_3^0$
electron - sneutrino	$\tilde{\nu}_e$	(left, right) strange squark	$\tilde{s}_{L,R}$	heaviest neutralino	$\tilde{\chi}_4^0$
muon - sneutrino	$\tilde{\nu}_\mu$	(left, right) top squark	$\tilde{t}_{L,R}$	lightest chargino	$\tilde{\chi}_1^\pm$
tau - sneutrino	$\tilde{\nu}_\tau$	(left, right) bottom squark	$\tilde{b}_{L,R}$	heaviest chargino	$\tilde{\chi}_2^\pm$
				gluino	\tilde{g}

Table 3.1.2: MSSM particle content and their symbols. The subscript L and R denote left- and right-handed sparticles, respectively.

3.2 Phenomenological Minimal Supersymmetric Standard Model

The unconstrained MSSM introduces a large number (> 100) of free parameters. Therefore, making generic predictions from MSSM is non-trivial. Using basic phenomenological assumptions [15, 35], the total number of free parameters can be drastically reduced. By including

- R-parity conservation and therefore a stable lightest supersymmetric particle
- electroweak and soft symmetry breaking
- no new source of CP-violation, thus all parameters are real
- no flavor changing neutral currents (FCNC) at tree level
- degenerate 1st and 2nd generation squark and slepton states
- negligible 1st and 2nd generation squark and slepton trilinear couplings $A_{q,l} \approx 0$

the number of free parameters is reduced to 19 (see table 3.2.1), as it is done in the so-called phenomenological Minimal Supersymmetric Standard Model (pMSSM).

It contains mass parameters for the sfermion sector for left- and right-handed 1st and 2nd generation squarks \tilde{q} ($M_{\tilde{q}_1} = M_{\tilde{q}_2}$, $M_{\tilde{u}_R} = M_{\tilde{c}_R}$, $M_{\tilde{d}_R} = M_{\tilde{s}_R}$) and sleptons \tilde{l} ($M_{\tilde{l}_1} = M_{\tilde{l}_2}$, $M_{\tilde{e}_R} = M_{\tilde{\mu}_R}$),

as well as for the left-handed 3rd generation squarks \tilde{Q} ($M_{\tilde{Q}}$) and sleptons \tilde{L} ($M_{\tilde{L}}$) and their right-handed opponents ($M_{\tilde{t}_R}$, $M_{\tilde{b}_R}$, $M_{\tilde{\tau}_R}$). The trilinear couplings for the 3rd generation sfermions connecting their left- and right-handed components are given by A_t , A_b and A_τ .

Furthermore it includes parameters for the gaugino/higgsino sector with mass parameters for binos and winos (M_1 , M_2), as well as for higgsinos (μ). Those parameters strongly influence the masses of neutralinos and charginos (see section 3.2.1). The gluino mass is given by M_3 .

Additional parameters arise from the Higgs sector with the pseudoscalar Higgs mass m_A and the ratio of the two Higgs doublet vacuum expectation values $\tan\beta = \nu_2/\nu_1$, which are used to e.g. calculate the Higgs masses on tree level (see section 3.2.1).

Parameter	Description
$M_{\tilde{l}_1} = M_{\tilde{l}_2}$	Left-handed 1 st - and 2 nd gen slepton
$M_{\tilde{e}_R} = M_{\tilde{\mu}_R}$	Right-handed 1 st - and 2 nd gen slepton
$M_{\tilde{L}}$	Left-handed 3 rd gen slepton
$M_{\tilde{\tau}_R}$	Right-handed 3 rd gen slepton
$M_{\tilde{q}_1} = M_{\tilde{q}_2}$	Left-handed 1 st - and 2 nd gen squark
$M_{\tilde{u}_R} = M_{\tilde{c}_R}$	Right-handed 1 st - and 2 nd gen up-type squark
$M_{\tilde{d}_R} = M_{\tilde{s}_R}$	Right-handed 1 st - and 2 nd gen down-type squark
$M_{\tilde{Q}}$	Left-handed 3 rd gen squark
$M_{\tilde{t}_R}$	Right-handed 3 rd gen up-type squark
$M_{\tilde{b}_R}$	Right-handed 3 rd gen down-type squark
M_1	Bino mass parameter
M_2	Wino mass parameter
M_3	Gluino mass parameter
μ	Higgsino mass parameter
m_A	CP-odd Higgs boson mass
$\tan\beta$	Ratio of the Higgs vev
A_t	Trilinear top quark coupling
A_b	Trilinear bottom quark coupling
A_τ	Trilinear τ lepton coupling

Table 3.2.1: Soft parameters in the phenomenological Minimal Supersymmetric Standard Model [15, 35].

3.2.1 The pMSSM Particle Content

Most of the particle mass eigenstates within the pMSSM model arise due to the mixture of sparticle states. While the electroweakinos are the result of the mixing of electroweak superpartners due to soft symmetry breaking, the scalar sparticles undergo a left-right mixing being influenced by the trilinear couplings. This section will introduce the procedure to calculate their sparticle masses in pMSSM. Furthermore, the properties of the five Higgs bosons are introduced.

Electroweakinos in pMSSM

The introduction of soft symmetry breaking in MSSM leads to the mixture of sfermions with equal charge. Thus, superpartners of SM bosons mix to so-called electroweakinos, which can be separated into neutral and charged neutralinos and charginos, respectively. The characteristics of neutralinos (higgsino-, wino- or bino-like) and charginos (higgsino- or wino-like) are highly dependent on the higgsino-gaugino-mixture and therefore the soft parameters M_1 , M_2 , μ and $\tan\beta$. Their masses are derived from the diagonalization of the neutralino- (chargino-) mass matrix \mathcal{M}_N (\mathcal{M}_C)

$$\mathcal{M}_N = \begin{pmatrix} M_1 & 0 & -m_Z s_W c_\beta & m_Z s_W s_\beta \\ 0 & M_2 & m_Z c_W c_\beta & -m_Z c_W s_\beta \\ -m_Z s_W c_\beta & m_Z c_W c_\beta & 0 & -\mu \\ m_Z s_W s_\beta & -m_Z c_W s_\beta & -\mu & 0 \end{pmatrix} \quad (3.2.1)$$

$$\mathcal{M}_C = \begin{pmatrix} M_2 & \sqrt{2}m_W s_\beta \\ \sqrt{2}m_W c_\beta & \mu \end{pmatrix} \quad (3.2.2)$$

using the 4×4 (2×2) unitary mixing matrices \mathcal{Z} (\mathcal{U} , \mathcal{V})

$$\mathcal{M}_N^D = \mathcal{Z}^* \mathcal{M}_N \mathcal{Z}^{-1} \quad (3.2.3)$$

$$\mathcal{M}_C^D = \mathcal{U}^* \mathcal{M}_C \mathcal{V}^{-1} \quad (3.2.4)$$

where $s_W \equiv \sin\theta_W$, $c_W \equiv \cos\theta_W$, θ_W is the Weinberg-angle, $s_\beta \equiv \sin\beta$, $c_\beta \equiv \cos\beta$ and m_Z (m_W) is the mass of the Z (W) boson [35]. The mixing matrices for the chargino sector can be written as⁶

$$\mathcal{U} = O_u \quad (3.2.5)$$

$$\mathcal{V} = \begin{cases} O_v & \text{for } \det(\mathcal{M}_C) > 0 \\ \sigma_3 O_v & \text{for } \det(\mathcal{M}_C) < 0 \end{cases} \quad (3.2.6)$$

$$O_{u,v} = \begin{pmatrix} c_{\phi_{u,v}} & s_{\phi_{u,v}} \\ -s_{\phi_{u,v}} & c_{\phi_{u,v}} \end{pmatrix} \quad (3.2.7)$$

where $s_{\phi_{u,v}} \equiv \sin\phi_{u,v}$, $c_{\phi_{u,v}} \equiv \cos\phi_{u,v}$ and σ_3 is the third Pauli matrix [35]. The mixing angles ϕ_u and ϕ_v are given by

$$\tan 2\phi_u = \frac{2\sqrt{2}m_W(\mu \sin\beta + M_2 \cos\beta)}{M_2^2 - \mu^2 - 2m_W^2 \cos 2\beta} \quad (3.2.8)$$

$$\tan 2\phi_v = \frac{2\sqrt{2}m_W(\mu \cos\beta + M_2 \sin\beta)}{M_2^2 - \mu^2 + 2m_W^2 \cos 2\beta}. \quad (3.2.9)$$

The diagonalization of the chargino mixing matrix \mathcal{M}_C has been performed within the scope of this work and is given in appendix A.1. The diagonalization of the neutralino mixing matrix was obtained numerically.

The neutralino (chargino) mass-eigenstates are labeled in the ordering $|m_{\tilde{\chi}_1^0}| < |m_{\tilde{\chi}_2^0}| < |m_{\tilde{\chi}_3^0}| < |m_{\tilde{\chi}_4^0}|$ ($|m_{\tilde{\chi}_1^\pm}| < |m_{\tilde{\chi}_2^\pm}|$). Those eigenvalues can become negative, having a crucial impact on

⁶Here, a positive value of M_2 is assumed.

the branching ratio of heavy Higgs bosons decaying to electroweakinos. They then need to be redefined using chiral rotations [35]. The lightest neutralino $\tilde{\chi}_1^0$ is typically handled as the Lightest Supersymmetric Particle (LSP), as it has to have no color or electric charge⁷. For minimal mixed LSPs, and therefore (at least) one soft parameter of M_1 , M_2 or μ being significantly smaller than the others, they can be classified as bino-like ($M_1 \ll M_2, \mu$), wino-like ($M_2 \ll M_1, \mu$) or higgsino-like LSPs ($\mu \ll M_1, M_2$)⁸.

Sfermions in pMSSM

For sfermions heavier than the electroweak gauge bosons, their masses arise due to the $SU(2)_L \otimes U(1)_Y$ invariant soft terms in the superpotential V_{soft} (see eq. 3.3.4). The sfermion mass eigenstates are derived from the diagonalization of the 2×2 Hermitian mass matrix $\mathcal{M}_{\tilde{f}}$, with 3×3 blocks for left- and right-handed components ($M_{\tilde{f}_L}, M_{\tilde{f}_R}$). Off-diagonal matrices mix left- and right-handed states, where the trilinear couplings A_f and terms originating from higgsino mass terms in the superpotential are contributing [15].

$$\mathcal{M}_{\tilde{f}} = \begin{pmatrix} m_f^2 + M_L^2 & m_f X_f \\ m_f X_f & m_f^2 + M_R^2 \end{pmatrix} \quad (3.2.10)$$

with

$$M_L^2 = M_{\tilde{f}_L}^2 + (I_f^{3L} - Q_f s_W^2) m_Z^2 c_{2\beta} \quad (3.2.11)$$

$$M_R^2 = M_{\tilde{f}_R}^2 + Q_f s_W^2 m_Z^2 c_{2\beta} \quad (3.2.12)$$

$$X_f = A_f - \mu (\tan \beta)^{-2I_f^{3L}} \quad (3.2.13)$$

where m_f is the mass of the SM fermion, Q_f is the electromagnetic charge and I_f^{3L} is the third component of the weak isospin [35]. To diagonalize the sfermion mass-matrix, a rotation-matrix for each sfermion state with a corresponding mixing angle is introduced [15].

$$O_{\tilde{f}} = \begin{pmatrix} c_{\phi_{\tilde{f}}} & s_{\phi_{\tilde{f}}} \\ -s_{\phi_{\tilde{f}}} & c_{\phi_{\tilde{f}}} \end{pmatrix} \quad \sin 2\phi_{\tilde{f}} = \frac{2m_f X_f}{m_{\tilde{f}_1}^2 - m_{\tilde{f}_2}^2} \quad (3.2.14)$$

The masses of the two sfermionic states arise then as a mixture of the left- and right-handed component and is given by

$$m_{\tilde{f}_{1,2}}^2 = m_f^2 + \frac{1}{2} \left(M_L^2 + M_R^2 \mp \sqrt{(M_L^2 - M_R^2)^2 + 4m_f^2 X_f^2} \right) \quad (3.2.15)$$

Large off-diagonal terms $m_f X_f$ in the square root lead to strong mixing and thus creates splitted sfermionic mass states with $m_{\tilde{f}_1} \ll m_{\tilde{f}_2}$. Furthermore, for the special case of $X_f \approx 0$ or $m_f \ll M_L, M_R$, the off-diagonal terms in the mass-matrix become negligible and no $L - R$ mixing is obtained.

⁷As discussed in section 3.4.3, the left-handed sneutrinos is disfavored as a DM candidate due to its strong coupling to the Z boson.

⁸The numerical implementation of the characterization of the LSP is done according to the mixing matrix \mathcal{Z} for bino-like ($\mathcal{Z}_{11}^2 > \max(\mathcal{Z}_{12}^2, \mathcal{Z}_{13}^2 + \mathcal{Z}_{14}^2)$), wino-like ($\mathcal{Z}_{12}^2 > \max(\mathcal{Z}_{11}^2, \mathcal{Z}_{13}^2 + \mathcal{Z}_{14}^2)$) and higgsino-like LSPs ($(\mathcal{Z}_{13}^2 + \mathcal{Z}_{14}^2) > \max(\mathcal{Z}_{11}^2, \mathcal{Z}_{12}^2)$) (see section 4.4).

The Heavy Higgs Bosons in pMSSM

Supersymmetric models contain two Higgs doublets (H_u, H_d) ⁹ to break the electroweak and the soft symmetry. The ratio of their vacuum expectation values, ν_d and ν_u , is given by $\tan \beta = \nu_u/\nu_d$, which is one of the free parameters in pMSSM models. The vevs are normalized to the SM value $\nu_d^2 + \nu_u^2 = \nu_{\text{SM}}^2 \approx (246 \text{ GeV})^2$ [11].

Due to their two Higgs doublets, MSSM models predict the existence of two neutral CP-even (h, H), one neutral CP-odd (A) and a pair of charged scalar bosons (H^\pm). In addition, a neutral and a pair of charged Goldstone bosons (G^0, G^\pm) are retrieved from the mixing of the real (ϕ) and complex (χ) components of the Higgs doublets using the mixing angles α and β , within their ranges $-\pi/2 \leq \alpha \leq 0$ and $0 \leq \beta \leq \pi/2$ [14, 15, 35].

$$H_1 = H_d = \begin{pmatrix} H_d^0 \\ H_d^- \end{pmatrix} = \begin{pmatrix} (\nu_d + \phi_d^0 + i\chi_d^0)/\sqrt{2} \\ \phi_d^- \end{pmatrix} \quad \langle H_d \rangle = \frac{\nu_d}{\sqrt{2}} \quad (3.2.16)$$

$$H_2 = H_u = \begin{pmatrix} H_u^+ \\ H_u^0 \end{pmatrix} = \begin{pmatrix} \phi_u^+ \\ (\nu_u + \phi_u^0 + i\chi_u^0)/\sqrt{2} \end{pmatrix} \quad \langle H_u \rangle = \frac{\nu_u}{\sqrt{2}} \quad (3.2.17)$$

$$\begin{pmatrix} H \\ h \end{pmatrix} = \begin{pmatrix} c_\alpha & s_\alpha \\ -s_\alpha & c_\alpha \end{pmatrix} \begin{pmatrix} \phi_d^0 \\ \phi_u^0 \end{pmatrix} \quad \begin{pmatrix} G^0 \\ A \end{pmatrix} = \begin{pmatrix} c_\beta & s_\beta \\ -s_\beta & c_\beta \end{pmatrix} \begin{pmatrix} \chi_d^0 \\ \chi_u^0 \end{pmatrix} \\ \begin{pmatrix} G^\pm \\ H^\pm \end{pmatrix} = \begin{pmatrix} c_\beta & s_\beta \\ -s_\beta & c_\beta \end{pmatrix} \begin{pmatrix} \phi_d^\pm \\ \phi_u^\pm \end{pmatrix} \quad (3.2.18)$$

The mixing angles are connected due to the relation

$$\sin 2\alpha = -\frac{m_H^2 + m_h^2}{M_H^2 - m_h^2} \sin 2\beta \quad (3.2.19)$$

where m_h and m_H are the masses of the neutral CP-even Higgs bosons. On tree-level, the Higgs masses are determined by the two independent parameters $\tan \beta$ and the mass of the pseudoscalar m_A [14, 15, 35].

$$(m_{H,h}^{LO})^2 = \frac{1}{2} \left[m_A^2 + m_Z^2 \pm \sqrt{(m_A^2 + m_Z^2)^2 - 4m_A^2 m_Z^2 \cos^2 2\beta} \right] \xrightarrow{m_A \gg m_Z} \approx m_A^2 \quad (3.2.20)$$

$$(m_{H^\pm}^{LO})^2 = m_A^2 + m_W^2 \xrightarrow{m_A \gg m_Z} \approx m_A^2 \quad (3.2.21)$$

Fig 3.2.1 was created using `SusHi-1.6.1` [37, 38] and `FeynHiggs-2.10.4` [39] and shows the dependence of CP-even Higgs boson masses on m_A . It is seen, that the light Higgs mass cannot exceed the Z boson mass for leading order (LO) calculations. Therefore, radiative corrections play a crucial role in the determination of the MSSM Higgs masses. These radiative corrections arise mainly due to 3rd generation (s)particles leading to a dependence on the parameters for the squark and slepton masses. In the decoupling limit¹⁰ $m_A \gg m_Z$, h is SM-like and the masses of the heavy Higgs bosons are (almost) degenerate ($m_A \approx m_H \approx m_{H^\pm}$).

3.2.2 Heavy Higgs Couplings

In this section, the coupling of the CP-even neutral heavy Higgs bosons to SM particles, squarks and electroweakinos are described. Further details, as e.g. the coupling to the pseudoscalar A or the charged Higgs bosons H^\pm can be found in the literature [14, 15, 35].

⁹In the literature, this notation is often replaced by $H_d = H_1$ and $H_u = H_2$, with their vacuum expectation values $\nu_d = \nu_1$ and $\nu_u = \nu_2$.

¹⁰The decoupling limit is usually obtained for $m_A > 250 \text{ GeV}$ [35].

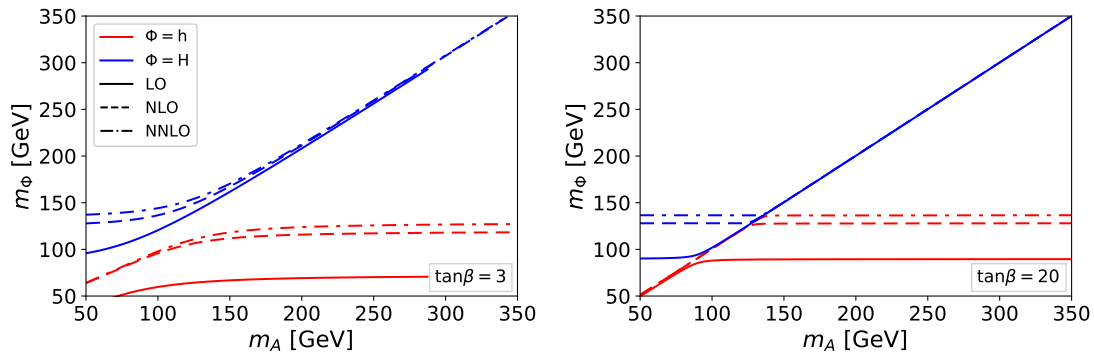


Figure 3.2.1: The CP-even Higgs boson masses in dependence of m_A for $\tan \beta = 3$ (left) and $\tan \beta = 20$ (right) including corrections up to NNLO QCD for one specific set of parameters.

Heavy Higgs Couplings to SM Particles

The mixing angles of the two Higgs doublet components α and β influence the couplings of pMSSM Higgs to SM particles. However, this reduces to a dependence on the pMSSM free parameter $\tan \beta$ for the decoupling regime ($m_A \gg m_Z$). In table 3.2.2, the couplings of the neutral Higgs bosons to up- and down-type fermions ($g_{\Phi u\bar{u}}$, $g_{\Phi d\bar{d}}$), as well as to vector bosons ($g_{\Phi VV}$), normalized to the SM couplings (g^{SM}) are given.

As seen in the table, the pseudoscalar A has no coupling to vector bosons at tree-level and therefore their production in vector boson fusion or Higgs radiation processes (see section 3.2.4) is suppressed. For $m_A \gg m_Z$, the couplings of the heavy neutral Higgs bosons (H , A) to fermions are strongly dependent on $\tan \beta$ leading to crucial effects in heavy Higgs production mechanisms. For large values of $\tan \beta$, the coupling to down-type fermions can be significantly enhanced. Since the interaction vertex to fermions is proportional to its mass ($g_{\Phi f\bar{f}} \propto m_f$), the coupling to the bottom quark becomes dominant for $\tan \beta > \sqrt{m_t/m_b} \sim 6.4$ [14, 15, 35].

Φ	$g_{\Phi u\bar{u}}/g_{\Phi u\bar{u}}^{\text{SM}}$	$g_{\Phi d\bar{d}}/g_{\Phi d\bar{d}}^{\text{SM}}$	$g_{\Phi VV}/g_{\Phi VV}^{\text{SM}}$
h	$\cos \alpha / \sin \beta \rightarrow 1$	$-\sin \alpha / \cos \beta \rightarrow 1$	$\sin(\beta - \alpha) \rightarrow 1$
H	$\sin \alpha / \sin \beta \rightarrow \cot \beta$	$\cos \alpha / \cos \beta \rightarrow \tan \beta$	$\cos(\beta - \alpha) \rightarrow 0$
A	$\cot \beta$	$\tan \beta$	0

Table 3.2.2: Neutral MSSM Higgs couplings normalized to SM-Higgs couplings (g^{SM}) for up-type fermions ($g_{\Phi u\bar{u}}$), down-type fermions ($g_{\Phi d\bar{d}}$) and vector bosons ($g_{\Phi VV}$) and the decoupling limit $m_A \gg m_Z$ [40].

The coupling of the CP-even heavy Higgs H to vector bosons becomes negligible for $m_A \gg m_Z$ and the behavior of the light neutral Higgs h becomes SM-like. Furthermore, the vertex ZAh is also proportional to $\cos(\beta - \alpha)$ ($\rightarrow 0$ for $m_A \gg m_Z$), while the vertex ZAH is proportional to $\sin(\beta - \alpha)$ ($\rightarrow 1$ for $m_A \gg m_Z$). The trilinear couplings Zhh and ZHH are forbidden by the spin of the particles and ZhH is forbidden due to CP-invariance¹¹ [35].

¹¹Since the CP-symmetry is broken, the coupling ZhH can exist [35].

Heavy Higgs Couplings to Sfermions

The couplings of heavy neutral Higgs bosons to sfermions are potentially large, as they include terms proportional to their SM partner mass squared m_f^2 and terms proportional to their trilinear couplings A_f . Furthermore, couplings to the bottom squark are enhanced for large values of $\tan\beta$ and can exceed the values to top squarks. It should be noted, that the coupling to sfermions is not proportional to their mass, but to their SM partner mass. Therefore, mainly decays to 3rd generation sfermions are considered. For the decay of Higgs bosons to squarks, the Lagrangian for the interaction¹² of heavy Higgs bosons to squarks can be written as

$$\mathcal{L}_{H\tilde{q}\tilde{q}} = \sum_{\tilde{q}} C_{H\tilde{q}\tilde{q}} H \tilde{q}^* \tilde{q} \quad (3.2.22)$$

$$C_{H\tilde{q}\tilde{q}} = \begin{pmatrix} (I_q^{3L} - Q_q s_W^2) m_Z^2 \cos(\beta + \alpha) + m_q^2 r_1^q & \frac{1}{2} m_q (A_q r_1^q + \mu r_2^q) \\ \frac{1}{2} m_q (A_q r_1^q + \mu r_2^q) & Q_q s_W^2 m_Z^2 \cos(\beta + \alpha) + m_q^2 r_1^q \end{pmatrix} \quad (3.2.23)$$

where $C_{H\tilde{q}\tilde{q}}$ contains the couplings to squarks, $r_1^u = \sin\alpha/\sin\beta$, $r_2^u = -\cos\alpha/\sin\beta$, $r_1^d = -\cos\alpha/\cos\beta$ and $r_2^d = -\sin\alpha/\cos\beta$. For the decoupling regime, where $m_H \gg m_Z$, the Higgs mixing angle α is negligible and thus, only r_2^u and r_1^d are non-vanishing. Furthermore, the trilinear couplings of the 1st and 2nd generation squarks are set to zero in pMSSM. Due to the light mass of the SM light quarks, the coupling of 1st and 2nd generation squarks can be approximately reduced to the diagonal terms in the matrix given above, leading to a strong dependence on $\cos\beta$, and thus the pMSSM soft parameter $\tan\beta$.

The interaction matrices to sleptons can be found in Ref. [35].

Heavy Higgs Couplings to Electroweakinos

The couplings to electroweakinos is affected by the soft symmetry breaking and the gaugino-higgsino mixing to neutralinos and charginos (see section 3.2.1). Therefore, the couplings for left- and right-handed electroweakinos to the CP-even neutral heavy Higgs

$$g_{\tilde{\chi}_i^\pm \tilde{\chi}_j^\mp H}^L = g_{\tilde{\chi}_j^\pm \tilde{\chi}_i^\mp H}^R = \frac{1}{\sqrt{2} s_W} (\cos\alpha \mathcal{V}_{j1} \mathcal{U}_{i2} + \sin\alpha \mathcal{V}_{j2} \mathcal{U}_{i1}) \quad (3.2.24)$$

$$g_{\tilde{\chi}_i^0 \tilde{\chi}_j^0 H}^{L,R} = \frac{1}{2 s_W} (\mathcal{Z}_{j2} - t_W \mathcal{Z}_{j1}) (\cos\alpha \mathcal{Z}_{i4} - \sin\alpha \mathcal{Z}_{i3}) + i \leftrightarrow j \quad (3.2.25)$$

is strongly dependent on the neutralino (chargino) mixing matrices \mathcal{Z} (\mathcal{U} , \mathcal{V}) and therefore on the soft parameters M_1 , M_2 , μ and $\tan\beta$ [14, 35]. Furthermore, due to the appearance of the Higgs doublet mixing angle α , the couplings also depend on the Higgs masses, thus the parameter m_A . For the decoupling regime ($m_A \gg m_Z$), the mixing angle α is small, thus, terms proportional to $\sin\alpha$ become negligible.

3.2.3 Heavy Higgs Decays

As squarks and slepton masses are expected to be heavy, the decay of heavy Higgs bosons to SUSY particles was not in the main focus of previous analyses. However, it is possible for some sparticles to be light, as it is for electroweakinos or in limited cases, as e.g. for strong sfermion mixing, for 3rd generation sfermions. Studies of the pMSSM parameter space demonstrated a branching ratio for heavy Higgs bosons H decaying to SUSY particles of up to 90 %, depending on $\tan\beta$ [1]. As it is of importance for this work, this section will focus on the decay of heavy Higgs bosons to electroweakinos.

¹²Here, no quartic interaction terms are considered.

The decay width Γ of a neutral heavy Higgs boson H decaying to electroweakinos is defined as

$$\Gamma(H \rightarrow \tilde{\chi}_i \tilde{\chi}_j) \sim m_H \left[((g_{Hij}^L)^2 + (g_{Hij}^R)^2) \left(1 - \frac{m_{\tilde{\chi}_i}^2}{m_H^2} - \frac{m_{\tilde{\chi}_j}^2}{m_H^2} \right) - 4 \epsilon_i \epsilon_j g_{Hij}^L g_{Hij}^R \frac{m_{\tilde{\chi}_i} m_{\tilde{\chi}_j}}{m_H^2} \right] \quad (3.2.26)$$

where $\tilde{\chi}_i \tilde{\chi}_j$ can be a pair of neutralinos ($\tilde{\chi}_i^0 \tilde{\chi}_j^0$) or charginos ($\tilde{\chi}_i^\pm \tilde{\chi}_j^\mp$), ϵ_i (ϵ_j) is the sign of the i^{th} (j^{th}) electroweakino mass-eigenvalue and g_{Hij}^L (g_{Hij}^R) is the coupling constant for left- (right-) handed electroweakinos (see section 3.2.2) [14, 15, 35]. As seen, the coupling is enhanced for one negative mass eigenvalue ($\epsilon_i \neq \epsilon_j$) or unequal sign of the left- and right-handed couplings ($\text{sign}(g_{Hij}^L) \neq \text{sign}(g_{Hij}^R)$). Thus, an asymmetric decay into a light and a heavy electroweakino is preferred if kinematically allowed.

Fig. 3.2.2 shows the calculated branching ratios $\mathcal{B}(H \rightarrow \tilde{\chi}\tilde{\chi}) = \Gamma(H \rightarrow \tilde{\chi}\tilde{\chi})/\Gamma_{\text{total}}$ for the decay of H to neutralinos (left plot) and to charginos (right plot) for one specific set of parameters (bino-like LSP, $M_1 < \mu < M_2$) in dependence of the Higgs mass. As seen in eq. 3.2.26 and fig. 3.2.2, the decay width is enhanced for asymmetric decays ($H \rightarrow \tilde{\chi}_1^0 \tilde{\chi}_2^0$ or $H \rightarrow \tilde{\chi}_1^\pm \tilde{\chi}_2^\mp$) if kinematically allowed. Furthermore, these plots show a preferred decay to a pair of charginos.

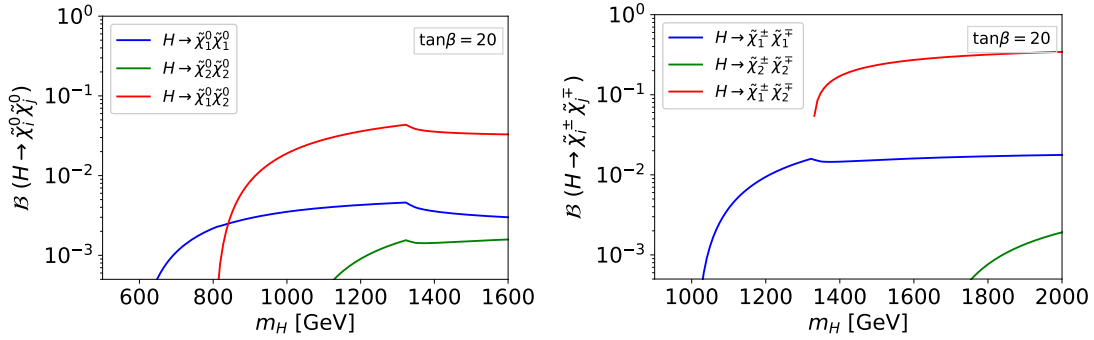


Figure 3.2.2: Branching ratios of heavy CP-even Higgs bosons (H) decaying to a pair of neutralinos (left) and a pair of charginos (right) for a bino-like LSP dataset ($M_1 < \mu < M_2$).

3.2.4 Higgs Boson Production Processes

The production of neutral Higgs bosons at the LHC is mainly given through the processes given in table 3.2.3, where V (V^*) are on-shell (off-shell) vector bosons and Q are 3rd generation quarks [14, 15, 25]. In fig. 3.2.3, the Feynman diagrams for the main production processes of MSSM Higgs bosons are given.

Production Mechanism	Process
Higgs Radiation	$q\bar{q} \rightarrow V^* \rightarrow V + h/H$
Vector Boson Fusion	$qq \rightarrow V^* q V^* q \rightarrow qq + h/H$
Gluon Fusion	$gg \rightarrow h/H/A$
Bottom Quark Annihilation	$gg \rightarrow Q\bar{Q}Q\bar{Q} \rightarrow Q\bar{Q} + h/H/A$ $b\bar{b} \rightarrow h/H/A$

Table 3.2.3: Main processes of neutral Higgs production at the LHC.

The production of the pseudoscalar A is suppressed for Higgs radiation and vector boson fusion processes, as it does not couple to SM vector bosons on tree-level (see section 3.2.2). The coupling to vector bosons to the neutral CP-even heavy Higgs boson is negligible for the decoupling regime, which is why these processes are not considered in this work (see table 3.2.2). Therefore, the dominating production processes are gluon fusion, where 3rd generation (s)quarks mainly contribute to the triangle diagram, and the bottom quark annihilation processes, where two bottom quarks annihilate to the Higgs boson.

For the gluon fusion process, two Feynman diagrams contribute equally to the total cross section of heavy Higgs productions (see fig. A.2.1). The cross section is calculated using Feynman rules and Feynman parameters (see Ref. [24]) with the final result for leading order calculations and SM fermion contributions being

$$\sigma(gg \rightarrow H) \propto \alpha_S^2 m_H^2 [\tau(1 + (1 - \tau)f(\tau))]^2 \quad (3.2.27)$$

$$f(\tau) = \begin{cases} \arcsin^2\left(\frac{1}{\sqrt{\tau}}\right) & \text{for } \tau \geq 1 \\ \left(\log\left(\frac{1+\sqrt{1-\tau}}{1-\sqrt{1-\tau}}\right) - i\pi\right)^2 & \text{for } \tau < 1 \end{cases} \quad (3.2.28)$$

where $\tau = (2m_f/m_H)^2$, α_S is the strong coupling parameter, m_f is the mass of the fermion considered in the triangle and m_H is the Higgs mass [41]. Due to their large mass, 3rd generation quarks dominate in the calculation of the cross section in gluon fusion processes, with the contribution of down-type quarks being enhanced for large $\tan\beta$. The contribution of 3rd generation sfermions \tilde{f} is suppressed by a factor of $m_f/m_{\tilde{f}}$, but can become important for low sfermion masses $m_{\tilde{f}}$. The calculation of the triangle diagram in gluon fusion processes was reproduced within the scope of this work and is given in appendix A.2.

As a result of up-type (down-type) couplings being suppressed (enhanced) by a factor of $1/\tan\beta$ ($\tan\beta$) (see table 3.2.2), large $\tan\beta$ ($\gtrsim 7$) lead to bottom quark annihilation being the dominant production channel of H [14, 15, 35]. Thus, two b -quark jets in the detector give an additional handle on the search for resonant heavy Higgs bosons at the LHC.

Study on the Heavy Higgs Production Cross Section

Fig. 3.2.4 visualizes the calculated cross sections for neutral CP-even heavy Higgs boson productions in both processes, gluon fusion and bottom quark annihilation. The Higgs mass (upper plots) and $\tan\beta$ dependence (lower plots) is visualized for one specific set of parameters. For these calculations, all sfermions are assumed to be heavy ($m_{\tilde{f}} \approx 1.5$ TeV).

The behavior of the calculated cross section in gluon fusion changes for $\tan\beta \gtrsim 7$ as a result of b -quark contributions dominating the triangle diagram. The bump at $m_H \sim 350$ GeV (see fig. 3.2.4, upper left) arises as a result of additional on-shell t -quark contributions in the triangle diagram of gluon fusion processes, which is again suppressed for large $\tan\beta$ values.

The center-of-mass energy dependence for both production processes is shown in fig. 3.2.4 (lower plots). In this work, the cross sections are calculated for $\sqrt{s} = 14$ TeV to determine the sensitivity of the High-Luminosity LHC (HL-LHC) [42, 43] with 3 ab^{-1} integrated luminosity. For future colliders with center-of-mass energies of about $\sqrt{s} \approx 100$ TeV (e.g. the hadronic Future Circular Collider FCC-hh [44]), an increase of the computed cross sections of more than one order of magnitude is expected.

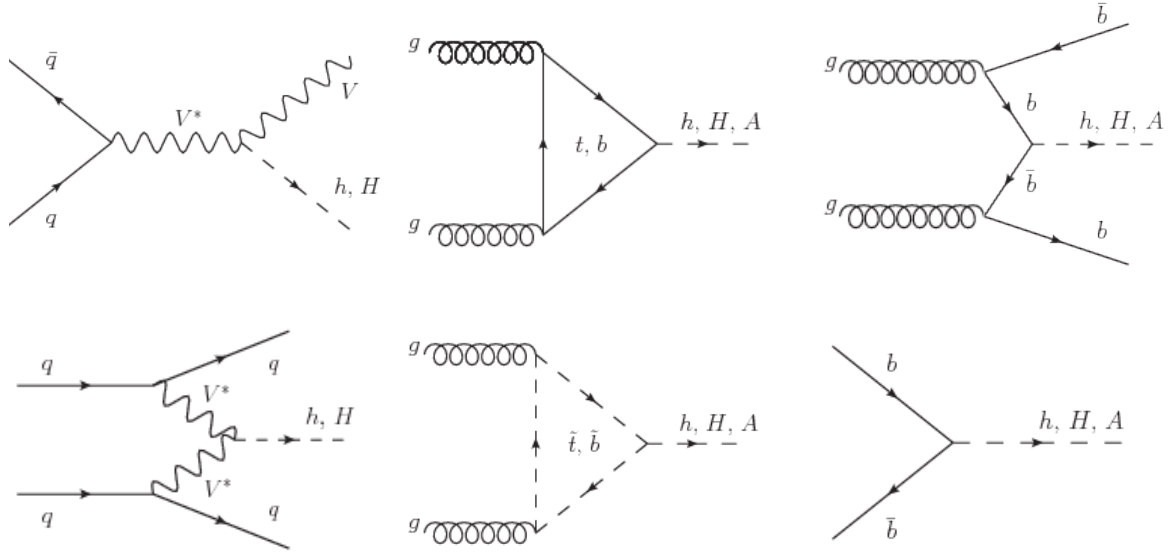


Figure 3.2.3: Main production channels for heavy Higgs bosons at the LHC. Higgs radiation (upper left) and vector boson fusion (lower left) are negligible for the decoupling regime ($m_H \gg m_Z$). The main production processes are gluon fusion (middle), and bottom quark annihilation (right). The figures were created using Jaxodraw-2.1 [4].

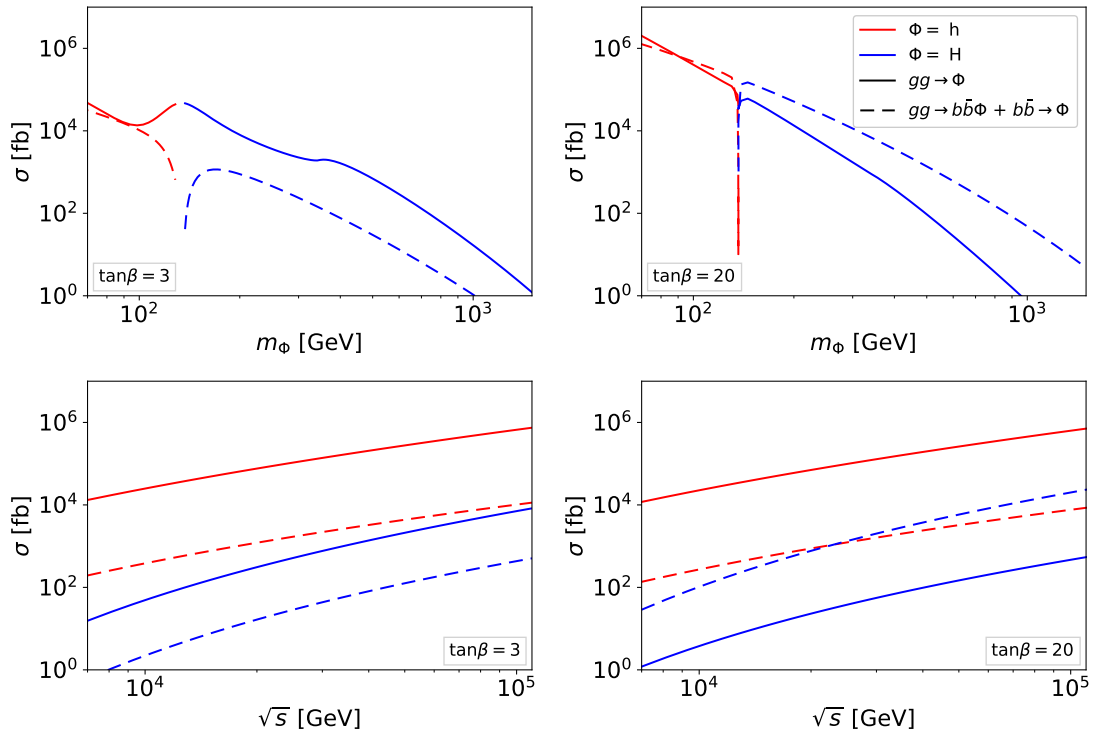


Figure 3.2.4: The Higgs boson production cross sections of gluon fusion (solid) and bottom quark annihilation (dashed) processes in dependence of the Higgs mass (m_Φ) (upper plots, $\sqrt{s} = 14$ TeV) and the center-of-mass energy \sqrt{s} (lower plots) for $\tan\beta = 3$ (left) and $\tan\beta = 20$ (right) for one specific set of parameters. These figures were calculated using SusHi-1.6.1 [37, 38].

3.3 Soft Symmetry Breaking in MSSM

Since the Higgs mechanism, as applied in the SM (see section 2.2), does not break supersymmetry, a term leading to soft symmetry breaking (SSB) has to be added to the Lagrangian of MSSM. SSB is necessary to allow heavier masses of sparticles compared to their SM partners. Furthermore, if supersymmetry and the electroweak symmetry are broken, sparticles with same electric charge mix.

In SUSY, two Higgs doublets with opposite hypercharge generate the masses of fermions with a given isospin. In addition, they are responsible for generating the masses of the W and Z boson. The superpotential V_H , which is minimized to create soft symmetry breaking, is given by

$$V_H = V_D + V_F + V_{\text{soft}} \quad (3.3.1)$$

$$V_D = \frac{g_2^2}{8} \left[4|H_1^\dagger \cdot H_2|^2 - 2|H_1|^2|H_2|^2 + (|H_1|^2)^2 + (|H_2|^2)^2 \right] + \frac{g_1^2}{8} (|H_2|^2 - |H_1|^2)^2 \quad (3.3.2)$$

$$V_F = \mu^2 (|H_1|^2 + |H_2|^2) \quad (3.3.3)$$

$$V_{\text{soft}} = m_{H_1}^2 H_1^\dagger H_1 + m_{H_2}^2 H_2^\dagger H_2 + B\mu (H_2 H_1 + h.c.) \quad (3.3.4)$$

where V_D contains the quartic Higgs interactions, V_F is the F term and V_{soft} is the potential arising from the soft SUSY breaking Higgs mass and the bilinear term. To achieve electroweak symmetry breaking in MSSM, a soft SUSY breaking is a requirement [15]. Minimizing the superpotential with

$$\frac{\partial V_H}{\partial H_1^0} = \frac{\partial V_H}{\partial H_2^0} = 0 \quad (3.3.5)$$

leads to the two necessary conditions for SSB

$$B\mu = \frac{(m_{H_1}^2 - m_{H_2}^2) \tan 2\beta + m_Z^2 \sin 2\beta}{2} \quad (3.3.6)$$

$$\mu^2 = \frac{m_{H_2}^2 \sin^2 \beta - m_{H_1}^2 \cos^2 \beta}{\cos 2\beta} - \frac{m_Z^2}{2} \quad (3.3.7)$$

where m_{H_1} and m_{H_2} are the scalar masses¹³. These conditions are especially important for pMSSM, as it allows to lower the number of free parameters.

A detailed calculation of minimizing the superpotential was performed within the scope of this work and is given in appendix A.3.

3.4 Standard Model Issues within Supersymmetry

There are many reasons, why SUSY is considered as the most promising extension of the SM. Despite its simplicity, it is able to tackle some of the main problems of the Standard Model. This section will give a brief overview of the main shortcomings of the SM (see section 2.3), and how SUSY introduces a solution.

¹³The scalar masses m_{H_1} and m_{H_2} can be replaced with the more physical soft parameters μ and m_A [15].

3.4.1 Hierarchy Problem in SUSY

A possible solution to the hierarchy problem, as described in section 2.3.1, arises due to the equal contribution of fermionic and bosonic (s)particles to the corrections of the Higgs mass. Their equal contribution, but with opposite sign, cancels the quadratic terms in the calculation of the Higgs mass (see eq. 2.3.1). In addition to the one example of the top quark contribution (see fig. 3.4.1, left), corrections to the Higgs mass are added as a result of the top squark loop (see fig. 3.4.1, right).

However, an exact cancellation of the quadratic contributions of the corrections is only possible for particles and sparticles with equal (or close to equal) mass. To make the Higgs mass renormalized, the supersymmetry breaking scale, and therefore the lightest MSSM particles, are expected to be not far from 1 TeV. This effect has strong impacts on the heavy Higgs bosons arising in MSSM (see section 3.2.1), resulting in an upper limit for their mass.

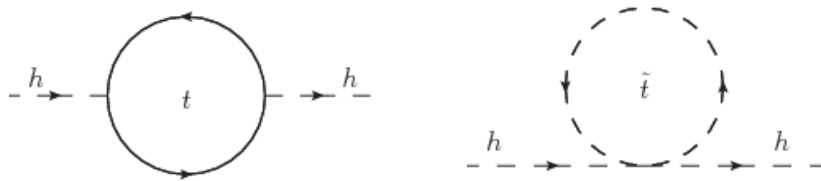


Figure 3.4.1: Feynman diagram for corrections to the Higgs mass due to top quarks (left) and stops (right). The figure was created using Jaxodraw-2.1 [4].

3.4.2 Gauge Coupling Unification in SUSY

In the SM, the gauge couplings of the symmetry groups $SU(3)_C$, $SU(2)_L$ and $U(1)_Y$, labeled as g_3 , g_2 and g_1 , respectively, do not exactly unify at the GUT-scale (see section 2.3.2). Many theories of BSM physics address this problem by introducing new multiplets and therefore new particles at high energy scales leading to corrections of the energy dependence of the couplings. This can lead to gauge coupling unification at the GUT scale, paving the way for a Grand Unified Theory.

Sparticles, introduced in Supersymmetric Grand Unified Theories (SUSY GUT), are held to have masses at the TeV-scale. Thus, additional corrections to the gauge couplings arise due to the contribution of those particles [45]. Fig. 3.4.2 shows the inverse couplings for SUSY GUT in dependence of the logarithm of the energy, where $\alpha_i = g_i^2/4\pi$ for MSSM. As seen, the couplings unify at an energy scale of about $m_{\text{GUT}} \approx 10^{16}$ GeV due to additional sparticle contributions at 10^4 GeV.

The boundary conditions as a result of enforcing gauge coupling unification reduces the number of free parameters and constraints the SUSY GUT models. One example is the extension of MSSM with enforced GUT scale unification, the minimal supergravity model (mSUGRA) [36], with only 5 free parameters.

The gauge coupling unification at the GUT scale is not enforced in pMSSM and therefore not considered in this work.

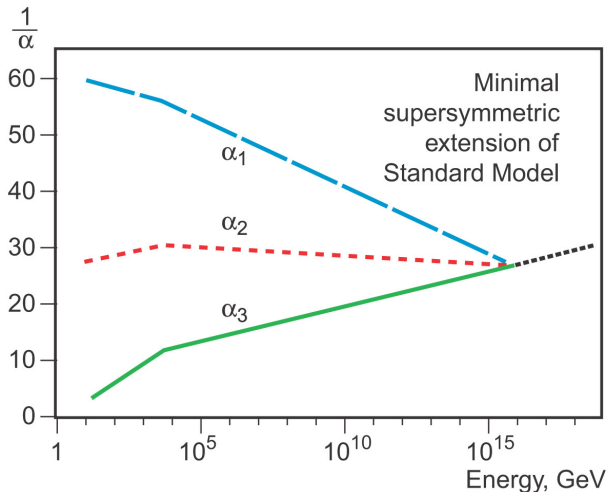


Figure 3.4.2: Energy-dependence of the gauge coupling constants in MSSM. Figure taken from Ref. [26].

3.4.3 Dark Matter Candidates

Another aspect of supersymmetry is that, other than the Standard Model, it is able to provide a neutral stable particle, which can act as a DM candidate. In MSSM, the baryon (B) and lepton number (L) is no longer conserved due to gauge invariant terms in the superpotential. The introduction of a \mathbb{Z}_2 symmetry, the R-parity

$$R = (-1)^{3(B-L)+2s} \quad (3.4.1)$$

where s is the spin of the particle, assures the conservation of those quantities again [15]. As a result, supersymmetric particles are produced in even numbers and decay in odd numbers of sparticles. The latter leads to a stable supersymmetric particle which can act as a DM candidate.

Models containing the Lightest Supersymmetric Particle (LSP) as a DM candidate have to fulfill the requirements concerning the DM relic density $\Omega_{\tilde{\chi}_1^0} h^2$ [46], the density of the DM particle at the freeze-out in the early universe, where h is the Hubble constant. Thus, neutralinos have to be produced in sufficient quantities in the early universe, leading to constraints on the neutralino mass and the DM to SM annihilation cross section.

Left-handed sneutrinos are disfavored as a DM candidate due to their strong coupling to the Z boson and therefore they are either excluded by direct DM experiments or annihilate too rapidly, leading to a small relic abundance [47]. The lightest neutralino $\tilde{\chi}_1^0$ is therefore held as a DM candidate in supersymmetry, as it has no color or electric charge.

4 Analysis Setup

The main goal of this work is the systematic analysis of heavy Higgs bosons decaying to SUSY particles within pMSSM for the full 19-dimensional parameter space. Therefore, a pre-collected dataset of the ATLAS collaboration is used. This set is particularly useful, as it applied a full 19-dimensional pMSSM parameter scan. In addition to the already applied constraints, the parameter sets are checked against current constraints of the Higgs and flavor sector by using the codes `HiggsBounds-4.3.1`, `HiggsSignals-1.4.0` and `SuperIso-3.6`, respectively. The `SModelS-1.1.1` framework allows to characterize decays in a model independent way using Simplified Model Spectra (SMS) and is able to apply current constraints of the CMS and ATLAS experiment.

This section gives an introduction to simplified models and the codes used in this work. The `SModelS` framework is discussed in more detail, as it is crucial for characterizing decay modes of the heavy Higgs boson. Furthermore, the ATLAS pMSSM dataset is introduced. A detailed study of the excluded parameter space within this dataset has been performed, with its results given in this section.

4.1 Simplified Model Spectra

The general interpretation of experimental results from BSM physics searches in collider experiments has become difficult, as their results can be interpreted in a variety of theoretical BSM models. One approach is the use of Simplified Model Spectra (SMS), where effective Lagrangians¹⁴ with only a limited number of new particles are used. In this interpretation technique, the process can be described using the masses and branching ratios of the new particles, as well as the the production cross section of the effective interaction. These parameters are directly related to observables in high-energy physics experiments. Thus, SMS approach assumptions are not a function of the color, spin or polarization of the particles.

The results then are typically given in upper limits for the product of the cross section and the branching ratio $\sigma \times \mathcal{B}$ for given particle masses [48] or in so-called efficiency map results, where constraints are given on the total signal of one specific signal region (see section 4.2.3). As an example for upper limit results, constraints on the decay of a supersymmetric quark into a quark and a neutralino $\tilde{q} \rightarrow q + \tilde{\chi}_1^0$ can be given as an upper limit on $\sigma \times \mathcal{B}$ as a function of the sparticle masses $m_{\tilde{q}}$, $m_{\tilde{\chi}_1^0}$ [49]. Even though, limits derived in the form of Simplified Model Spectra are significantly weaker, they can be interpreted in any theoretical full model.

The Feynman diagrams for full models can also be reduced to SMS topologies with Feynman-like graphs. One example is given in fig. 4.1.1, where the full model (left) of a Drell-Yan-like neutralino and chargino production is re-drawn in an SMS equivalent topology (right), only showing the detectable SM particles and missing transverse energy (MET) at the end of each branch [49]. The production of the W boson in proton-proton collisions is redrawn in an effective interaction, visualized as a circle with two outgoing legs.

¹⁴Here, ‘effective Lagrangians’ is meant in a sense that only a limited number of parameters are used.

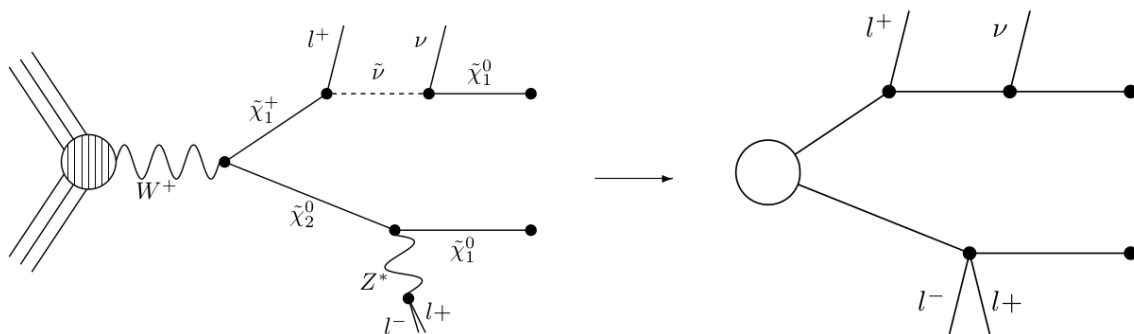


Figure 4.1.1: Feynman diagram for a full model (left) and the SMS topology (right). Figure taken from Ref. [49].

4.2 The SModelS Framework

Current searches for supersymmetry at the LHC are still without success, pushing the constraints on sparticle masses to the TeV scale. As simple BSM models are already excluded, the systematic scan for new particles has become difficult. Due to a varying mass spectrum of theoretical models, thus having different branching ratios of the included particles, an interpretation of current collider constraints is non-trivial.

The SModelS-1.1.1 framework [49–51] addresses this problem by creating SMS topologies of a given input in an SLHA file format. These SLHA files contain the mass spectrum, the production cross sections and the decay branching ratios. The PySLHA [52] reader is used to read the input SLHA files. By decomposing the supersymmetric input spectra for the given model into SMS topologies, each resulting topology can then be tested separately against limits from LHC direct SUSY searches. Fig. 4.2.1 gives a schematic overview of the SModelS working principle.

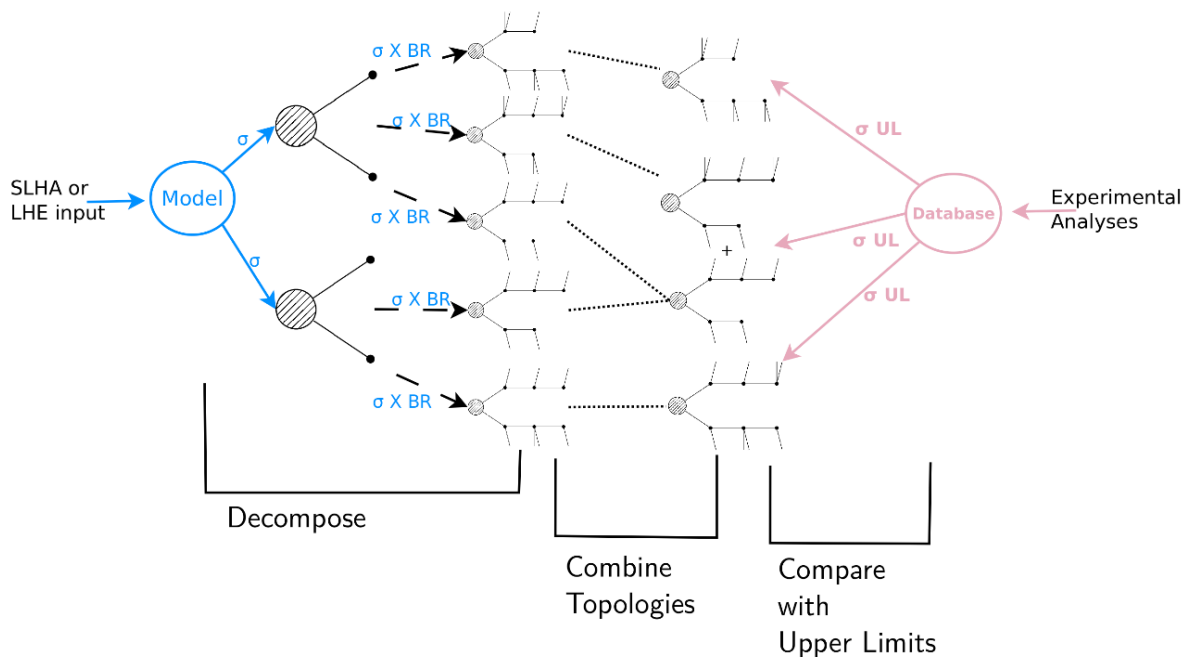


Figure 4.2.1: The working principle of the SModelS framework. Figure taken from Ref. [49].

Simplified Models are defined by taking all possible decay modes into account (see fig. 4.2.2). For each resulting topology, the output is reduced to the relevant signal. Thus, it only contains the SM particles visible to the detector and MET in every branch, where only the $\sigma \times \mathcal{B}$ values associated with the topology are stored (see fig. 4.1.1, right plot). The information of intermediate new particles is not of particular interest for the analysis and therefore not stored. This allows to decompose an input spectrum in a model independent way.

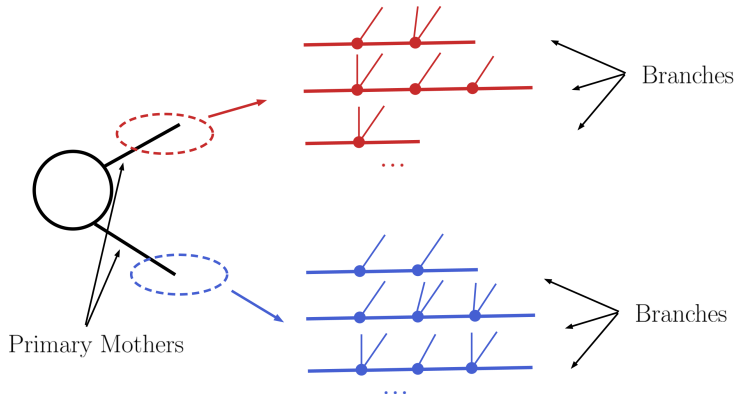


Figure 4.2.2: The decomposition procedure in the `SModelS` framework. Figure taken from Ref. [51].

To reduce the computing time of the decomposition, `SModelS` provides a σ_{cut} parameter. It allows to neglect topologies with cross sections below the cut value. Since in this work `SModelS` is used for the calculation of an unusually low production cross section of the mother particle and therefore have to use an unusually low absolute σ_{cut} value of 10^{-9} fb, a change of the input parameter so a relative cut-value compared to the initial state production cross section is proposed. This is particularly important for using `SModelS` for BSM searches, as it is done here.

After decomposing the input of the theoretical model, the predicted $\sigma \times \mathcal{B}$ values of the SMS topologies are compared to current upper limits from LHC direct SUSY searches at the CMS and ATLAS experiment (see section 4.2.4). This is trivial for analyses of one particular topology, as the experimental results provide the cross section and the masses of the analyzed BSM particles (see section 4.2.3). However, most analyses constrain the sum of topologies, as e.g. mass degenerate light sleptons \tilde{l} ($m_{\tilde{l}} = m_{\tilde{e}} = m_{\tilde{\mu}}$). For those, it is a necessity to combine the decomposed spectra before applying experimental constraints (see fig. 4.2.1, middle part).

Currently, `SModelS` is applicable for any BSM scenarios obeying a \mathbb{Z}_2 symmetry (e.g. R-Parity). New particles are produced in even numbers, which then decay to an odd number, resulting in a missing transverse energy (MET) in the final state at the LHC.

Within `SModelS`, the production process is represented as an effective production, where the detailed interaction is unknown and shown as a circle with two legs. The formalism is not capable of directly decomposing resonant searches, as e.g. the heavy Higgs and its decay to supersymmetric particles for this work. Therefore, the effective interaction is computed using the product of the MSSM Higgs production cross section and the branching ratio of its decay to SUSY particles $\sigma(pp \rightarrow H) \times \mathcal{B}(H \rightarrow \text{SUSY SUSY})$. This value is provided as an input to the code, which is a particularly new and innovative way to classify the signatures from resonant searches using `SModelS`. Fig. 4.2.3 visualizes the resonant heavy Higgs production, with its decay to SUSY particles (left) and how it is provided in `SModelS` (right).

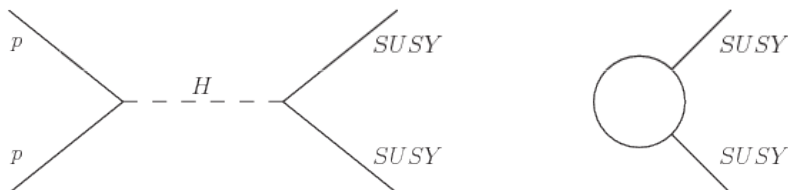


Figure 4.2.3: Feynman-like diagram for resonant heavy Higgs productions at proton-proton collisions with its decay to SUSY particles (left) in SMS topologies and how it is provided to the SModelS framework (right). The figures were created using Jaxodraw-2.1 [4]

4.2.1 The SModelS Notation

During the decomposition procedure and in the final output, the SModelS framework uses bracket notation describing the simplified model topologies. Since SModelS can deal with BSM obeying the \mathbb{Z}_2 symmetry, the output includes two branches enclosed by square brackets. In each branch, again the vertices are enclosed by brackets and separated with commas. However, for better readability and due to the simple signatures in the output, a simplified version of the bracket notation is used in this work.

As the \mathbb{Z}_2 symmetry leads to BSM particle pair productions, every branch includes MET at the end of the decay chain. In the output, electrons and muons are combined to light leptons (labeled l), as well as gluons and light quarks (u , d , c , s) are combined to *jets*.

Fig. 4.2.4 visualizes the SModelS notation principle with an example of a simple decay process. There, the outermost brackets enfold each branch ($[[l^+], [\nu]]$ and $[[l^-, l^+]]$), separated with a comma. The branches are sorted in size, each containing a list of vertices, again separated with commas. The notation for the vertices include the final state SM particles of the decay process. In the example given in fig. 4.2.4, the BSM particle of the upper branch decays to a light lepton (l^+) and an intermediate new particle. The latter again decays into a neutrino ($[\nu]$) and the final BSM particle, detectable as MET. The particle in the lower branch decays with an off-shell neutral particle (e.g. the Z boson), visualized as two light leptons in one vertex ($[[l^-, l^+]]$).

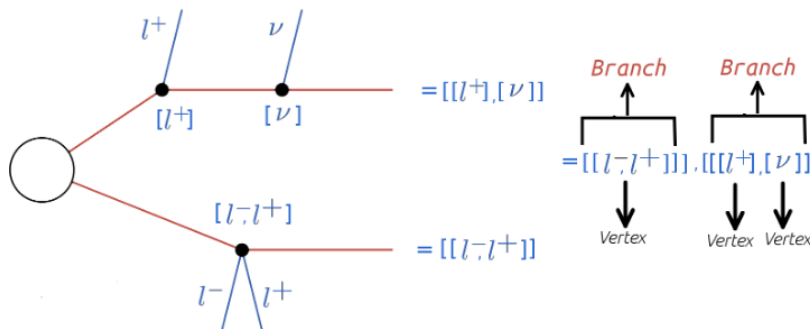


Figure 4.2.4: Conversion of a Simplified Models Spectrum to the bracket notation used in SModelS. Figure taken from Ref. [50].

4.2.2 Compression of Elements within SModelS

The SModelS framework uses two simplifications during the decomposition procedure, mass compressions and invisible compressions. These processes are useful to reduce the output in having fewer cascade decays. Thus, the result is more likely to be experimentally constrained.

- **Invisible Compression**

The process of invisible compression is used to neglect invisible decay products in the SMS topologies. One example is given in fig. 4.2.4, where the decay into a neutrino will not be visible to the detector. This vertex is then compressed, with the effective final state momentum being the sum of the neutrino and the final state momenta. Thus, the analysis performed by the framework results in equivalent topologies compared to experimental searches.

- **Mass Compression**

Mass compression is performed for small mass splittings between two BSM states. `SModelS` uses mass compressions to omit decays to nearly degenerate states. The parameter for the mass difference can be adjusted to the experimental setup. The main advantage is the resulting simplified topology being shorter and soft final states are reduced. The procedure for mass compression is illustrated in fig. 4.2.5.

In this work, a limit on the mass splittings of $\Delta m = 5$ GeV is used for this procedure. This is of particular importance for the higgsino-like LSP dataset, where the mass difference between the lightest chargino and the two lightest neutralinos is small. Therefore the decay of a heavy Higgs to a pair of charginos can lead to mono- W signatures, where the light chargino decays invisibly (‘soft’) to the LSP (see fig. 5.0.1).

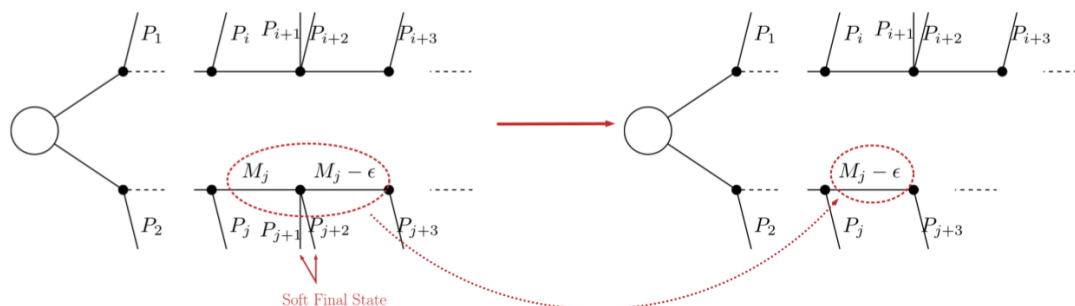


Figure 4.2.5: Mass compression in `SModelS`. Final states with masses lower than 5 GeV (soft final states) will not be visible in the software output. Figure taken from Ref. [50].

4.2.3 The `SModelS` Database

The database of the `SModelS` framework is based on SMS results from current LHC direct SUSY searches. It takes the constraints from publications and preliminary results from the CMS and ATLAS experiments into account. However, the user is able to specify the database for their purposes. The experimental results can be categorized in upper limit and efficiency map results.

- **Upper Limit Results**

Upper limit (UL) results provide experimental limits on the product of the cross section and the branching ratio $\sigma \times \mathcal{B}$ and are thus able to constrain one specific simplified model. The 95 % C.L. limits are typically provided by experiments in UL maps as a function of the BSM particle masses. One example is the previously mentioned decay of a squark into a quark and a neutralino $\tilde{q} \rightarrow q + \tilde{\chi}_1^0$, where upper limit constraints on the signal $(\sigma \times \mathcal{B})_{\text{UL}}$ are given as a function of the sparticle masses $m_{\tilde{q}}, m_{\tilde{\chi}_1^0}$ [49].

- **Efficiency Map Results**

Efficiency map (EM) results constrain the total signal of one specific signal region, given by $\sum \sigma \times \mathcal{B} \times \epsilon$. Here, the efficiency ϵ is denoted for the product of the acceptance and

the efficiency $A \times \epsilon$. The total signal is calculated using efficiency maps, which are grids of simulated efficiencies for specific simplified models and signal regions. These maps are computed by determining the number of signal events after applying all cuts using Monte-Carlo data.

4.2.4 The SModelS Output

After performing the previously discussed decomposition procedure, the theoretical predictions (signal cross sections) are compared with experimental upper limits $(\sigma \times \mathcal{B})_{\text{UL}}$ for ATLAS and CMS results, where SMS interpretations are currently available.

The theory predictions for each topology are confronted with experimental constraints with 95 % C.L. by calculating the r -value

$$r = \frac{(\sigma \times \mathcal{B})_{\text{th}}}{(\sigma \times \mathcal{B})_{\text{UL}}} \begin{cases} > 1 & \text{(excluded)} \\ < 1 & \text{(not excluded)} \end{cases} \quad (4.2.1)$$

where a model is excluded for at least one prediction being $r > 1$. A detailed description about the procedure of comparing theoretical predictions to UL-type and EM-type results can be found in Ref. [50].

In addition, SModelS categorizes its output containing the SMS topologies and their calculated $\sigma \times \mathcal{B}$ values into blocks of missing topologies, long-cascade decays and asymmetric decays.

- **Missing Topologies**

The SModelS output provides useful information about so-called missing topologies. In other words, these are topologies for which no corresponding SMS result was found in the SModelS database, independent of the particle masses. Using the decomposition output, topologies with equal final states are summed, resulting in indistinguishable initial states. The topologies are accompanied by their theoretical prediction of $\sigma \times \mathcal{B}$.

As this work is classifying the Higgs decays to supersymmetric particles and defining new ways to search for MSSM Higgs at the LHC, the missing topologies module is of special interest. By applying SModelS with a reduced database¹⁵, the missing topology block categorizes the main possible decay modes of a particle. Missing topologies are further classified into long-cascade decays and asymmetric decays.

- **Long-Cascade Decays**

Long-cascade decays are a subgroup of the missing topologies module. This block provides information about the mother particles and the theoretical prediction of $\sigma \times \mathcal{B}$ of special decay chains with more than one intermediate state in at least one branch. The expected signal is grouped according to their mother particles.

To analyze the possible decays of the heavy Higgs boson in this work, the long-cascade module is used to study the complexity of the decay process. Long-cascade decays arise mainly from heavy mother particles with kinematically allowed sub-decays to intermediate sparticle states. Since large cross sections are the result of low Higgs masses, it is expected that they are suppressed within the conditions of this work.

¹⁵SModelS cannot be operated without a database. Therefore, a reduced database with only one insignificant entry is used to classify all possible decay modes. In this work, the decay into a stop pair ($pp \rightarrow H \rightarrow t\bar{t}$) has been chosen. The dataset mostly contains heavy top squarks, thus this decay process is kinematically forbidden, which has been checked numerically.

- **Asymmetric Decays**

Asymmetric decays are a subgroup of the missing topologies module, where one branch of the SMS topology differs from the other. The module provides information about the mother particles and the theoretical prediction of $\sigma \times \mathcal{B}$. The theoretical predictions are then grouped according to their initially produced particles. Long-cascade decays are not included in the output of this module.

4.3 Additional Frameworks

In order to obtain the valid parameter space of pMSSM for resonant heavy Higgs searches, constraints from the flavor and Higgs sector have been applied to the pre-collected dataset using `SuperIso-3.6`, `HiggsBounds-4.3.1` and `HiggsSignals-1.4.0`. Furthermore, the production cross section of the CP-even neutral heavy Higgs has been calculated as an input for the `SModelS-1.1.1` framework with `SusHi-1.6.1`. The following will give a brief introduction to those additional frameworks used in this work.

4.3.1 SuperIso

`SuperIso-3.6` [53, 54] computes flavor physics observables, such as the branching ratios, lifetime and masses of mesons (e.g. π^+ , K^+ , D_s^+ , B^+ , B_s), within the Standard Model, the general two Higgs doublet (2HDM) and a variety of supersymmetric models.

The computation of isospin symmetry breaking observables turn out to be very restrictive to the parameter space of BSM physics models, as sparticles strongly contribute to those measured values. Especially rare B meson decays, with the flavor changing neutral current (FCNC) transitions $b \rightarrow s\gamma$, constrain the parameter space of MSSM. This work uses `SuperIso` to calculate NLO supersymmetric contributions to FCNCs and other rare decays. Therefore, SM inputs and the 19 free parameters of pMSSM are used to calculate the branching ratios, where $\mathcal{B}(B \rightarrow X_s\gamma)$, $\mathcal{B}(B_s \rightarrow \mu^+\mu^-)$ and $\mathcal{B}(B^+ \rightarrow \tau^+\nu_\tau)$ are of special interest. Furthermore, the anomalous magnetic moment of the muon $a_\mu = \frac{1}{2}(g_\mu - 2)$ [55] is computed and checked against current observations.

Details about the applied constraints of the flavor sector are given in section 4.4, with the ranges of the calculated observables given in table 4.4.3.

4.3.2 HiggsBounds

Limits on the MSSM heavy Higgs sector are checked using `HiggsBounds-4.3.1` [56, 57], written in Fortran. It is able to handle a variety of BSM physics models containing both, neutral and charged Higgs bosons. `HiggsBounds` applies limits from heavy Higgs searches at LEP, Tevatron and the LHC, where for the latter, analyses performed at a center-of mass energy of $\sqrt{s} = 7$ TeV and 8 TeV are taken into account.

By using the SLHA input-files with specified values for the Higgs masses, branching ratios and their production cross section, `HiggsBounds` computes the predicted signal rates for specific search channels considered in its experimental database. Their relevant quantities are the product of the cross sections and the branching ratios, denoted with $Q_{\text{model}}(X)$, where X is the

production and decay process. `HiggsBounds` first determines the analysis with the highest statistical sensitivity X_0 using the expected experimental limits $Q_{\text{exp.}}$. In a second step, it performs the exclusion test by calculating the ratio to the observed limit Q_{obs}

$$k_0 = \frac{Q_{\text{model}}(X_0)}{Q_{\text{obs}}(X_0)} \begin{cases} > 1 & \text{(excluded)} \\ < 1 & \text{(not excluded)} \end{cases} \quad (4.3.1)$$

to be able to exclude parameter sets at 95 % C.L.. The detailed statistical method to ensure a true 95 % C.L. exclusion limit is given in Ref. [56].

For their calculations, `HiggsBounds` requires special input blocks in the SLHA file format to calculate the theoretical predictions Q_{model} . This block contains the effective couplings of neutral Higgs bosons (h, H, A) to SM bosons, and 3rd generation fermions and can be provided by e.g. `SPheno` [58, 59]. The dataset used in this work already contains these SLHA blocks, which is why `SPheno` is not used here¹⁶.

It is recommended to use `HiggsBounds` in combination with `HiggsSignals`, to probe the full Higgs sector.

4.3.3 HiggsSignals

`HiggsSignals-1.4.0` [60] is a Fortran code based on `HiggsBounds` and allows to test a given parameter set in the SLHA file format against current limits from LEP, Tevatron and the LHC for a variety of models (e.g. MSSM). `HiggsSignals` compares the expected signal of heavy Higgs bosons with current observations. It applies either a mass-centered or a peak-centered approach for calculating the compatibility of a given input with experimental results. These approaches are complementary.

- **The mass-centered χ^2 method**

In the mass-centered χ^2 method, `HiggsSignals` computes the expected signal of every neutral Higgs boson at the corresponding fixed Higgs mass in the given input-file and compares it to signal rate measurements of the above mentioned experiments. These calculations assume a fixed Higgs boson mass, with a χ^2 test being performed at that mass. The signal-rates of multiple Higgs bosons are combined, if it is not able to resolve them in experimental results.

- **The peak-centered χ^2 method**

The peak-centered χ^2 method tries to assign to each observed local excess in experimental results any number of Higgs bosons provided by the input model. For those signals, the corresponding Higgs masses enter in the calculation of the χ^2 value [60]. It is tested, if the observed Higgs boson signal at a given mass is compatible with the influences of all Higgs bosons in the given model. Therefore, typically channels with a high mass resolution, i.e. $h \rightarrow \gamma\gamma$ and $h \rightarrow ZZ \rightarrow 4l$, are used.

Thus, `HiggsSignals` is capable of comparing the (combined) expected signal rates from the neutral MSSM Higgs bosons with current light Higgs measurements. In this work, a mass-centered χ^2 approach with an exclusion limit of 90 % C.L. is applied. It was found, that the in this work used parameter sets are highly sensitive to the limit set by `HiggsSignals` (see section 4.4.1).

¹⁶An early self-collected flat-prior parameter scan of this work showed a calculation error within `SPheno`. This led to a large amount of parameter sets being mistakenly excluded by `HiggsBounds`. Therefore, collecting a dataset was not possible within this work. According to the creator of `SPheno`, this problem is solved in the upcoming version.

4.3.4 SusHi

The production of heavy Higgs bosons in MSSM are studied in this work using the `SusHi-1.6.1` framework [37, 38]. The provided input-files in the SLHA file format can be used to calculate the production cross section for the neutral and charged Higgs bosons within various BSM models, as MSSM, NMSSM, mSUGRA and 2HDM. The calculations include gluon-fusion and heavy quark annihilation processes (see fig. 3.2.3). For the latter, only bottom quark annihilations are taken into account in this work, as they can become dominant for large $\tan\beta$ values in 2HDM and (N)MSSM.

- **The gluon fusion process**

The gluon fusion process is the most dominating production channel for low values of $\tan\beta$ in 2HDM and (N)MSSM. In leading order calculations, the (virtual) 3rd generation (s)fermions are mainly contributing in the triangle (calculation given in appendix A.2). In `SusHi`, the gluon fusion process can be calculated up to NNLO QCD corrections and up to N³LO for the neutral CP-even Higgs boson production in the heavy-top limit [61]. In supersymmetric models, the contribution of squarks \tilde{q} is typically suppressed by a factor of $m_q/m_{\tilde{q}}$. Thus, only the contribution of light bottom squarks \tilde{b} in the triangle can become significant for low sbottom masses and large $\tan\beta$ with enhanced Yukawa coupling.

- **The bottom quark annihilation process**

Even though, the contribution of bottom quark annihilation processes for Higgs productions is negligible within SM calculations, it becomes the dominating process for a large parameter (sub-)space within 2HDM and (N)MSSM. The processes of $b\bar{b} \rightarrow \phi$ and $gg \rightarrow b\bar{b}\phi$ can be calculated up to NNLO QCD using bottom quark PDFs.

`SusHi` can be linked to various Higgs-related frameworks, as `FeynHiggs` [39] to calculate the MSSM Higgs boson masses, or `HiggsBounds` and `HiggsSignals` to check against current experimental constraints. `SusHi` is furthermore linked to the `LHAPDF` library [62], which provides a variety of PDF sets for (s)quarks and gluons, used within the calculations.

The detailed calculations of (N)NLO corrections within the `SusHi` framework are given in Ref. [37, 38]

4.4 The ATLAS pMSSM Dataset

For the study within this work, a pre-collected and categorized dataset from a multi-dimensional flat-prior pMSSM parameter scan is used [63–67]. The scan is performed for the full 19-dimensional parameter space with its ranges given in table 4.4.1. The upper limit of 4 TeV for the mass parameters are chosen to ensure all new states are kinematically accessible at the LHC. A further increase above 4 TeV has very little effects in most cases [67]. A higher maximal value for A_t is implied, as it especially affects corrections to the Higgs mass [67]. The point selection [67] of the scan requires the parameter sets to satisfy pMSSM assumptions (see section 3.2), positive mass-squared values (no tachyons) and the LSP being the lightest neutralino $\tilde{\chi}_1^0$. The SM input values for the scan are given in table 4.4.2.

The SUSY spectrum is calculated using `SOFTSUSY-3.4.0` [68–70], where all parameter sets resulting in an error within the spectrum computation are discarded¹⁷. To ensure the accuracy of the SUSY mass spectrum, the values are recalculated using `SuSpect` [71]. Parameter sets with deviations of more than 50 % are removed. The Higgs masses are re-computed using

¹⁷A detailed description about the occurring error messages can be found in the appendix of Ref. [67].

4 Analysis Setup

Lower Limit	Parameter	Upper Limit	Description
90 GeV	$\leq M_{\tilde{l}_1} = M_{\tilde{l}_2} \leq$	4000 GeV	Left-handed 1 st - and 2 nd gen slepton
90 GeV	$\leq M_{\tilde{e}_R} = M_{\tilde{\mu}_R} \leq$	4000 GeV	Right-handed 1 st - and 2 nd gen slepton
90 GeV	$\leq M_{\tilde{L}_3} \leq$	4000 GeV	Left-handed 3 rd gen slepton
90 GeV	$\leq M_{\tilde{\tau}_R} \leq$	4000 GeV	Right-handed 3 rd gen slepton
200 GeV	$\leq M_{\tilde{q}_1} = M_{\tilde{q}_2} \leq$	4000 GeV	Left-handed 1 st - and 2 nd gen squark
200 GeV	$\leq M_{\tilde{u}_R} = M_{\tilde{c}_R} \leq$	4000 GeV	Right-handed 1 st - and 2 nd gen up-type squark
200 GeV	$\leq M_{\tilde{d}_R} = M_{\tilde{s}_R} \leq$	4000 GeV	Right-handed 1 st - and 2 nd gen down-type squark
100 GeV	$\leq M_{\tilde{Q}_3} \leq$	4000 GeV	Left-handed 3 rd gen squark
100 GeV	$\leq M_{\tilde{t}_R} \leq$	4000 GeV	Right-handed 3 rd gen up-type squark
100 GeV	$\leq M_{\tilde{b}_R} \leq$	4000 GeV	Right-handed 3 rd gen down-type squark
0 GeV	$\leq M_1 \leq$	4000 GeV	Bino mass parameter
70 GeV	$\leq M_2 \leq$	4000 GeV	Wino mass parameter
80 GeV	$\leq \mu \leq$	4000 GeV	Higgsino mass parameter
200 GeV	$\leq M_3 \leq$	4000 GeV	Gluino mass parameter
0 GeV	$\leq A_t \leq$	8000 GeV	Trilinear top quark coupling
0 GeV	$\leq A_b \leq$	4000 GeV	Trilinear bottom quark coupling
0 GeV	$\leq A_\tau \leq$	4000 GeV	Trilinear τ lepton coupling
100 GeV	$\leq m_A \leq$	4000 GeV	CP-odd Higgs boson mass
1	$\leq \tan \beta \leq$	60	Ratio of the Higgs vacuum expectation values

Table 4.4.1: Parameter range for the pMSSM scan [67].

`FeynHiggs-2.10.0` [39], where the light Higgs mass includes corrections up to N³LO and has to be within 5 GeV of the calculations of `SOFTSUSY`. The branching ratios of the given parameter sets are computed using `SUSY-HIT-1.3` [72], `HDECAY-5.11` [73] and `MadGraph5_aMC@NLO-2.1.1` [74], where any sets resulting in a negative branching ratio or a decay width larger than $\Gamma_{\text{total}} > 1$ TeV are discarded [67].

The pre-collected data sample, stored in the SLHA file format, already satisfies current limits of 22 distinct ATLAS analyses, given in Ref. [67]. Table 4.4.3 shows the additionally applied constraints, where the observables within the flavor sector are computed using `micrOMEGAs-3.5.5` [75]. Here, especially the branching ratios of $\mathcal{B}(B \rightarrow X_s \gamma)$, $\mathcal{B}(B_s \rightarrow \mu^+ \mu^-)$ and $\mathcal{B}(B^+ \rightarrow \tau^+ \nu_\tau)$ are constraining pMSSM models, where 2σ constraints are applied. The computed value of $\mathcal{B}(B_s \rightarrow \mu^+ \mu^-)$ is rescaled by a factor of $(1 - 0.088)^{-1}$ to compare the values with experimental data, as proposed in Ref. [76]. Furthermore, the deviation of the anomalous magnetic moment of the muon $\Delta(g - 2)_\mu$ and the electroweak parameter $\Delta\rho$ are computed, where 3σ constraints are applied. The latter uses limits from the radiative corrections to the Z boson coupling strength ΔT , with $\Delta\rho = \alpha\Delta T$ and $\alpha(m_Z) = 1/128$.

The LSP is a stable DM candidate and thus has a cosmological abundance. Nevertheless it is not clear, if it solely responsible for the DM content in the universe. Therefore, the cold dark matter relic density $\Omega_{\text{CDM}} h^2$ is taken as an upper limit on the LSP abundance. The code `micrOMEGAs` is used to compute the neutralino-nucleon cross sections, which are then scaled to calculate the effective dark matter cross sections [67]. These values are allowed to be a factor of four higher

Parameter	Value	Description
$\alpha(m_Z)$	127.918	QED coupling parameter
$\alpha_s(m_Z)$	0.1198	QCD coupling parameter
m_Z	91.1875 GeV	Z boson mass
Γ_Z	2.4952 GeV	Total Z boson decay width
$\sin^2 \theta_W$	0.22264	\sin^2 of the Weinberg angle
m_W	80.398 GeV	W boson mass
Γ_W	2.140 GeV	Total W boson decay width
$m_s(1 \text{ GeV})$	0.128 GeV	Strange quark mass
m_c^{pole}	1.666 GeV	Charm quark pole-mass
m_b	4.164 GeV	Bottom quark mass
m_b^{pole}	4.80 GeV	Bottom quark pole-mass
m_t^{pole}	172.6 GeV	Top quark pole-mass
V_{us}	0.2255	CKM-matrix elements
V_{cb}	41.6×10^{-3}	
V_{ub}	4.31×10^{-3}	
V_{ub}/V_{cb}	0.104	
m_B	5.279 GeV	B -meson mass
f_B	0.216 GeV	B -meson decay constant
τ_B	1.643 ps	B -meson mean lifetime
f_{B_s}	0.230 GeV	B_s -meson decay constant
τ_{B_s}	1.47 ps	B_s -meson mean lifetime

Table 4.4.2: Standard Model input parameters for the pMSSM parameter scan [63].

than experimental limits, as uncertainties of nucleon form factors are taken into account [67].

Combined LEP results are applied to the parameter sets, where especially constraints on the invisible width of the Z boson ($\Gamma_{\text{inv}}(Z) < 2 \text{ MeV}$) and lower limits on sparticle masses are taken into account. Due to the latter, charged sparticles have to have a mass above 100 GeV, light squarks have to be heavier than 200 GeV. A lower limit for chargino masses of 103 GeV is the result of sneutrino masses being heavier than 160 GeV and the mass splitting between the lightest chargino and the LSP being at least 2 GeV [67].

Due to expected theory uncertainties, the range of the light Higgs boson mass is fixed to be between 124 and 128 GeV.

The above mentioned constraints are already applied in the pre-collected data sample. In addition, the parameter sets have to obey 2σ limits from experimental heavy Higgs searches, which are checked in this work using the code `HiggsBounds-4.3.1` [57, 60, 77]. Constraints in the light Higgs sector are checked using `HiggsSignals-1.4.0` [60], where a limit of 90 % C.L. is applied. As previous constraints only limit the range of the light Higgs boson, `HiggsSignals` strongly influence the valid parameter space (see section 4.4.1).

In addition to the already applied constraints within the flavor sector, the same conditions are used by checking the parameter sets with `SuperIso-3.6` [53, 54] to ensure no anomalies in the

Lower Limit	Parameter	Upper Limit	Description
-0.0005	$\leq \Delta\rho$	≤ 0.0017	Electroweak parameter
-17.7×10^{-10}	$\leq \Delta(g-2)_\mu$	$\leq 43.8 \times 10^{-10}$	Anomalous magnetic moment of the muon
2.69×10^{-4}	$\leq \mathcal{B}(b \rightarrow s\gamma)$	$\leq 3.87 \times 10^{-4}$	Branching ratio FCNC
1.6×10^{-9}	$\leq \mathcal{B}(B_s \rightarrow \mu^+\mu^-)$	$\leq 4.2 \times 10^{-9}$	Branching ratio $B_s \rightarrow \mu\mu$
66×10^{-6}	$\leq \mathcal{B}(B^+ \rightarrow \tau^+\nu_\tau)$	$\leq 161 \times 10^{-6}$	Branching ratio $B^+ \rightarrow \tau^+\nu_\tau$
	$\Omega_{\tilde{\chi}_1^0} h^2$	≤ 0.1208	Cold dark matter energy density
	$\Gamma_{\text{inv(SUSY)}}(Z)$	$\leq 2 \text{ MeV}$	Z boson decay width to invisible
100 GeV	$\leq m_{\tilde{\chi}^\pm}$		Lightest charged sparticle mass
103 GeV	$\leq m_{\tilde{\chi}_1^\pm}$		Lightest chargino mass
200 GeV	$\leq m_{\tilde{q}}$		Lightest squark mass
124 GeV	$\leq m_h$	$\leq 128 \text{ GeV}$	Light Higgs boson mass

Table 4.4.3: Constraints applied to the MSSM parameter scan [67].

applied codes.

SLHA files containing long-lived sparticles ($c\tau > 1 \text{ mm}$) are removed from the analysis, as the `SModelS` framework cannot handle the resulting displaced vertex signatures. Since the aim of this work is to characterize decays of the neutral CP-even heavy Higgs H to supersymmetric particles, parameter sets where H solely decays to SM particles are discarded.

A detailed list of the number of removed files is given in table 4.4.5.

The total parameter sample is, according to the dominant part of the neutralino mixing matrix \mathcal{Z} , categorized into three parts: bino-like, wino-like and higgsino-like (see table 4.4.4). In this work, we only use the bino- and higgsino-set. Due to the small mass difference between the lightest chargino $\tilde{\chi}_1^\pm$ and the wino-like LSP, a majority of the parameters in the wino-set result in long-lived charged particles, leading to displaced vertex signatures in the detector (see fig. 4.4.1 and table 4.4.5). Since the newest version of the `SModelS` framework, being able to process displaced vertex signatures, is currently under development, a future analysis of the wino-set using `SModelS` is proposed.

Type	Definition	Sample Size
Bino-like LSP	$\mathcal{Z}_{11}^2 > \max(\mathcal{Z}_{12}^2, \mathcal{Z}_{13}^2 + \mathcal{Z}_{14}^2)$	31.112
Higgsino-like LSP	$(\mathcal{Z}_{13}^2 + \mathcal{Z}_{14}^2) > \max(\mathcal{Z}_{11}^2, \mathcal{Z}_{12}^2)$	59.044
Wino-like LSP	$\mathcal{Z}_{12}^2 > \max(\mathcal{Z}_{11}^2, \mathcal{Z}_{13}^2 + \mathcal{Z}_{14}^2)$	39.816

Table 4.4.4: Sample size after applying all constraints and definition of the categorized parameter sets [67].

4.4.1 Study of the Excluded Parameter Space

Direct SUSY searches of the ATLAS experiment already constrain the pMSSM parameter space, especially those resulting in light 3rd generation squark and slepton masses. Upper limits from 22 ATLAS searches and constraints on the SUSY mass spectrum, the invisible Z boson decay

width, the cold dark matter relic density and the limits of the flavor sector (see section 4.4 and table 4.4.3), already exclude about 41 % of the initial sample size. Limits in the Higgs and flavor sector, as well as necessary conditions for this analysis further reduce the valid number of parameter sets. This section will give a detailed study on the excluded parameter sets due to the in this work applied constraints. A detailed listing of the excluded sets in the applied ordering is given in table 4.4.5.

About 5.4 % (12.1 %) of the initial higgsino-like LSP (bino-like LSP) dataset is excluded due to SLHA files not containing H decays to SUSY particles. Furthermore, 5.3 % (4.2 %) contain long-lived sparticles and can thus not be analyzed by the `SModelS` framework. A limited number of SLHA files are removed, as the resulting $\sigma \times \mathcal{B}$ values are below the σ_{cut} parameter of `SModelS` (see section 4.2). These parameter sets contain very heavy Higgs bosons, reducing their production cross section. Furthermore, heavy LSPs lead to small branching ratios to SUSY particles. Thus, these parameter sets are not significant for this work.

For the valid parameter sets it is interesting to note the large amount of excluded sets by `HiggsSignals`, using 90 % C.L. within its mass-centered χ^2 method. Initial limits only fix the light Higgs mass range. Therefore, `HiggsSignals` is able to exclude the sets as a result of limits on the Higgs boson signal rates. A check of current constraints within the light and heavy Higgs sector is proposed for all SUSY parameter scans, as fixing the light Higgs mass is not sufficient. It should be noted, that the dataset is highly sensitive to the applied limit of `HiggsSignals`. An increase to 95 % C.L. reduces the dataset to about 18.000 and 38.500 valid points for the bino-like and higgsino-like LSP set, respectively.

Constraints	Bino-like LSP	Higgsino-like LSP	Wino-like LSP
Initial sample size (ATLAS)	103.410	126.684	80.233
Initial valid sample size (ATLAS)	61.370	77.981	43.680
No decay mode to SUSY particles	7.432	4.223	3.864
Long-lived sparticles ($c\tau > 1$ mm)	2.591	4.128	(36.817)
Excluded by SuperIso ($2\sigma/3\sigma$)	1.781	1.957	
Excluded by HiggsBounds (2σ)	120	154	
Excluded by HiggsSignals (90 % C.L.)	18.168	8.122	
Not processed ($\max(\sigma \times \mathcal{B}) < 10^{-9}$ fb)	166	353	
Valid sample size	31.112	59.044	39.816

Table 4.4.5: Breakdown of the excluded parameter sets. The wino-like LSP dataset is not treated in the analysis using `SModelS` and therefore, no constraints are applied.

Fig. 4.4.1 visualizes the fraction of the ATLAS pMSSM parameter study as a function of the light chargino lifetime $c\tau$. SLHA files with lifetimes of sparticles above $c\tau > 1$ mm are discarded in this study. As seen, the majority of the parameter sets in the wino-like LSP sample contain charginos with a lifetime of about $c\tau(\tilde{\chi}_1^\pm) \approx 50$ mm as a result of the lowest electroweakino mass parameter being M_2 and thus, the small mass difference between the chargino and the LSP.

Due to the large amount of long-lived sparticles in the wino-like LSP dataset, this set has not been studied using `SModelS`. Nevertheless, the dependence of the chargino lifetime on the lightest chargino and the heavy Higgs mass has been analyzed for wino-like LSPs. For this study, no constraints from the light and heavy Higgs sector were applied. Decays of heavy Higgs bosons into wino-like LSPs mainly lead to displaced vertex signatures in the detector. Promising results

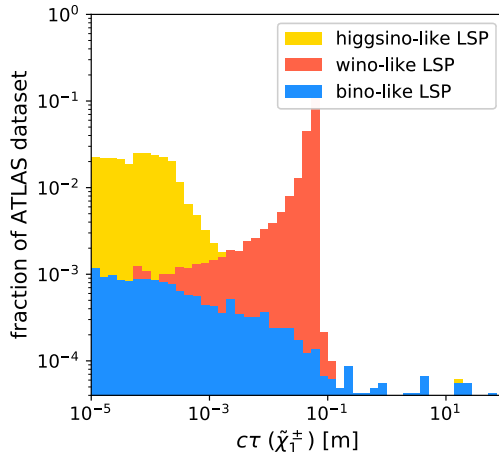


Figure 4.4.1: Lifetime of the lightest chargino $c\tau(\tilde{\chi}_1^\pm)$ for the categorized parameter sets.

can be found for the calculated cross sections, as discussed in section 5.7.

The excluded parameter sets in the $m_A - \tan\beta$ plane (upper plots) and in the relevant electroweakino soft parameter planes (middle/lower plots) for higgsino-like and bino-like LSPs are visualized in fig. 4.4.2 for the exclusion of long-lived sparticles and parameter sets with no decay mode of heavy Higgs bosons to SUSY particles. Fig. 4.4.3 gives the sets for the exclusion in the flavor and Higgs sector.

Removed parameter sets as a result of heavy Higgs bosons only decaying to SM particles are the result of low Higgs masses ($m_A \approx m_H$) and heavy sparticles. Therefore, a decay is kinematically forbidden. The large electroweakino masses are the result of large values of the relevant soft parameters M_1 , M_2 and μ (see fig. 4.4.2, middle/lower plots). Here, especially a large value of the lowest soft parameter (μ for higgsino-like LSPs, M_1 for bino-like LSPs) plays a crucial role, as it leads to heavy LSPs. Squarks and sleptons are in general heavy for those datasets.

Long-lived sparticles arise due to small mass-differences to the LSP. Typically, the lightest chargino $\tilde{\chi}_1^\pm$, or in limited cases light tau sleptons $\tilde{\tau}$ or bottom squarks \tilde{b} are long-lived in the underlying dataset. The latter are mainly due to strong mixing of left-/right-handed components and thus, one eigenstate having a mass close to the LSP mass. A decay into their SM superpartner and the LSP is then kinematically forbidden. Light charginos arise due to a highly mixed electroweakino sector, where the lightest neutralinos and the lightest chargino are nearly degenerate in mass (see fig. 4.4.2, middle/lower plots).

As seen in fig. 4.4.3, the analyses on heavy Higgs bosons included in **HiggsBounds** are mainly able to exclude specific regions with heavy Higgs masses of about $m_H \approx m_A \approx 1$ TeV for a range of $\tan\beta$ between $30 < \tan\beta < 50$, where the Yukawa couplings to down-type squark is strongly enhanced. It is expected, that other excluded parameter sets are not included in the initial dataset, as they are already removed due to limitations of ATLAS analyses.

Furthermore, a large amount of excluded parameter sets by **HiggsSignals** is found for positive values of the higgsino mass parameter $\mu > 0$. It is not known, if this is the result of strong constraints from the above mentioned experiments or an enhanced signal due to contributions of sparticles. No anomalies were found during the analysis of the excluded parameter space.

Excluded sets by **SuperIso** mainly arise due to small deviations in the calculation of the flavor sector observables of **SuperIso** to the previously applied code **micrOMEGAs**. Here, especially the increasing amount of excluded parameter sets for large $\tan\beta$ is seen. The enhanced Yukawa couplings to down-type squarks leads to non-negligible contributions of those sparticles to the flavor observables.

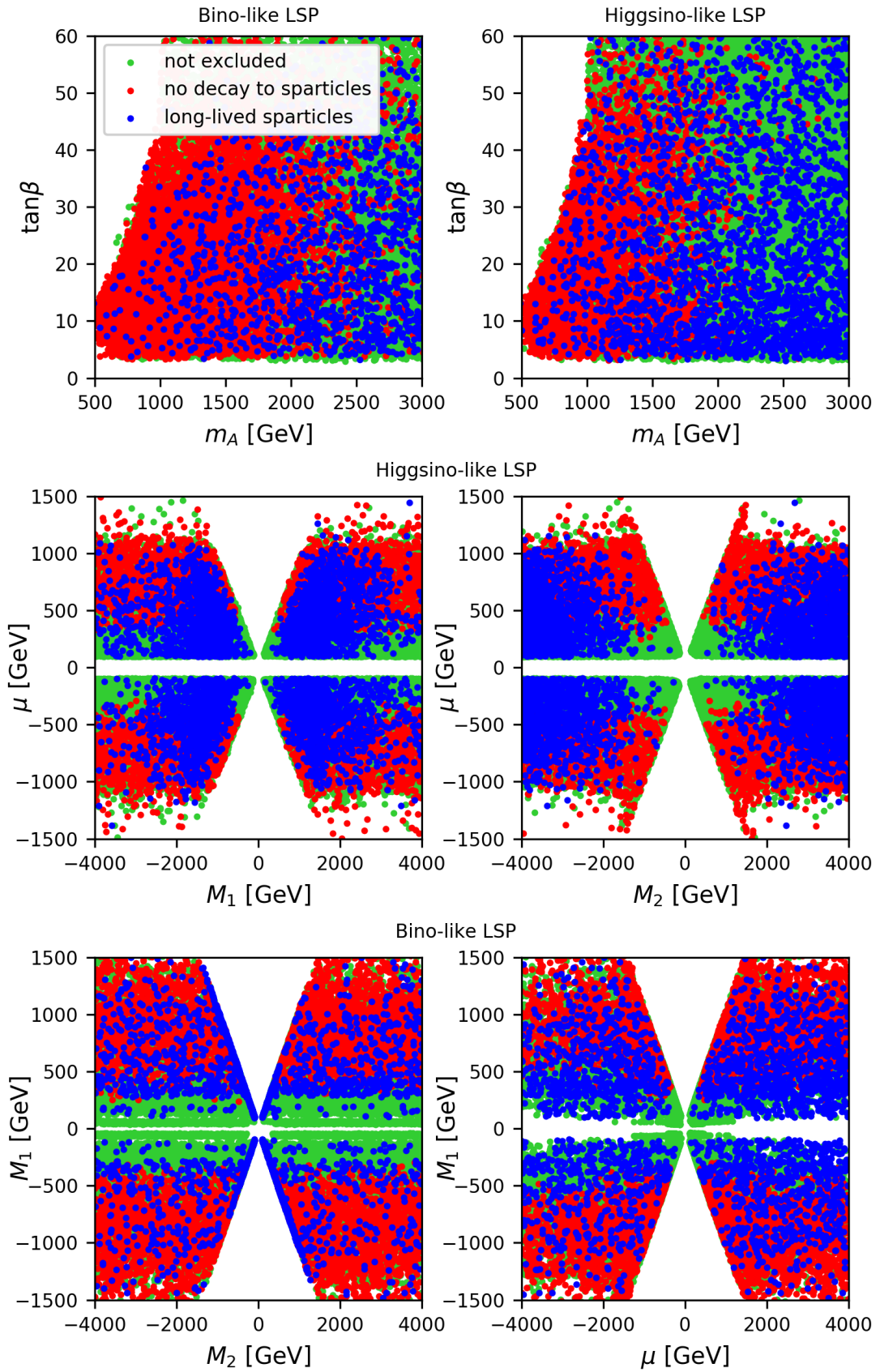


Figure 4.4.2: Study of the excluded parameter sets due to long-lived sparticles or no decay mode to sparticles in the relevant parameter planes for the higgsino-like and bino-like LSP datasets.

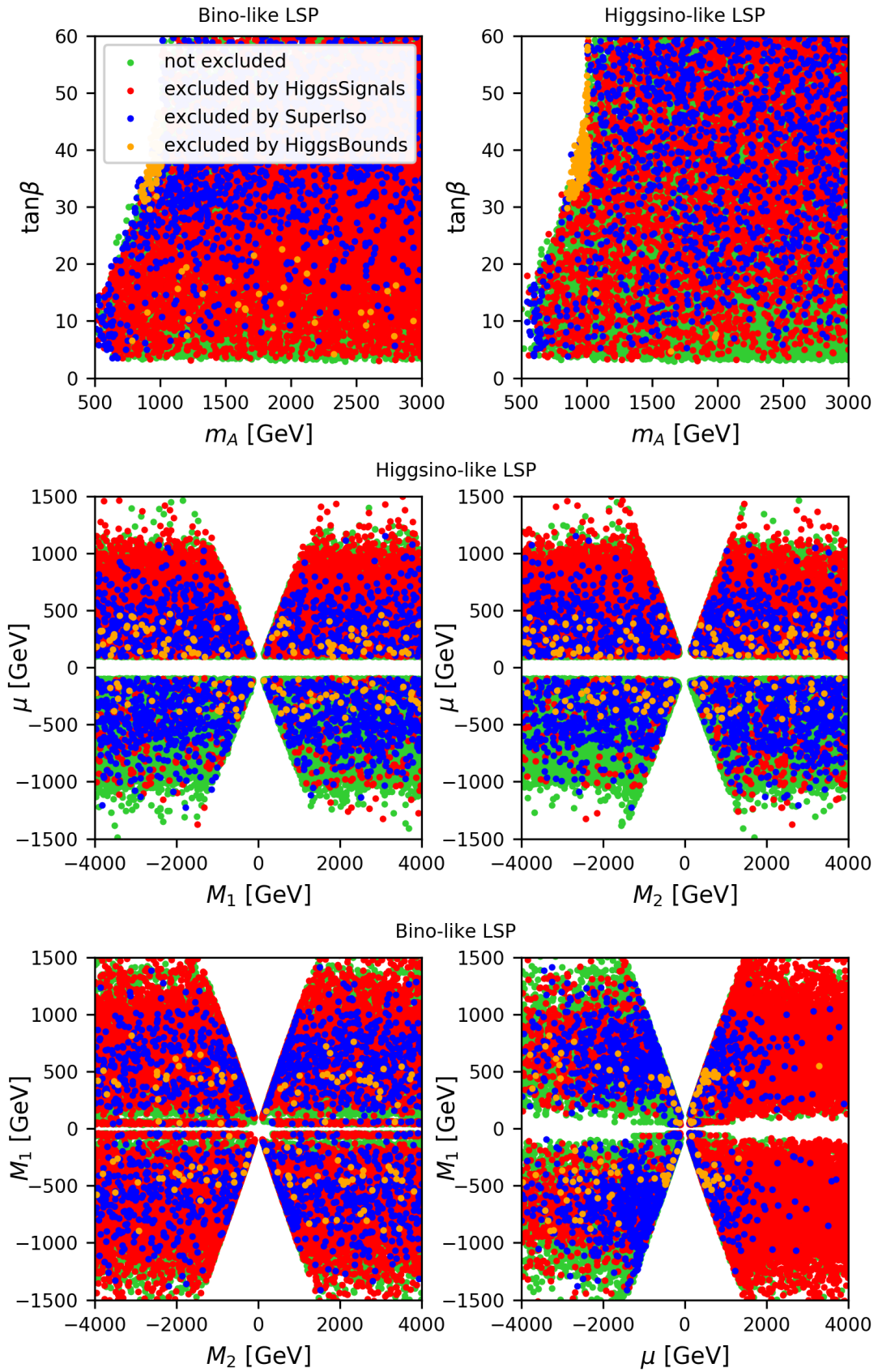


Figure 4.4.3: Study of the excluded parameter sets in the Higgs- and flavor sector in the relevant parameter planes for the higgsino-like and bino-like LSP datasets.

5 Results

The aim of this work is the systematic analysis of the viable pMSSM parameter space using `SusHi-1.6.1` [37, 38] to calculate the production cross sections and `SModelS-1.1.1` [49, 50, 52, 78–80] to classify decay channels of heavy Higgs bosons (H). A reduced database is used in the `SModelS` framework to retrieve all possible decay modes of H to sparticles within the missing topology block. Thus, no additional constraints from LHC direct SUSY searches are applied (see section 4). Nevertheless, studies on current constraints from LHC Run 1 and Run 2 are given in section 5.5. Furthermore, the regions with maximal signal at the LHC are identified for the signatures of heavy Higgs decays. A systematic study of the parameter dependence for heavy Higgs production and decays is done for the resulting signatures. Since the wino-like LSP dataset contains mostly long-lived charged particles, it is not possible to analyze it using `SModelS`. However, a brief study on the lifetime of light charginos in this set is performed.

The resulting missing topology signatures of the bino- and higgsino-like LSP dataset are dominated by the asymmetric decay of the heavy Higgs boson to a light and a heavy electroweakino state. The decay of the latter leaves an on- or off-shell vector boson (Z, W) or light Higgs (h) signature in the detector. For the off-shell states, the dominating channels are $Z^*, W^* \rightarrow jet\ jet$ and $Z^*, h^* \rightarrow b\bar{b}$, where *jets* are light quarks of the 1st and 2nd generation ($jet \in \{u, d, s, c\}$) or gluons. In a limited number of files, the soft W boson decays leptonically ($W^* \rightarrow l\nu_l$), where a single 1st or 2nd generation lepton ($l \in \{e, \mu\}$) is visible to the detector.

The analysis of the missing topologies can be presented in two ways, either by showing the most frequent missing topologies in a certain parameter space, or by selecting for each parameter point the missing topology with the highest cross section. The upper plots in fig. 5.0.2 visualizes the five most frequent occurring signatures from resonant heavy Higgs decays to supersymmetric particles. The most dominating ones is given in the lower plots.

Mono- X signatures ($X = h, W, Z$) are found to be the most frequent occurring, as well as the most dominant missing topologies, having the highest cross sections in up to 41 % of the data points. They occur as a result of the asymmetric decay of a heavy Higgs to a light and a heavy neutralino or chargino, as asymmetric decays are preferred for heavy Higgs bosons if kinematically allowed (see section 3.2.3). Fig. 5.0.1 visualizes the Feynman diagrams for the simplest heavy Higgs decays with mono- X signatures. In these decay processes, the heavier electroweakino state decays with an on-shell X ($X = h, W, Z$) to the final state, with the lighter state being stable or decaying to soft objects.

Mono- Z and mono- h signatures appear due to the asymmetric decay of H to neutralinos, with a soft decay of the lighter state and a decay of the heavier neutralino to a Z or h boson and the LSP¹⁸. Even though, the vertex $\tilde{\chi}_i^0 \rightarrow h\tilde{\chi}_1^0$ ($i \in \{2, 3\}$) is larger compared to $\tilde{\chi}_i^0 \rightarrow Z\tilde{\chi}_1^0$ [35] in the bino-like LSP dataset with highly mixed bino-/higgsino-like LSPs (see section 5.1.1), mono- Z signatures dominating the Higgs decay is found. This is the result of the following: The branching ratios of electroweakinos decaying to on-shell Z and h are very similar, even though,

¹⁸As given in table 5.0.1, the decay into the LSP can be replaced with a kinematically allowed decay to an electroweakino, which then decays soft.

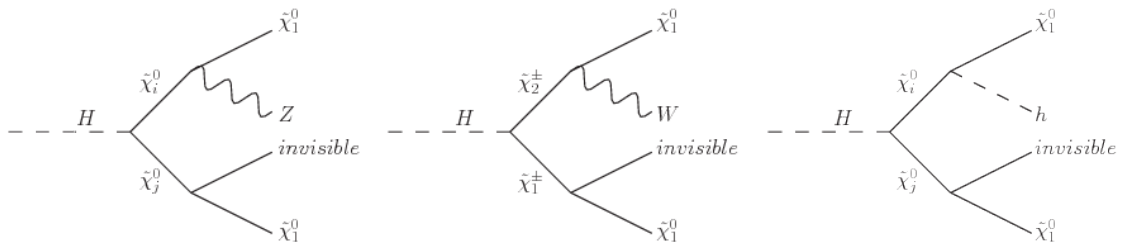


Figure 5.0.1: Feynman diagrams for heavy Higgs decays with mono- X signature ($i < j$). The figures were created using `Jaxodraw-2.1` [4].

the latter is slightly larger. The larger branching ratio for decays to h is the result of the coupling of the light Higgs to the admixture of bino-/higgsino-components, where Z stronger couples to the pure higgsino-component of electroweakinos [35]. However, for decays to Z bosons, more decay modes are possible, as e.g. the mass difference of two neutralinos being below the light Higgs mass and thus a decay into the latter is kinematically forbidden. `SModelS` sums over the initial states with same final signatures, leading to larger $\sigma \times \mathcal{B}$ values for mono- Z signatures.

Besides H decaying into a light and heavy neutralino state, mono- Z and mono- h signatures are also found for Higgs decaying to a pair of charginos. There, the heavier chargino $\tilde{\chi}_2^\pm$ decays to the lighter one ($\tilde{\chi}_2^\pm \rightarrow Z/h \tilde{\chi}_1^\pm$) and both light charginos decay to soft final states and the LSP. If kinematically allowed, this process can be dominant, as the decay to higgsino- and wino-like states are preferred (see section 5.1.1). Thus, decays of Higgs to charginos results in higher branching ratios compared to an asymmetric decay to neutralinos. Furthermore, both possible channels ($H \rightarrow \tilde{\chi}_1^+ \tilde{\chi}_2^-$ and $H \rightarrow \tilde{\chi}_1^- \tilde{\chi}_2^+$) are summed. The soft decay reduces the total $\sigma \times \mathcal{B} \times \mathcal{B}_{\text{soft}}$ only marginally, as the branching ratio to soft final states is summed over all possible decay modes ($W_{\text{soft}}^* \rightarrow jet\ jet$ and $W_{\text{soft}}^* \rightarrow l \nu_l$, with $l \in \{e^-, e^+, \mu^-, \mu^+\}$ and $jet \in \{u, d, s, c\}$).

Mono- W signatures are the result of H decaying into a light and heavy chargino, where the (light) heavy state decays to an (soft off-shell) on-shell W boson and the LSP, with $W_{\text{soft}}^* \rightarrow jet\ jet$, leading to two soft jets ($\Delta m < 5$ GeV) not visible to the detector.

In addition, this signature can be the result of a H decay to two neutralinos, where the heavier state further decays to a W boson and a light chargino. The latter then decays soft to the LSP. Only a minority of the bino-like LSP dataset contains mono- W signatures, as the lightest chargino state is higgsino-like and thus, a decay to a W boson is suppressed. Furthermore, suppressed decays of the higgsino-like neutralinos $\tilde{\chi}_2^0$ and $\tilde{\chi}_3^0$ to the lightest chargino are found, reducing the number of decay channels with mono- W signature. The wino-like chargino $\tilde{\chi}_2^\pm$ and neutralino $\tilde{\chi}_4^0$, where the decay into a W boson is preferred, are likely to be heavy, as the soft parameter M_2 is not expected to be low (see section 5.1.1).

Furthermore, additional on- and off-shell vector bosons are found in the dominating missing topologies in up to 12 % of the parameter sets. The more complex signatures $((W), (jet, jet)), (jet, jet)$ and $((Z), (jet, jet)), (jet, jet)$ in the bino-like LSP dataset is the result of the preferred coupling of Higgs to mixed higgsino-/wino-like states (see section 5.1.1). Thus, large Higgs masses allow a decay to the wino-like $\tilde{\chi}_4^0$ and the higgsino-like $\tilde{\chi}_2^0$ or $\tilde{\chi}_3^0$, where the latter is preferred. Due to this decay being kinematically allowed and having large branching ratios, additional decays of the heavier neutralinos to the LSP leads to more complex signatures with on- and off-shell bosons in the detector. It should be noted, that this is not the only process playing a role. As `SModelS` sums over all initial states, the same signature can be a result of many initial states. Thus, for high Higgs masses, more complex signatures can become dominant.

The (inv),(inv) signature is the result of H decaying to a pair of LSPs, light neutralinos (e.g.

$\tilde{\chi}_2^0$) or charginos ($\tilde{\chi}_1^\pm$), where the latter two have to decay soft. These processes are often the only possible decays of H to SUSY particles, as all other states are heavy. Thus, this signature is dominant for low Higgs or large sparticle masses. This is especially the case for the bino-like LSP dataset, where the mass difference of the LSP and next-to LSP (NLSP) can be large.

Decays of a heavy electroweakino (neutralino or chargino) to an intermediate slepton state can be dominant in up to 4 % of the dataset, leading to two single light leptons in one branch. To this signature, the H decay to a LSP and a heavy neutralino state are contributing in addition. The heavy neutralino then decays with an intermediate chargino state into the LSP, where two leptonically decaying off-shell W bosons ($W^* \rightarrow l\nu_l$) leave each a single lepton in the detector. This process can be enhanced, as the final $\sigma \times \mathcal{B}$ value is a sum over all final light lepton states ($l \in \{e^-, e^+, \mu^-, \mu^+\}$).

Heavy Higgs bosons with low masses ($m_H \lesssim 700$ GeV) are disfavored by ATLAS direct SUSY searches or do not contain a decay to SUSY particles. Thus, the analyzed data includes only decoupled Higgs states leading to the coupling of the heavy Higgs bosons to vector bosons being suppressed (see section 3.2.2).

Furthermore, lower bounds on the stop and sbottom masses disfavor a direct decay to those pairs ($H \rightarrow \tilde{t}\tilde{t}/\tilde{b}\tilde{b}$) or stops and sbottoms as an intermediate state. Due to strong constraints on the squark and slepton mass, only a minority of the parameter sets contain direct decays of heavy Higgs to light squarks and light sleptons leading to the signatures (jet),(jet) and (l),(l) (see section 5.3). Therefore, these signatures are dominant for large Higgs masses or due to the enhancement as a result of low $\tan\beta$ values. Nevertheless, the dilepton signature can be interesting, as additional contributions of H decaying into a chargino pair can result in the same signature and thus, the total signal is enhanced. There, the charginos decay to the LSP and an off-shell W boson each, where the leptonic decay of the latter leave each a single lepton in the detector.

The detailed physical process of those missing topologies is given in table 5.0.1. It should be noted, depending on the characteristics of the electroweakinos and thus the hierarchy of the soft parameters, the decay to two heavier states (e.g. $H \rightarrow \tilde{\chi}_3^0\tilde{\chi}_2^0$) can be preferred compared to e.g. $H \rightarrow \tilde{\chi}_3^0\tilde{\chi}_1^0$. Thus, in the table, the LSP can be replaced by any other light electroweakino, which then decays soft. Additionally, more complex decays have to be considered, as `SModelS` sums over all mother particles with the same final signature.

MSSM Higgs decaying to supersymmetric particles and possible mono- X signatures have been previously discussed in [1–3]. However, this study differs from the previous attempts, as it is a systematic and complete survey of all pMSSM Higgs productions and decay modes. Furthermore, it allowing for squarks and sleptons to be light. This is the result of the full 19-dimensional pMSSM parameter scan of this work.

5.1 Heavy Higgs Decays with Mono- X Signature

In this section, the mono- X signatures ($X = h, W, Z$) of heavy Higgs bosons are discussed in more detail, as they are the most interesting signatures for experimental analyses. Fig. 5.1.1 shows the production cross section of heavy Higgs bosons in proton-proton collisions decaying to a chargino or neutralino pair with mono- W signatures for higgsino-like LSPs (upper plots) calculated with `SusHi-1.6.1` [37, 38] and `SModelS-1.1.1` [49, 50, 52, 78–80]. It is given in the $\tilde{\chi}_2^\pm - \tilde{\chi}_1^\pm$ chargino mass plane, and in the $m_A - \tan\beta$ parameter plane, including cross sections up to $\mathcal{O}(10)$ fb for $\sqrt{s} = 14$ TeV. Future colliders, as e.g. the hadronic Future Circular Collider (FCC-hh) [44], are expected to have a center-of-mass energy of about $\sqrt{s} \approx 100$ TeV, leading to

Topology	Decay Processes	Information
(inv),(inv)	$H \rightarrow \tilde{\chi}_k^\pm \tilde{\chi}_l^\mp \rightarrow W_{\text{soft}}^* \tilde{\chi}_1^0 W_{\text{soft}}^* \tilde{\chi}_1^0$	$k, l \in \{1, 2\}$
	$H \rightarrow \tilde{\chi}_1^0 \tilde{\chi}_1^0$	$i, j \in \{1, 2, 3, 4\}$
	$H \rightarrow \tilde{\chi}_i^0 \tilde{\chi}_j^0 \rightarrow X_{\text{soft}}^* \tilde{\chi}_1^0 X_{\text{soft}}'^* \tilde{\chi}_1^0$	$X, X' \in \{Z, h\}$
(inv),(higgs)	$H \rightarrow \tilde{\chi}_1^0 \tilde{\chi}_j^0 \rightarrow \tilde{\chi}_1^0 h \tilde{\chi}_1^0$	$j \in \{2, 3, 4\}$
	$H \rightarrow \tilde{\chi}_1^\pm \tilde{\chi}_2^\mp \rightarrow W_{\text{soft}}^* \tilde{\chi}_1^0 h \tilde{\chi}_1^\mp \rightarrow W_{\text{soft}}^* \tilde{\chi}_1^0 Z W_{\text{soft}}^* \tilde{\chi}_1^0$	
(inv),(Z)	$H \rightarrow \tilde{\chi}_1^0 \tilde{\chi}_j^0 \rightarrow \tilde{\chi}_1^0 Z \tilde{\chi}_1^0$	$j \in \{2, 3, 4\}$
	$H \rightarrow \tilde{\chi}_1^\pm \tilde{\chi}_2^\mp \rightarrow W_{\text{soft}}^* \tilde{\chi}_1^0 Z \tilde{\chi}_1^\mp \rightarrow W_{\text{soft}}^* \tilde{\chi}_1^0 Z W_{\text{soft}}^* \tilde{\chi}_1^0$	
(inv),(W)	$H \rightarrow \tilde{\chi}_1^\pm \tilde{\chi}_2^\mp \rightarrow W_{\text{soft}}^* \tilde{\chi}_1^0 W \tilde{\chi}_1^0$	$j \in \{3, 4\}$
	$H \rightarrow \tilde{\chi}_1^0 \tilde{\chi}_j^0 \rightarrow \tilde{\chi}_1^0 W \tilde{\chi}_1^\pm \rightarrow \tilde{\chi}_1^0 W W_{\text{soft}}^* \tilde{\chi}_1^0$	
(inv),(jet,jet)	$H \rightarrow \tilde{\chi}_1^0 \tilde{\chi}_j^0 \rightarrow \tilde{\chi}_1^0 Z^* \tilde{\chi}_1^0$	$j \in \{2, 3, 4\}$
	$H \rightarrow \tilde{\chi}_1^\pm \tilde{\chi}_2^\mp \rightarrow W_{\text{soft}}^* \tilde{\chi}_1^0 W^* \tilde{\chi}_1^0$	
	$H \rightarrow \tilde{\chi}_1^\pm \tilde{\chi}_2^\mp \rightarrow W_{\text{soft}}^* \tilde{\chi}_1^0 Z^* \tilde{\chi}_1^\mp \rightarrow W_{\text{soft}}^* \tilde{\chi}_1^0 Z^* W_{\text{soft}}^* \tilde{\chi}_1^0$	
(W),(jet,jet)	$H \rightarrow \tilde{\chi}_1^\pm \tilde{\chi}_2^\mp \rightarrow W^* \tilde{\chi}_1^0 W \tilde{\chi}_1^0$	$i, j \in \{2, 3, 4\},$
	$H \rightarrow \tilde{\chi}_i^0 \tilde{\chi}_j^0 \rightarrow Z^* \tilde{\chi}_1^0 W \tilde{\chi}_1^\pm \rightarrow Z^* \tilde{\chi}_1^0 W W_{\text{soft}}^* \tilde{\chi}_1^0$	$i < j$
((Z),(jet, jet)),(jet,jet)	$H \rightarrow \tilde{\chi}_1^\pm \tilde{\chi}_2^\mp \rightarrow W^* \tilde{\chi}_1^0 Z \tilde{\chi}_1^\mp \rightarrow W^* \tilde{\chi}_1^0 Z W^* \tilde{\chi}_1^0$	$i, j, k \in \{2, 3, 4\},$
	$H \rightarrow \tilde{\chi}_i^0 \tilde{\chi}_j^0 \rightarrow Z^* \tilde{\chi}_1^0 Z \tilde{\chi}_k^0 \rightarrow Z^* \tilde{\chi}_1^0 Z Z^* \tilde{\chi}_1^0$	$i, k < j$
((W),(jet, jet)),(jet,jet)	$H \rightarrow \tilde{\chi}_1^\pm \tilde{\chi}_2^\mp \rightarrow W^* \tilde{\chi}_1^0 W \tilde{\chi}_j^0 \rightarrow W^* \tilde{\chi}_1^0 W Z^* \tilde{\chi}_1^0$	$i, j \in \{2, 3, 4\}, i < j$
	$H \rightarrow \tilde{\chi}_i^0 \tilde{\chi}_j^0 \rightarrow Z^* \tilde{\chi}_1^0 W \tilde{\chi}_k^\pm \rightarrow Z^* \tilde{\chi}_1^0 W W^* \tilde{\chi}_1^0$	$k \in \{1, 2\}$
(inv),((jet),(jet))	$H \rightarrow \tilde{\chi}_1^0 \tilde{\chi}_j^0 \rightarrow \tilde{\chi}_1^0 jet \tilde{q} \rightarrow \tilde{\chi}_1^0 jet jet \tilde{\chi}_1^0$	$j \in \{2, 3, 4\}$
	$H \rightarrow \tilde{\chi}_1^\pm \tilde{\chi}_2^\mp \rightarrow W_{\text{soft}}^* \tilde{\chi}_1^0 jet \tilde{q} \rightarrow W_{\text{soft}}^* \tilde{\chi}_1^0 jet jet \tilde{\chi}_1^0$	$\tilde{q} \in \{\tilde{u}, \tilde{d}, \tilde{c}, \tilde{s}\}_{L,R}$
(inv),(l),(l)	$H \rightarrow \tilde{\chi}_1^0 \tilde{\chi}_j^0 \rightarrow \tilde{\chi}_1^0 l \tilde{l} \rightarrow \tilde{\chi}_1^0 l l \tilde{\chi}_1^0$	$j \in \{2, 3, 4\}$
	$H \rightarrow \tilde{\chi}_1^\pm \tilde{\chi}_2^\mp \rightarrow W_{\text{soft}}^* \tilde{\chi}_1^0 l' \tilde{l} \rightarrow W_{\text{soft}}^* \tilde{\chi}_1^0 l' l \tilde{\chi}_1^0$	$\tilde{l} \in \{\tilde{e}, \tilde{\mu}\}_{L,R}$
	$H \rightarrow \tilde{\chi}_1^0 \tilde{\chi}_j^0 \rightarrow \tilde{\chi}_1^0 W^* \tilde{\chi}_1^\pm \rightarrow \tilde{\chi}_1^0 W^* W^* \tilde{\chi}_1^0$	$W^* \rightarrow l \nu_l$
(jet),(jet)	$H \rightarrow \tilde{q} \tilde{q} \rightarrow jet \tilde{\chi}_1^0 jet \tilde{\chi}_1^0$	$\tilde{q} \in \{\tilde{u}, \tilde{d}, \tilde{c}, \tilde{s}\}_{L,R}$
	$H \rightarrow \tilde{q} \tilde{q} \rightarrow jet \tilde{\chi}_k^\pm jet \tilde{\chi}_k^\pm \rightarrow jet W_{\text{soft}}^* \tilde{\chi}_1^0 jet W_{\text{soft}}^* \tilde{\chi}_1^0$	$k \in \{1, 2\}$
(l),(l)	$H \rightarrow \tilde{l} \tilde{l} \rightarrow l \tilde{\chi}_1^0 l \tilde{\chi}_1^0$	$\tilde{l} \in \{\tilde{e}, \tilde{\mu}\}_{L,R}$
	$H \rightarrow \tilde{l} \tilde{l} \rightarrow l \tilde{\chi}_k^\pm l \tilde{\chi}_k^\pm \rightarrow l W_{\text{soft}}^* \tilde{\chi}_1^0 l W_{\text{soft}}^* \tilde{\chi}_1^0$	$k \in \{1, 2\}$
	$H \rightarrow \tilde{\chi}_k^\pm \tilde{\chi}_k^\pm \rightarrow W^* \tilde{\chi}_1^0 W^* \tilde{\chi}_1^0$	$W^* \rightarrow l \nu_l$

Table 5.0.1: Missing topologies for heavy Higgs decays and their detailed decay process given by the `SModelS` output. The subscript ‘soft’ represents undetected soft decay products ($M_{\text{soft}} < 5$ GeV) and ‘*’ notes off-shell particles. The latter will be visible to the detector due to the dominant decays $W^*, Z^* \rightarrow jet jet$ and $Z^*, h^* \rightarrow b\bar{b}$. Electrons and muons are combined to light leptons (l), as well as gluons and light quarks (u, d, c, s) are combined to *jets* as mentioned in the text. It should be noted, that LSPs as decay product can be replaced by the process $\tilde{\chi} \rightarrow X_{\text{soft}}^* \tilde{\chi}_1^0$, where $\tilde{\chi}$ can be any neutralino or chargino and X_{soft}^* can be any non-colored state not visible to the detector.

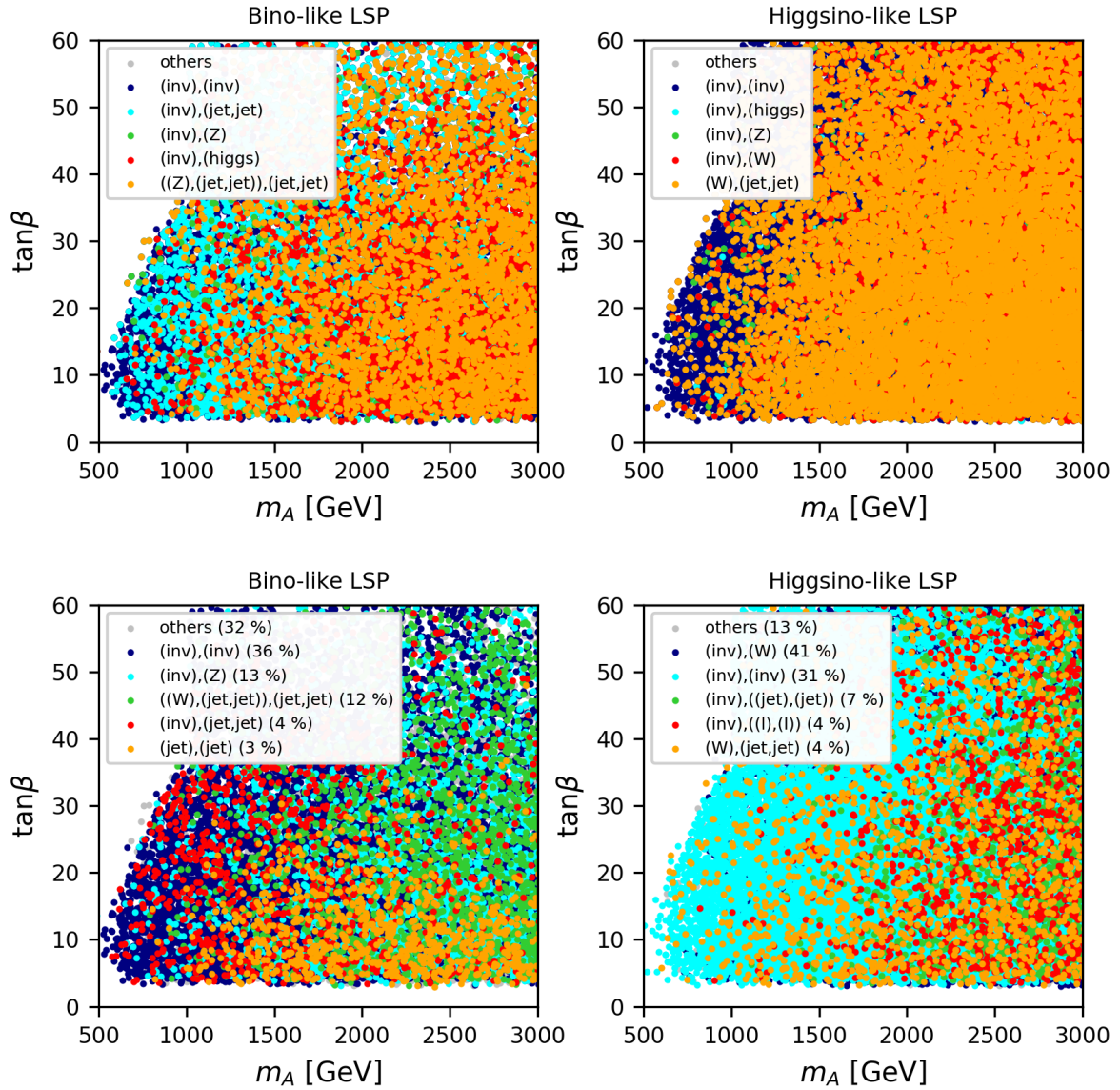


Figure 5.0.2: Most frequent occurring (upper plots) and most dominating (lower plots) missing topologies in the $m_A - \tan\beta$ parameter plane for bino-like LSPs (left) and higgsino-like LSPs (right).

an increase of the cross sections of more than one order of magnitude (see fig. 3.2.4, lower plots). Furthermore, the computed cross sections for mono- Z signatures for bino-like LSPs (lower plots) are given in the $\tilde{\chi}_3^0 - \tilde{\chi}_1^0$ neutralino mass plane and the $m_A - \tan\beta$ parameter plane, leading to similar results. The Feynman diagram presenting the processes of heavy Higgs decays resulting in mono- X signatures are shown in fig. 5.0.1. The plots for other mono- X topologies for both datasets are given in appendix B.1.

In each of the cases, a large cross section for the mono- X topology can be obtained for a light MSSM Higgs mass (here: $m_A \approx m_H$), it falls smoothly as the mass of the Higgs increases as expected. The nearly constant behavior of $\sigma \times \mathcal{B}$ with $\tan\beta$ is the result of a strongly decreasing branching ratio being compensated by an increasing total production cross section of the heavy Higgs boson as given in section 5.6.

It is interesting to note that the mass difference of the LSP and the next-to LSP (NLSP) or next-to-next-to LSP (NNLSP) can be large giving rise to potentially hard X in the final state. Mono- X signatures come most-likely with up to two b -jets as a result of the heavy Higgs production process, giving an additional handle on resonant heavy Higgs searches at the LHC (see section 5.1.2).

5.1.1 Study of the Parameter Dependence

The behavior of the cross sections for mono- X signatures are studied in dependence of the underlying soft parameters. Fig. 5.1.2, upper plots, show the production cross section of heavy Higgs bosons with mono- W signatures in the electroweakino soft parameter plane $M_1 - \mu$ (left) and $M_2 - \mu$ (right). For higgsino-like LSPs and thus, a low μ , large cross sections are found for low M_2 values. Therefore, the plots show a preferred coupling of heavy Higgs bosons to highly mixed higgsino-like and wino-like electroweakinos. Results with the highest cross sections are independent of the M_1 soft parameter and thus, no preferences for the bino-like component are obtained. Due to the low wino and higgsino mass parameters, a large coupling of the lightest electroweakinos to the W and Z bosons, thus mono- $W^{(*)}$ and mono- $Z^{(*)}$ signatures, is expected.

The lower plots visualize the production cross section of heavy Higgs bosons with mono- Z signatures in the $M_2 - M_1$ (left) and $\mu - M_1$ (right) soft parameter plane for bino-like LSPs. The highest cross sections are found for low values of μ and therefore a heavy Higgs decay to mixed bino- and higgsino-like states. Even though, decays to wino-/higgsino-mixed electroweakinos are preferred, the necessity of a large gaugino-higgsino mixing for heavy Higgs couplings leads to low values of μ for bino-like LSPs. Nevertheless, the wino-like $\tilde{\chi}_4^0$ and $\tilde{\chi}_2^\pm$ play a crucial role in the dominating signatures of heavy Higgs decays, as the decay into those particles has large branching ratios if kinematically allowed. This leads to either more complex signatures (e.g. ((Z/W),(jet,jet)),(jet,jet)) or potentially hard final state bosons.

The results for other signatures are given in appendix B.1.1. For the higgsino-like LSP dataset with mono- Z (upper plots) and mono- h (middle plots), the highest cross sections are again found for low values of M_2 and μ . The results for the bino-like LSP dataset with mono- h signature (lower plots) show large cross sections for low values of μ and M_1 .

Thus, a maximal signal at the LHC is found for Higgs decaying to highly mixed higgsino-gaugino states, independent of the decay mode. Decays to mixed states dominate over decays to pure higgsino-, bino-, or wino-like LSPs. Therefore, a future analysis of the wino-like LSP dataset with the next update of the `SModelS` framework is proposed. This update will be able to process long-lived particles, as they dominate in the wino-like LSP dataset (see table 4.4.5). Large cross

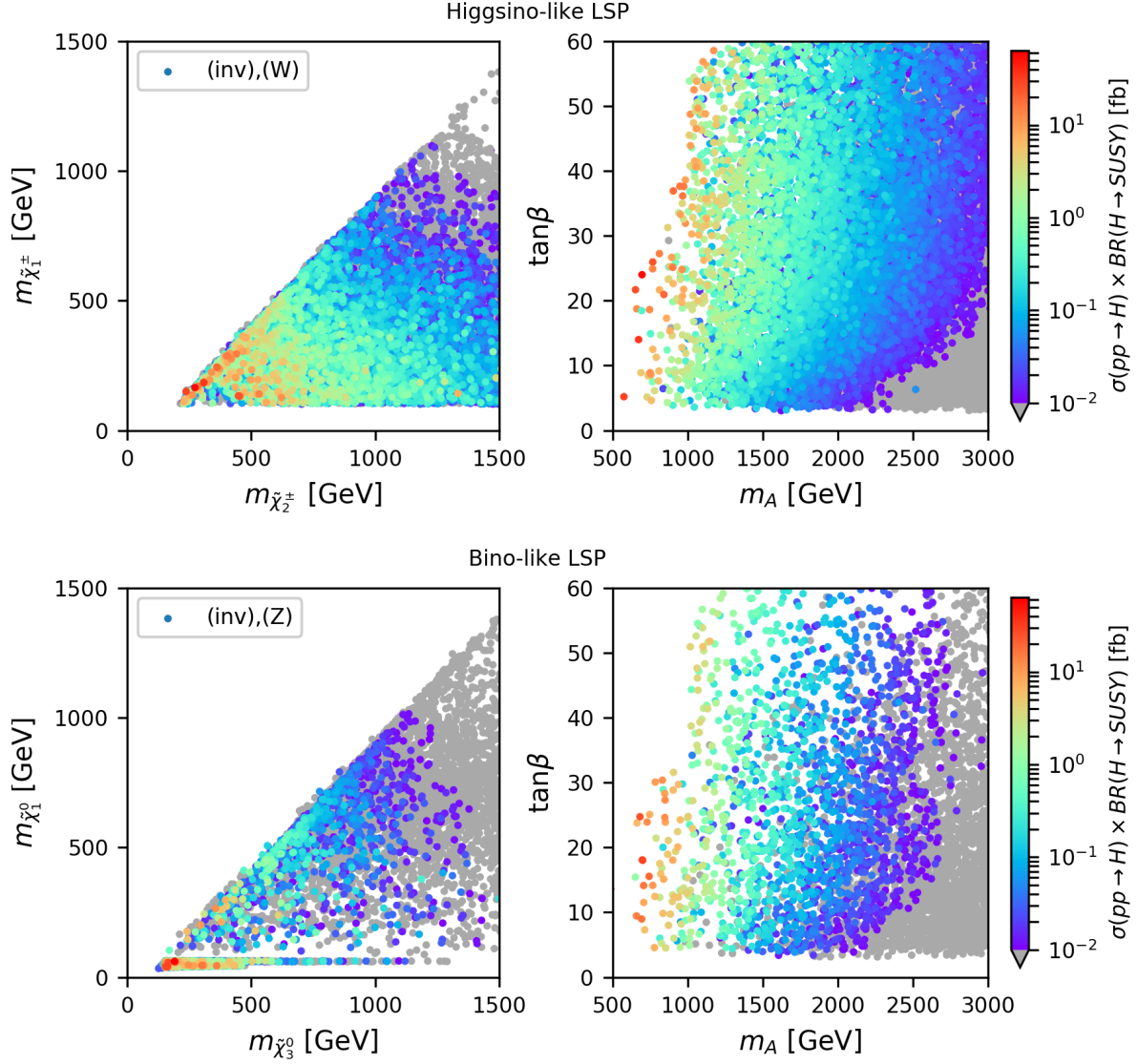


Figure 5.1.1: Cross sections for heavy Higgs searches with mono- W (upper plots) signature in the $\tilde{\chi}_2^\pm - \tilde{\chi}_1^\pm$ mass plane (left) and the $m_A - \tan\beta$ parameter plane (right) for higgsino-like LSPs, as well as with mono- Z (lower plots) signature in the $\tilde{\chi}_3^0 - \tilde{\chi}_1^0$ mass plane (left) and the $m_A - \tan\beta$ parameter plane (right) for bino-like LSPs.

sections for resonant heavy Higgs searches for low values of the higgsino mass-parameter μ are expected in this dataset (see section 5.7).

5.1.2 Study of the Production Process

In addition, the production channel of a heavy Higgs decaying with mono- X signatures are studied in this work. Fig. 5.1.3 show the ratio of the cross sections for the two production channels from proton-proton collisions, gluon fusion ggH and bottom quark annihilation bbH . The upper plots visualize the results for higgsino-like LSPs resulting in mono- W signatures. Since the gluon fusion process is only dominant for low $\tan\beta$ ($\lesssim 7$) given in green, mono- X signatures from heavy Higgs decays with large cross sections are mainly the result of H being produced in bottom quark annihilation processes (red). Thus, up to two additional b -jets in the detector are expected, giving an additional handle on the search for resonant heavy Higgs bosons at the LHC.

The bino-like LSP dataset with mono- Z signature (lower plots) show similar results. Bottom quark annihilation is the dominating production process of heavy Higgs bosons for about 98 % of the analyzed parameter space.

The outlier points with high $\tan\beta$ and a large cross section due to gluon fusion contain light bottom squarks (\tilde{b}_1, \tilde{b}_2). Therefore the domination gluon fusion production mechanism is the result of light sbottoms in the triangle-diagram with its contribution being enhanced by a large $\tan\beta$ value.

The results for other mono- X signatures are given in appendix B.1.2. Similar results are found for the higgsino-like LSP dataset with mono- Z (upper plots) and mono- h signature (middle plots) and for the bino-like LSP dataset with mono- h signature (lower plots). The Feynman diagram for those production processes are given in fig. 3.2.3.

5.2 Invisible Heavy Higgs Decays

For low masses of the Higgs bosons H , a decay to heavy SUSY particles can become kinematically forbidden. Thus, the only relevant decay products are two stable LSPs, where this process results in solely missing transverse momentum in the detector. In principle, this process is similar to the expected (reversed) thermal DM freeze-out mechanism in the early universe, where the LSP acts as a suitable dark matter candidate. There, the annihilation of SM particles to DM can work for a wide range of couplings and DM masses. Nevertheless, the assumption is made, that the DM particle interact sufficiently with SM particles.

Due to this link to the thermal freeze-out, the search for MET at the LHC becomes interesting. This work suggests the production of DM in SM annihilations to heavy Higgs bosons. However, to design a successful experimental search strategy, the production have to include at least one QCD jet resulting from initial state radiation. For heavy Higgs bosons produced in bottom quark annihilation processes, the additional production of up to two potentially hard b -jets can thus be used to trigger events with large missing transverse momentum.

Fig. 5.2.1 visualizes the calculated cross sections for heavy Higgs productions at 14 TeV center-of-mass energy times the branching ratio leading to these signatures. As seen, potentially large cross sections for fairly light Higgs bosons are found. The $\sigma \times \mathcal{B}$ values reduce drastically for increasing Higgs masses, as then other decay processes become dominant. The (inv),(inv) signature is the

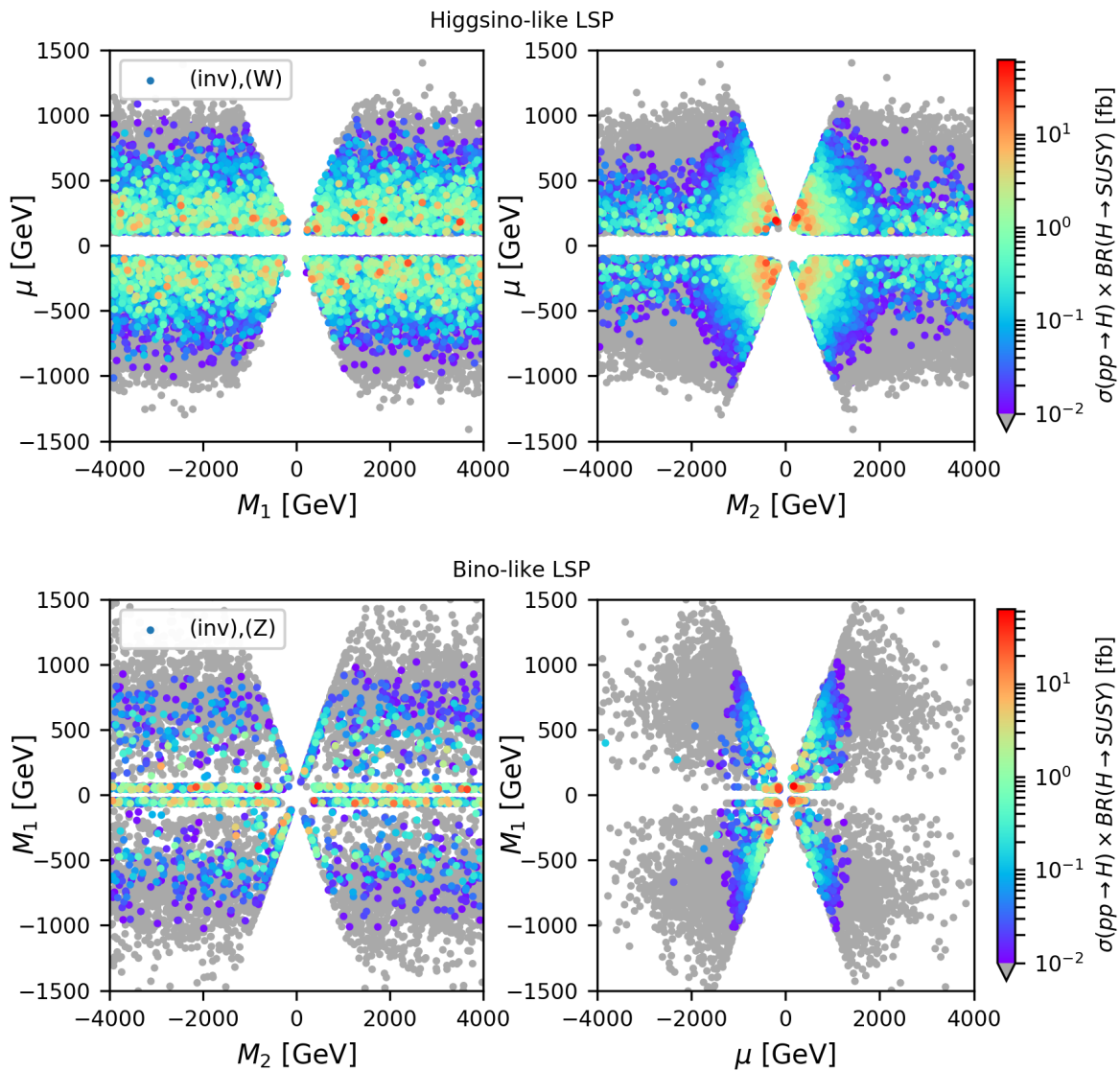


Figure 5.1.2: Cross sections for heavy Higgs searches with mono- W (upper plots) signature in the $M_1 - \mu$ (left) and the $M_2 - \mu$ soft parameter plane (right) for higgsino-like LSPs, as well as with mono- Z (lower plots) signature in the $M_2 - M_1$ (left) and the $\mu - M_1$ soft parameter plane (right) for bino-like LSPs.

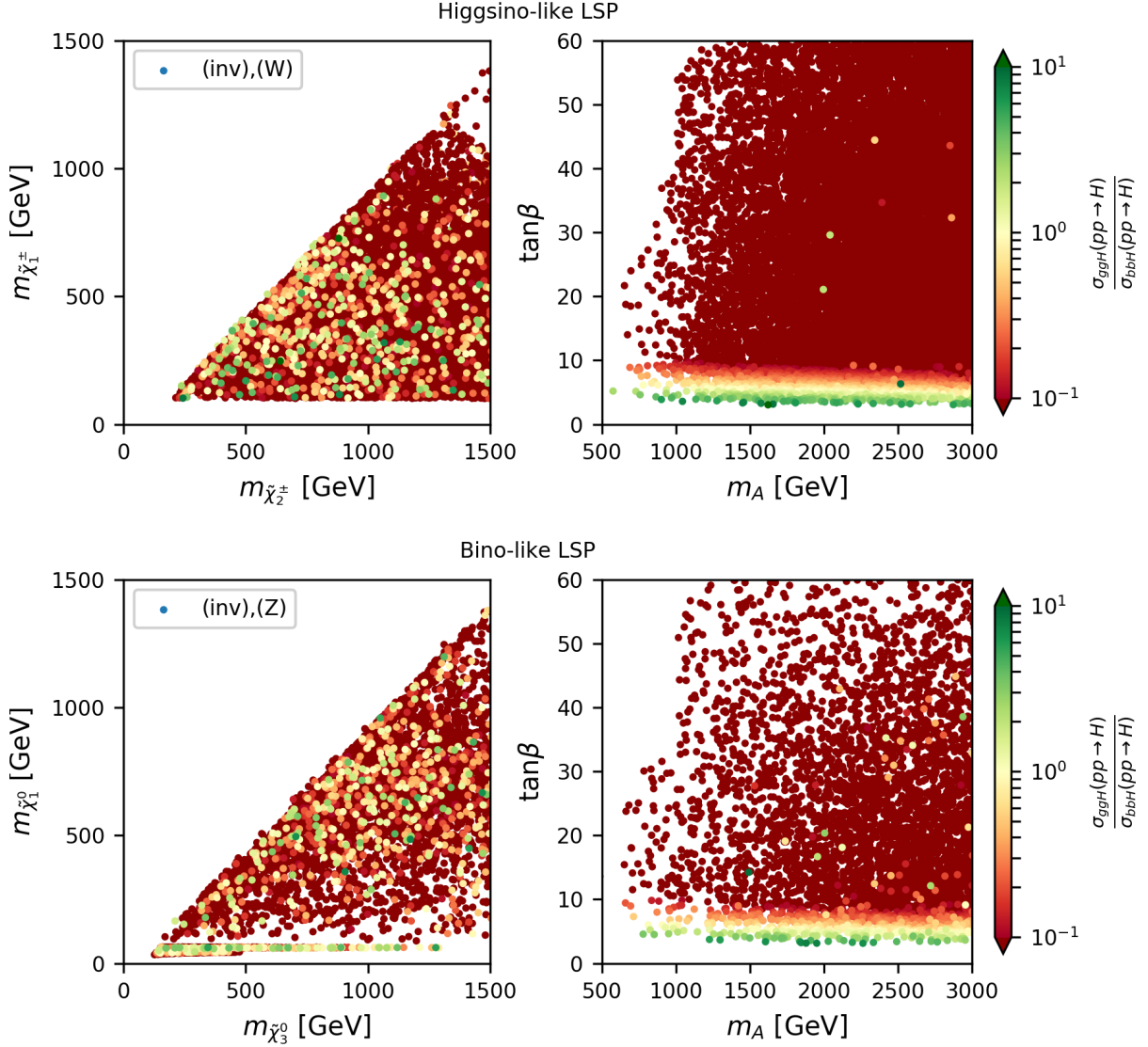


Figure 5.1.3: Fraction of gluon-fusion (σ_{ggH}) to bottom quark annihilation (σ_{bbH}) cross sections for heavy Higgs production with mono- W (upper plots) signature in the $\tilde{\chi}_2^\pm - \tilde{\chi}_1^\pm$ mass plane (left) and the $m_A - \tan\beta$ parameter plane (right) for higgsino-like LSPs, as well as with mono- Z (lower plots) signature in the $\tilde{\chi}_3^0 - \tilde{\chi}_1^0$ mass plane (left) and the $m_A - \tan\beta$ parameter plane (right) for bino-like LSPs.

dominating process, having the highest cross section, for the majority of the bino-like LSP dataset and a significant amount of the higgsino-like LSP dataset (see fig. 5.0.2, lower plots).

5.3 Heavy Higgs Decays with Dijet and Dilepton Signature

Even though, the coupling of heavy Higgs bosons to 3rd generation sfermions is preferred, strong lower limits on squark masses disfavor a decay to those sparticles. They are kinematically forbidden for regions in the parameter space, where large production cross sections of H are expected. However, the initial decay of H to a pair of light squarks $\left(\tilde{q} \in \left\{\tilde{u}, \tilde{d}, \tilde{c}, \tilde{s}\right\}_{L,R}\right)$ or light sleptons $\left(\tilde{l} \in \left\{\tilde{e}, \tilde{\mu}\right\}_{L,R}\right)$ can be interesting, as it leaves dilepton or dijet signatures in the detector. Fig. 5.3.1 shows the $\sigma \times \mathcal{B}$ values for heavy Higgs bosons decaying to squarks for bino-like LSPs in the $\tilde{q} - \tilde{\chi}_1^0$ and the $m_A - \tan \beta$ plane. As seen, a dijet signature in the detector can have potentially large cross sections in a very limited parameter space. Future results on direct SUSY searches and their limits on the mass of light squarks are able to probe the parameter space resulting in this signature.

The results with dilepton signature and results for higgsino-like LSPs with dijet and dilepton signature are less promising and are given in appendix B.2. Here, the strong dependence on $\tan \beta$ is visible. As given in section 3.2.2, the pMSSM coupling of H to 1st and 2nd generation squarks can be reduced to the diagonal terms of $C_{H\tilde{q}\tilde{q}}$, as the decoupling regime leads to a negligible $\sin \alpha$ and the mass of the SM quarks is low. Thus, the light squark coupling strongly depends on $\cos \beta$ and is therefore enhanced for low values of $\tan \beta$.

However, only a limited number of parameter sets contain light squarks and light sleptons and are thus kinematically reachable for Higgs decaying to those particles. Nevertheless, additional contributions of H decaying into a chargino pair can result in the same signature and thus, the total $\sigma \times \mathcal{B}$ value is enhanced for the dilepton signature. There, the charginos decay to the LSP and an off-shell W boson each, where the leptonic decay of the latter leave each a single lepton in the detector.

5.4 Long-Cascade Decays

Additionally, the SModelS framework is used to classify complex long-cascade decays, with more than one intermediate sparticle per branch (see section 4.2.4). These signatures are the result of heavy Higgs bosons decaying to heavy electroweakino states. For the latter, decays to intermediate sparticle states become then kinematically allowed.

Fig. 5.4.1 shows the ratio of the cross section to long-cascade decays $\sigma(pp \rightarrow H \rightarrow \text{long cascade})$ to the total cross section of heavy Higgs productions in proton-proton collisions $\sigma(pp \rightarrow H)$ in the $m_A - \tan \beta$ parameter plane. Long-cascade decays are negligible in regions of the $m_A - \tan \beta$ parameter plane where large production cross sections are expected. Thus, simple decay processes with e.g. mono- X signatures in the detector are dominating the heavy Higgs boson decay to sparticles.

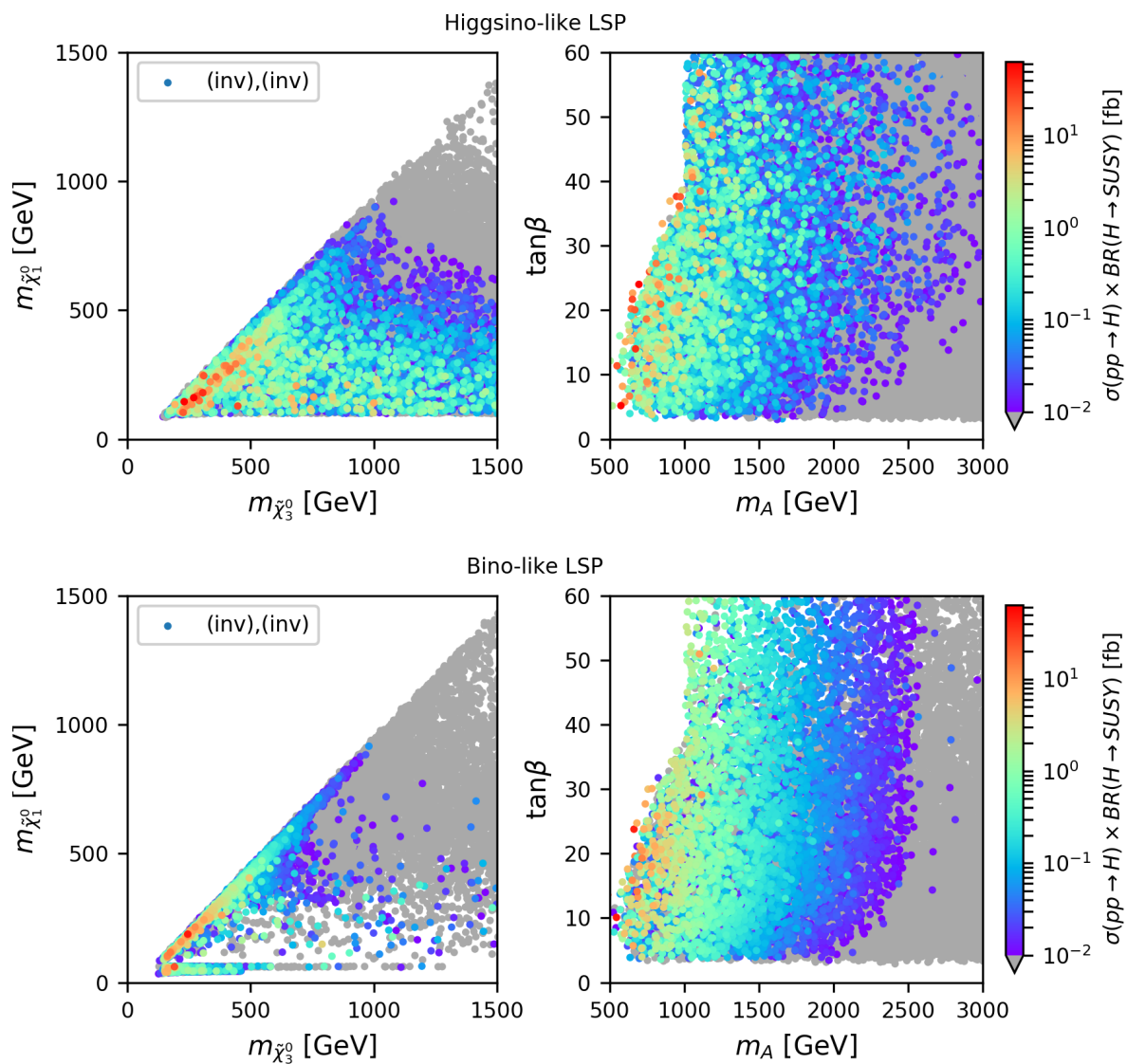


Figure 5.2.1: Cross sections of invisible heavy Higgs decays in the $\tilde{\chi}_3^0 - \tilde{\chi}_1^0$ mass plane (left) and the $m_A - \tan\beta$ parameter plane (right) for higgsino-like (upper plots) and bino-like LSPs (lower plots).

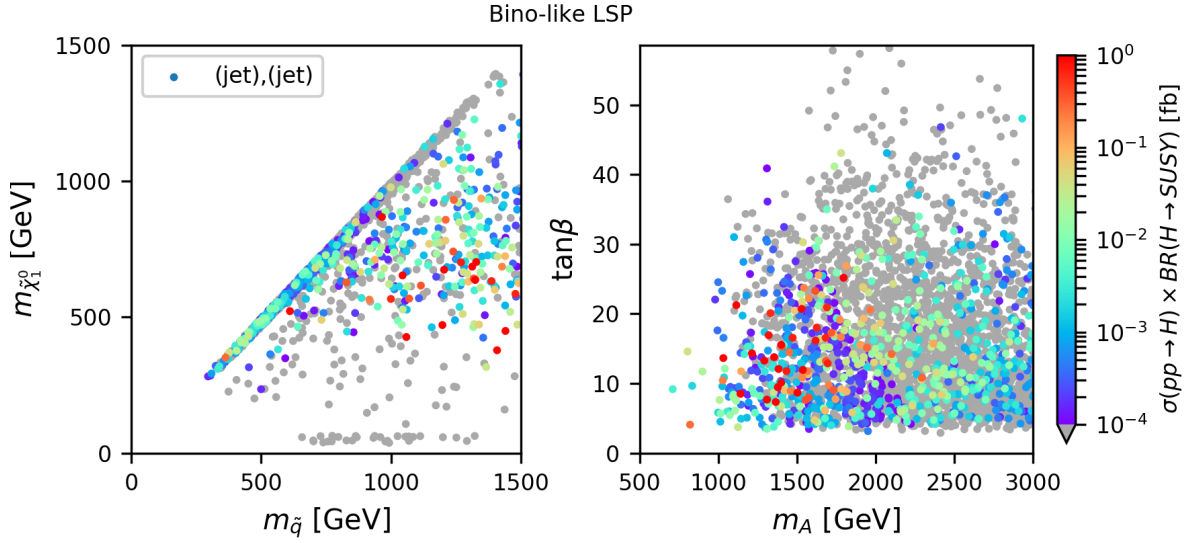


Figure 5.3.1: Cross sections for heavy Higgs searches with dijet signature in the $\tilde{q} - \tilde{\chi}_1^0$ mass plane (left) and the $m_A - \tan\beta$ parameter plane (right) for bino-like LSPs.

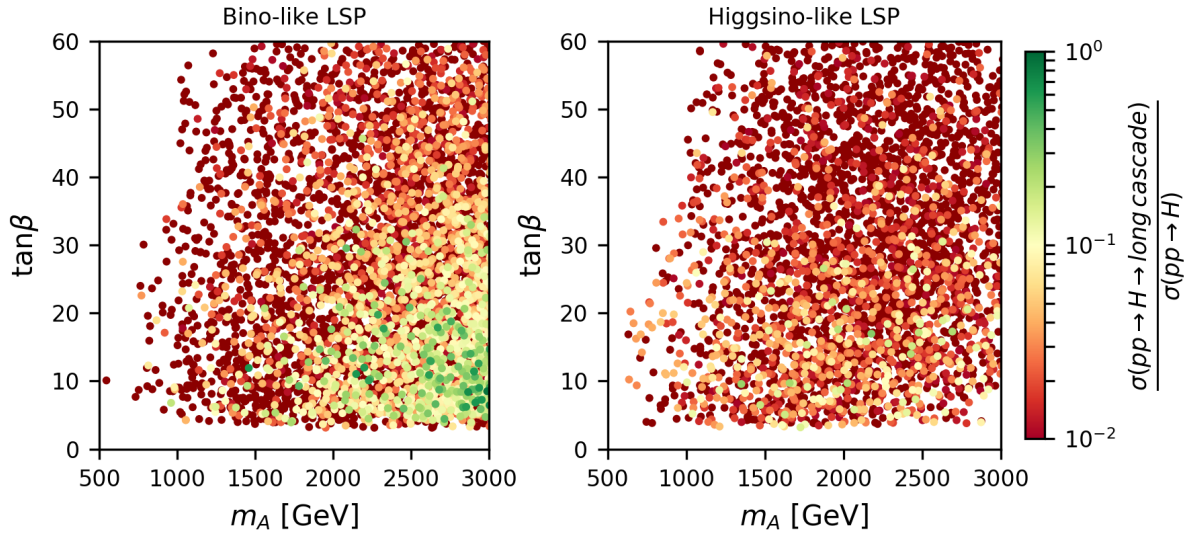


Figure 5.4.1: Ratio of the cross section to long-cascade decays $\sigma(pp \rightarrow H \rightarrow long\ cascade)$ to the total cross section $\sigma(pp \rightarrow H)$ in the $m_A - \tan\beta$ parameter plane for bino-like LSPs (left) and higgsino-like LSPs (right).

5.5 Constraints from LHC Direct SUSY Searches

The previous analyses used `SModelS` with a reduced database. It is thus able to classify all possible heavy Higgs boson decays without considering current SUSY analyses at the LHC. To apply constraints from CMS and ATLAS searches, the SLHA files are tested against the most updated simplified model limits from 8 TeV LHC direct SUSY searches using the full `SModelS` database. Two analyses from CMS [81] and ATLAS [82] are able to exclude about 3.67 % (1.27 %) of the remaining SLHA files for the higgsino-like (bino-like) LSP dataset, with the excluded points given in fig. 5.5.1, upper (lower) plots. The low number of excluded files is expected, as constraints from 22 distinct ATLAS analyses [67] are already applied to the initial dataset (see section 4.4). Excluded SLHA files are therefore not included in this analysis.

It should be noted, that the exclusion due to the ATLAS constraints arise from a preliminary conference note, not their follow-up final publication. The latter applies weaker constraints on the parameter space. It is expected, that this is the result of the changed number of signal regions in the final publication.

Studies of the pMSSM parameter set with hadronic 13 TeV LHC Run 2 ATLAS constraints from early direct SUSY searches with 3.2 fb^{-1} integrated luminosity exclude additionally 13.8 % (18.4 %) of the higgsino-like (bino-like) LSP dataset [83, 84]. The excluded points are shown in fig. 5.5.2 in the $m_A - \tan\beta$ parameter plane for higgsino-like LSPs (upper plots) on top (left) and below (right) the valid parameter sets. Similar results are found for the bino-like LSP dataset (lower plots). The excluded SLHA files have no influence on the most frequent and most dominant missing topologies given in fig. 5.0.2 and are not able to exclude a certain region of the $m_A - \tan\beta$ parameter plane.

5.6 Complementarity with Direct Heavy Higgs Searches

Current analyses of heavy Higgs boson decays assume a decay to SM particles. Previous works already showed a potentially high branching ratio of H to supersymmetric particles for low $\tan\beta$ values [1]. A study of the branching ratio of H to all SUSY particles for the full 19-dimensional MSSM parameter space of the ATLAS pMSSM dataset shows similar results. Fig. 5.6.1, upper plots, show a peak branching ratio of about $\mathcal{B}(H \rightarrow SUSY SUSY) \approx 60\%$ for low $\tan\beta$ values. Therefore, a solely analysis of $H \rightarrow SM SM$ is insufficient for certain regions of the parameter space.

As a result of this work, analyses taking decays to sparticles into account are proposed to probe the full pMSSM parameter space.

For low $\tan\beta$, the contribution of decays to squarks is enhanced. However, the main contribution comes from decays to electroweakinos, where the $\tan\beta$ dependence is highly non-trivial.

The branching ratio value is decreasing to about 10% for high $\tan\beta$ being nearly independent on m_A . However, the approximately constant $\sigma \times \mathcal{B}$ in dependence of $\tan\beta$ (see fig. 5.1.1) is the result of increasing heavy Higgs production cross sections (see fig. 5.6.1, lower plots) for regions with decreasing branching ratios. This is the result of increasing couplings of heavy Higgs bosons to down-type quarks and bottom quark annihilations becoming the dominant production process.

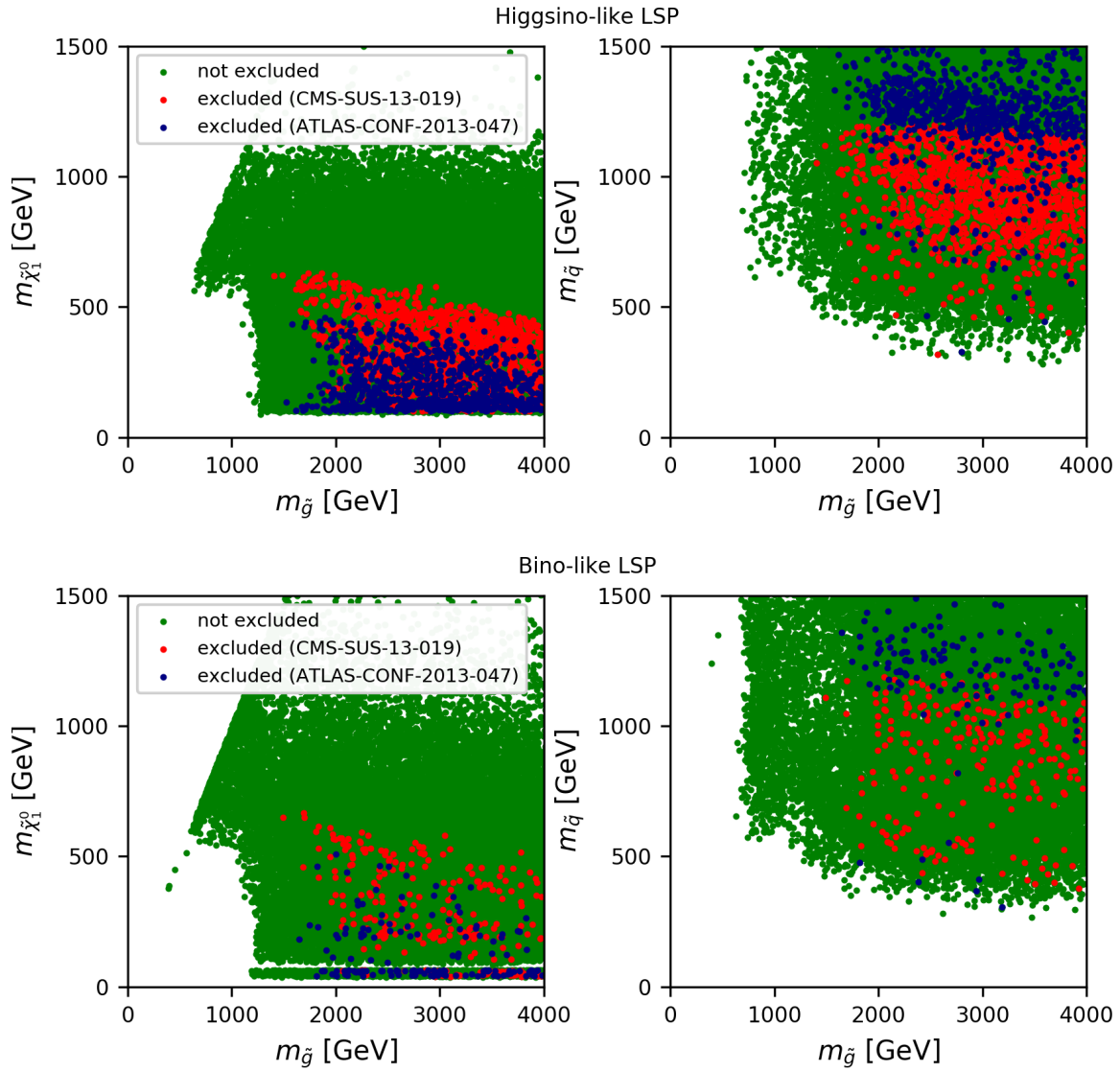


Figure 5.5.1: Parameter sets excluded by 8 TeV LHC Run 1 SUSY searches performed in the $\tilde{g} - \tilde{\chi}_1^0$ (left) and the $\tilde{g} - \tilde{q}$ (right) mass plane for higgsino-like (upper plots) and bino-like (lower plots) LSPs, where \tilde{q} is the lightest squark.

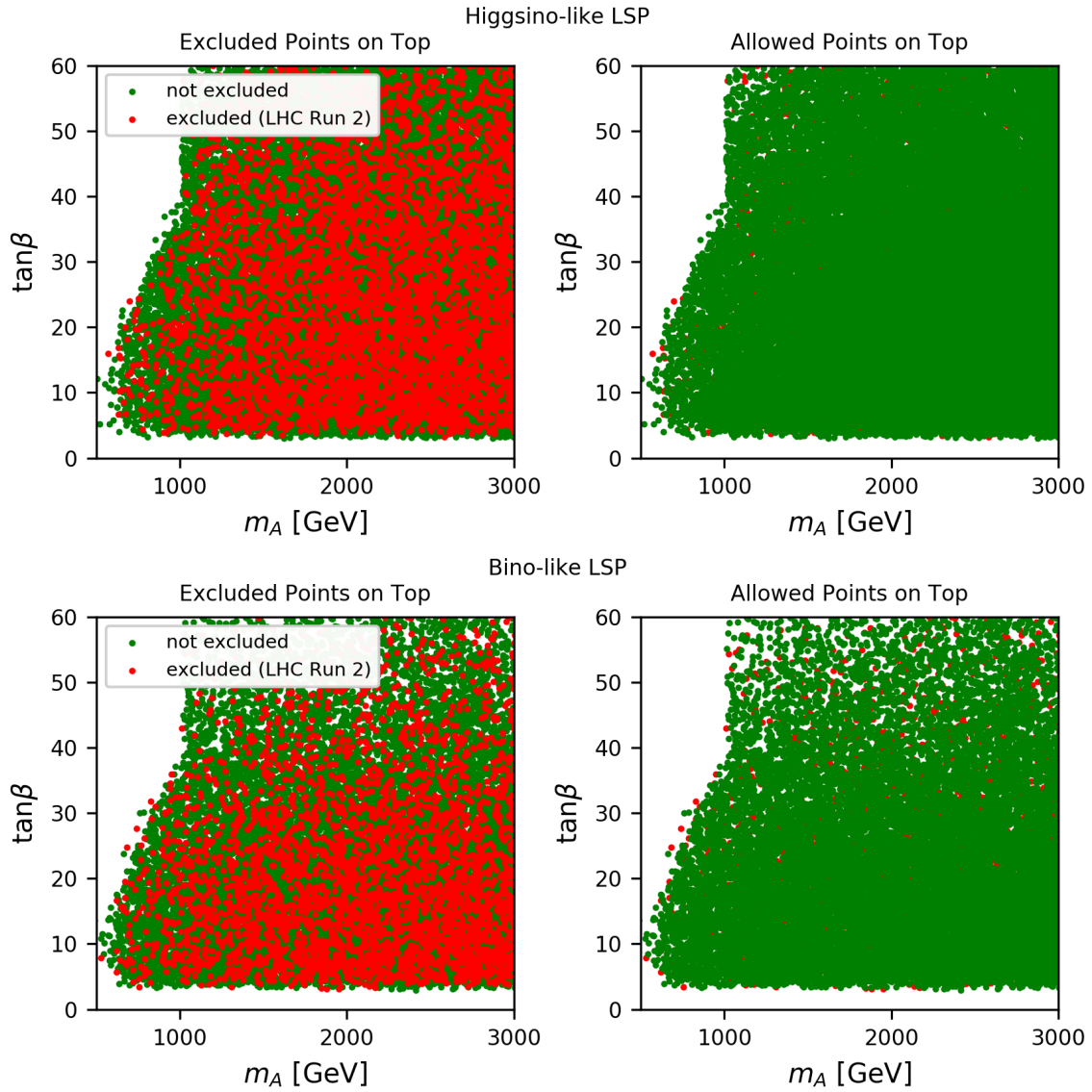


Figure 5.5.2: Parameter sets excluded by 13 TeV LHC Run 2 SUSY searches performed by [83, 84] in the $m_A - \tan\beta$ parameter plane for higgsino-like (upper plots) and bino-like (lower plots) LSPs. The left plot shows the excluded sets on top, the right plot below the valid parameter sets.

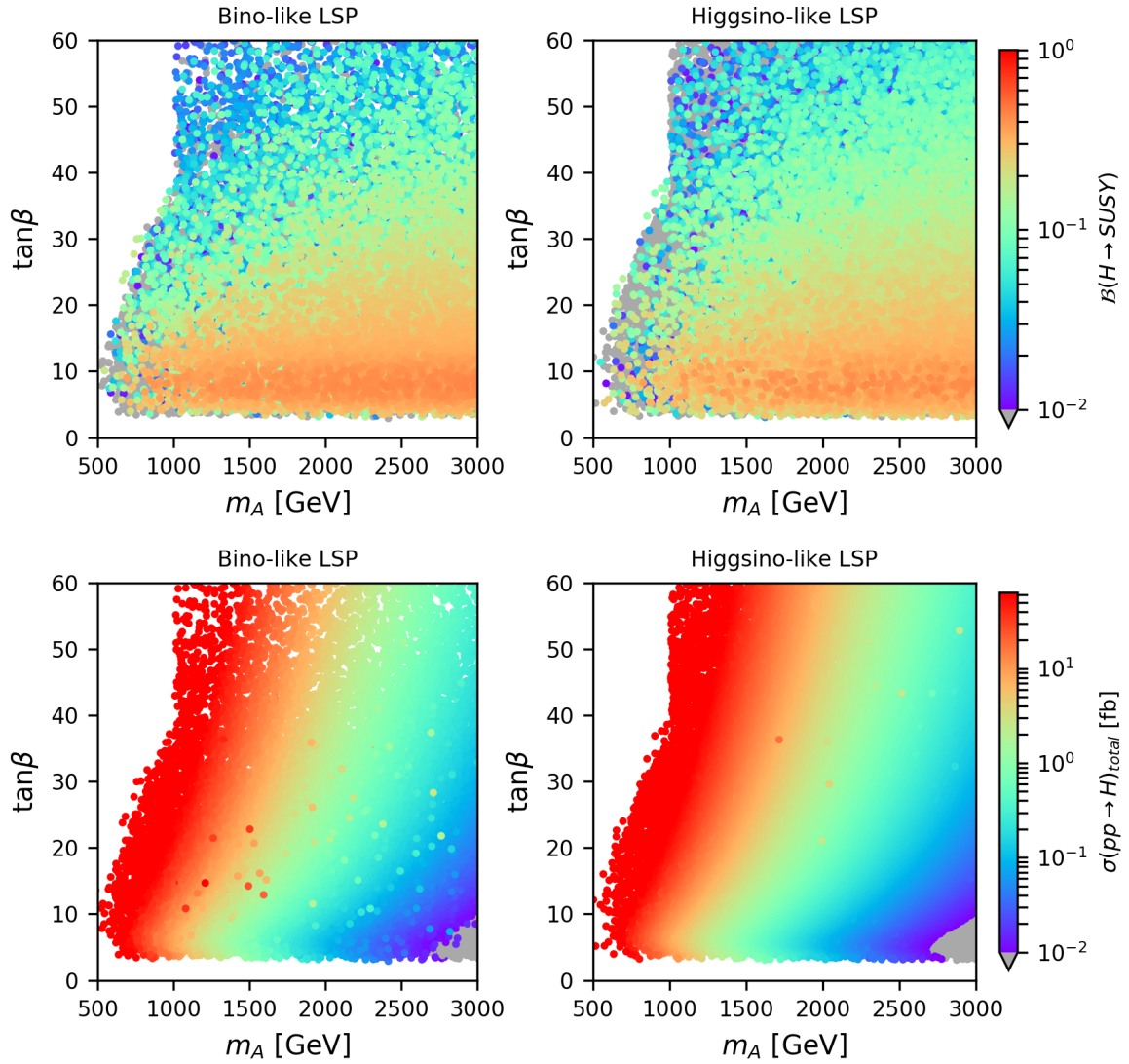


Figure 5.6.1: Branching ratio of heavy Higgs bosons decaying to SUSY particles (upper plots) and the total cross section of heavy Higgs boson production in the $m_A - \tan\beta$ parameter plane for bino-like LSPs (left) and higgsino-like LSPs (right).

5.7 Results for Wino-like LSPs

The small mass difference of the LSP to the light chargino $\tilde{\chi}_1^\pm$ leads to a long lifetime of the latter and therefore displaced vertex signatures in the detector. As the current version of **SModelS** cannot handle displaced vertices, the wino-like LSP dataset was not included in the previous study. The cross sections in dependence of the lifetime $c\tau$ and the light chargino (heavy Higgs) mass of heavy Higgs bosons decaying to a pair of charginos including the long-lived light chargino ($H \rightarrow \tilde{\chi}_1^\pm \tilde{\chi}_i^\mp$, $i \in \{1, 2\}$) for wino-like LSPs is given in fig. 5.7.1, left (right). Promising results with cross sections up to 50 fb for $\sqrt{s} = 14$ TeV are found, as a highly mixed higgsino-/wino-like LSP state is preferred for heavy Higgs decays (see section 5.1.1).

Thus, resonant heavy Higgs searches for wino-like LSPs with displaced vertex signatures are a potentially good candidate for future long-lived sparticle searches at the LHC. It should be noted, that constraints from the light and heavy Higgs sector have not been applied to the wino-like LSP dataset.

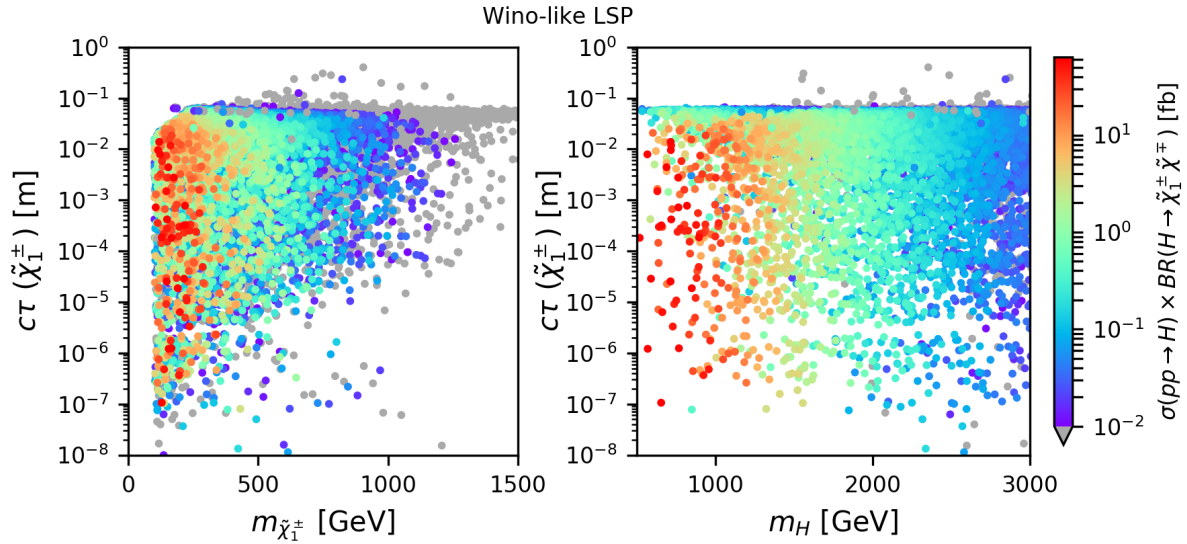


Figure 5.7.1: Cross sections for heavy Higgs bosons decaying to charginos ($H \rightarrow \tilde{\chi}_1^\pm \tilde{\chi}_i^\mp$, $i \in \{1, 2\}$) in dependence of the light chargino lifetime $c\tau(\tilde{\chi}_1^\pm)$ and its mass (left) and the heavy Higgs mass (right) for wino-like LSPs.

6 Conclusion

The discovery of the Higgs boson at the LHC in 2012 has been a remarkable success for the Standard Model of Particle Physics. Nevertheless, it is incomplete, as e.g. it is only able to describe about 4.9 % of the energy density in the universe. One possibility of physics beyond the SM is the introduction of supersymmetry. It tackles a number of issues arising within the SM by introducing superpartner particles in addition to the SM particle content. Due to the high number of free parameters within the Minimal Supersymmetric Standard Model, it is difficult to make predictions within the model. By applying basic assumptions, this number can be reduced to 19 free parameters, being called the phenomenological Supersymmetric Standard Model.

Supersymmetric models contain two Higgs doublets, leading to the existence of three neutral and a pair of charged Higgs bosons. While the light CP-even neutral Higgs is held as the SM Higgs boson with a mass of $m_h \approx 125$ GeV [11], the others are approximately degenerate in mass for the decoupling regime. The search for heavy Higgs bosons is therefore an important step to probe the full parameter space of MSSM.

For this analysis, a pre-collected data sample of a full 19-dimensional flat prior parameter scan is used. The dataset is categorized into higgsino-like, bino-like and wino-like LSP sets, according to the characteristics of the lightest neutralino. It already applies constraints from the dark matter relic density, LEP and ATLAS searches for SUSY particles, and requires the light Higgs to be within a certain mass range. Furthermore, constraints from the Higgs and the flavor sector are applied by using the frameworks `HiggsBounds`, `HiggsSignals` and `SuperIso`.

The `SModelS` framework is applied to analyze the remaining parameter sets and characterize possible signatures resulting from heavy Higgs bosons decaying to supersymmetric particles. `SModelS` is able to decompose a given input spectra into simplified models, which are then matched with results from direct SUSY searches of the CMS and ATLAS experiment at the LHC. Furthermore, it detects missing topologies, which have not been considered by experimental searches yet. A reduced database of the `SModelS` framework is used to identify all possible heavy Higgs decays within the missing topology block. Since it is not able to handle resonant searches, a unique method of using the framework is proposed. By providing the calculated product of the production cross section, computed with `SusHi`, and the branching ratio of the decay to SUSY particles $\sigma(pp \rightarrow H) \times \mathcal{B}(H \rightarrow SUSY SUSY)$ in the input-file, it is possible to apply `SModelS` for resonant heavy Higgs searches.

The analyzed datasets for higgsino-like and bino-like LSPs show mono- X ($X = h, W, Z$) signatures being the most frequent occurring and most dominating topologies in resonant heavy Higgs searches. These signatures are the result of the asymmetric decay of H to a pair of neutralinos or charginos, where the lighter state decays soft to the LSP ($\Delta m < 5$ GeV) and the heavier state decays to the LSP and X . The calculated production cross section resulting in those signatures revealed values up to $\mathcal{O}(10)$ fb for a center-of-mass energy of $\sqrt{s} = 14$ TeV. For bino-like LSPs, the lightest chargino being higgsino-like suppresses a decay to W bosons. Thus, mono- W signatures, where the main underlying process is a heavy Higgs boson decaying to a pair of charginos, are not found in the most frequent and most dominating missing topology block for the bino-like LSP dataset.

In any case, large cross sections are obtained for a light MSSM Higgs mass. Furthermore, a detailed study of their underlying parameter sets showed large cross sections for highly mixed electroweakino states, preferring mixed higgsino-/wino-like LSPs. Mono- X signatures will have additional b -jets in the detector as a result of bottom quark annihilation being the dominant heavy Higgs production process for about 98 % of the analyzed pMSSM parameter space. Since cross sections with long-cascade decay signatures are negligible, the decay of heavy Higgs bosons to sparticles will dominantly result in simple topologies.

Furthermore, constraints on sparticle masses from hadronic LHC Run 1 analyses are applied to the dataset. Especially two analyses are able to exclude approximately 3.67 % (1.27 %) of the parameter sets for higgsino-like (bino-like) LSPs. Studies, performed in Ref. [83] and [84] used early results from LHC Run 2, with 3.2 fb^{-1} integrated luminosity to additionally constrain the pMSSM dataset. By applying this study, it was possible to show the additional exclusion of 13.8 % (18.4 %) of the remaining higgsino-like (bino-like) LSP dataset. However, these constraints resulting from hadronic SUSY searches are not able to exclude a certain region of the pMSSM parameter space.

Since the branching ratio of heavy Higgs bosons to supersymmetric particles can be up to 60 % for low $\tan\beta$ values, the solely consideration of direct Higgs search analyses, where the heavy Higgs decays to SM particles, is insufficient to probe the full pMSSM parameter space. Thus, e.g. resonant heavy Higgs searches with a decay to SUSY particles are crucial for future analyses.

As a preferred decay of the heavy Higgs boson to highly mixed higgsino-/wino-like LSPs is found, large cross sections are expected for the signatures of the analyzed wino-like LSP dataset. However, the small mass difference of the LSP to the light chargino $\tilde{\chi}_1^\pm$ results in displaced vertex signatures not able to be handled by `SModelS` yet. A brief analysis showed expected $\sigma(pp \rightarrow H) \times \mathcal{B}(H \rightarrow \tilde{\chi}^\pm \tilde{\chi}^\mp)$ values for decays to a pair of charginos of up to 50 fb for a center-of-mass energy of $\sqrt{s} = 14 \text{ TeV}$.

Even though, the production process of heavy Higgs boson in proton-proton collisions, as well as its decay to supersymmetric particles is highly dependent on the underlying parameters of the 19-dimensional pMSSM parameter space, the process mainly results in simple signatures, as e.g. mono- X ($X = h, W, Z$). This study showed large cross sections for those topologies being reachable for the future LHC update. The high-luminosity LHC, with a total of 3 ab^{-1} integrated luminosity will therefore be able to probe the pMSSM parameter space by searching for heavy Higgs bosons decaying to sparticles. For future colliders with a center-of-mass energy of about $\sqrt{s} \approx 100 \text{ TeV}$, an increase of the cross sections of more than one order of magnitude is expected.

Thus, a re-interpretation of current mono- X analyses for dark matter searches is proposed. Furthermore, the search for heavy Higgs bosons decaying to wino-like LSPs is a promising candidate for future displaced vertex analyses.

A Detailed Calculations

The detailed calculations performed within the scope of this work are given in the following in addition to the theoretical background of section 3. It includes the diagonalization of the chargino mass matrix and the computation of their mixing angles (see section A.1), the calculation of the production cross section for heavy Higgs bosons from gluon fusion processes with a top quark triangle (see section A.2) and the minimization of the superpotential to retrieve the parameter conditions leading to soft symmetry breaking (see section A.3).

A.1 The Diagonalization of the Chargino Mass Matrix

The diagonalization of chargino mass matrix \mathcal{M}_C (see eq. 3.2.2) is an important step to derive the chargino masses. Here, a detailed calculation of the chargino mixing angles ϕ_u and ϕ_v (see eq. 3.2.19) is performed according to Ref. [35]. The diagonalization of the neutralino mixing matrix \mathcal{Z} was obtained numerically.

The chargino masses are derived from the diagonalization of the chargino mass matrix

$$\mathcal{M}_C = \begin{pmatrix} M_2 & \sqrt{2}m_W s_\beta \\ \sqrt{2}m_W c_\beta & \mu \end{pmatrix}$$

by using the 2×2 unitary mixing matrices \mathcal{U} and \mathcal{V}

$$\begin{aligned} \mathcal{M}_C^D &= \mathcal{U}^* \mathcal{M}_C \mathcal{V}^{-1} \\ (\mathcal{M}_C^D)^2 &= \mathcal{U}^* \mathcal{M}_C \mathcal{M}_C^\dagger (\mathcal{U}^*)^{-1} = \mathcal{V} \mathcal{M}_C^\dagger \mathcal{M}_C \mathcal{V}^{-1} \end{aligned}$$

and the rotation matrix $O_{u,v}$

$$\begin{aligned} \mathcal{U} &= O_u \\ \mathcal{V} &= \begin{cases} O_v & \text{for } \det(\mathcal{M}_C) > 0 \\ \sigma_3 O_v & \text{for } \det(\mathcal{M}_C) < 0 \end{cases} \\ O_{u,v} &= \begin{pmatrix} c_{\phi_{u,v}} & s_{\phi_{u,v}} \\ -s_{\phi_{u,v}} & c_{\phi_{u,v}} \end{pmatrix} \end{aligned}$$

where $s_{\phi_{u,v}} \equiv \sin \phi_{u,v}$ and $c_{\phi_{u,v}} \equiv \cos \phi_{u,v}$. For the case $\det(\mathcal{M}_C) > 0$, the masses of the charginos are derived with

$$\begin{aligned} (\mathcal{M}_C^D)^2 &= O_v \mathcal{M}_C^\dagger \mathcal{M}_C O_v^{-1} = \\ &= \begin{pmatrix} c_{\phi_{u,v}} & s_{\phi_{u,v}} \\ -s_{\phi_{u,v}} & c_{\phi_{u,v}} \end{pmatrix} \begin{pmatrix} M_2 & \sqrt{2}m_W c_\beta \\ \sqrt{2}m_W s_\beta & \mu \end{pmatrix} \begin{pmatrix} M_2 & \sqrt{2}m_W s_\beta \\ \sqrt{2}m_W c_\beta & \mu \end{pmatrix} \begin{pmatrix} c_{\phi_{u,v}} & -s_{\phi_{u,v}} \\ s_{\phi_{u,v}} & c_{\phi_{u,v}} \end{pmatrix} = \\ &= \begin{pmatrix} Ac_{\phi_v}^2 + 2BCs_{\phi_v}c_{\phi_v} + Ds_{\phi_v}^2 & BC(c_{\phi_v}^2 - s_{\phi_v}^2) + (D-A)s_{\phi_v}c_{\phi_v} \\ BC(c_{\phi_v}^2 - s_{\phi_v}^2) + (D-A)s_{\phi_v}c_{\phi_v} & As_{\phi_v}^2 - 2BCs_{\phi_v}c_{\phi_v} + Dc_{\phi_v}^2 \end{pmatrix} \stackrel{!}{=} \begin{pmatrix} m_{\tilde{\chi}_i^\pm}^2 & 0 \\ 0 & m_{\tilde{\chi}_j^\pm}^2 \end{pmatrix} \end{aligned}$$

where $i, j \in \{1, 2\}$ and the substitutions

$$\begin{aligned} A &= M_2^2 + 2m_W^2 c_\beta^2 \\ B &= \sqrt{2}m_W \\ C &= M_2 s_\beta + \mu c_\beta \\ D &= 2m_W^2 s_\beta^2 + \mu^2. \end{aligned}$$

are used. The comparison of the results leads to the conditions

$$\begin{aligned} m_{\tilde{\chi}_i^\pm}^2 &= A c_{\phi_v}^2 + 2BC s_{\phi_v} c_{\phi_v} + D s_{\phi_v}^2 \\ m_{\tilde{\chi}_j^\pm}^2 &= A s_{\phi_v}^2 - 2BC s_{\phi_v} c_{\phi_v} + D c_{\phi_v}^2 \\ 0 &= BC(c_{\phi_v}^2 - s_{\phi_v}^2) + (D - A)s_{\phi_v} c_{\phi_v} \end{aligned}$$

where from the latter, the mixing angles are derived using $t_{\phi_v} \equiv \tan \phi_v$.

$$\begin{aligned} BC(c_{\phi_v}^2 - s_{\phi_v}^2) &= (A - D)s_{\phi_v} c_{\phi_v} \\ BCc_{\phi_v}^2(1 - t_{\phi_v}^2) &= (A - D)c_{\phi_v}^2 t_{\phi_v} \\ t_{2\phi_v} &= \frac{2t_{\phi_v}}{1 - t_{\phi_v}^2} = \frac{2BC}{A - D} \\ &= \frac{2\sqrt{2}m_W (M_2 s_\beta + \mu c_\beta)}{M_2^2 - \mu^2 + 2m_W^2 \underbrace{(c_\beta^2 - s_\beta^2)}_{2c_{2\beta}}} \end{aligned}$$

The calculation is similar for deriving the mixing angle ϕ_u . The final result is thus given by

$$\begin{aligned} \tan 2\phi_u &= \frac{2\sqrt{2}m_W (\mu \sin \beta + M_2 \cos \beta)}{M_2^2 - \mu^2 - 2m_W^2 \cos 2\beta} \\ \tan 2\phi_v &= \frac{2\sqrt{2}m_W (\mu \cos \beta + M_2 \sin \beta)}{M_2^2 - \mu^2 + 2m_W^2 \cos 2\beta} \end{aligned}$$

A.2 The Calculation of Gluon Fusion Processes

The production cross section of CP-even neutral heavy Higgs bosons is calculated on leading order for the gluon fusion processes visualized in fig. A.2.1. Only the top quark contribution with its mass $m_t = m$ and SM processes are taken into account. This calculation is done using Feynman rules and Feynman parameters according to Ref. [24, 41].

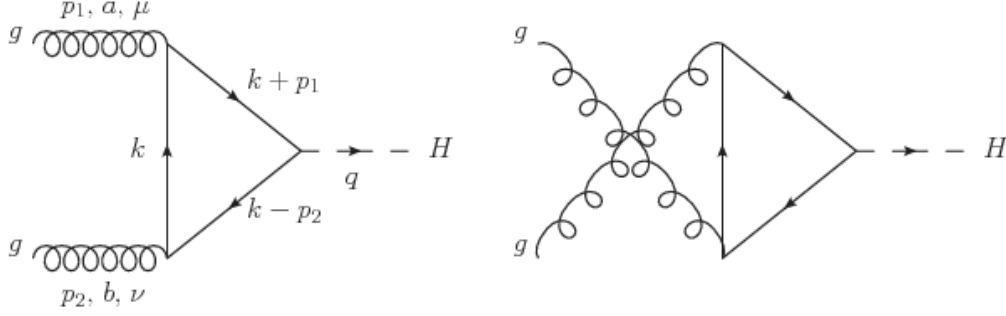


Figure A.2.1: The two Feynman diagrams for heavy Higgs production in gluon fusion processes at leading order with equal contributions. The figures were created using Jaxodraw-2.1 [4].

The Feynman rules for each propagator given in fig. A.2.1 are

Description	Factor
External gluon	$\epsilon_\mu(p)$
External scalar	1
Fermion loop	-1
Fermion propagator	$\frac{i(\not{p}+m)}{p^2-m^2+i\epsilon}$
Quark-gluon vertex	$ig\gamma^\mu t^a$
Yukawa vertex	$-i\lambda$

Table A.2.1: Feynman rules for the calculation of the cross section in gluon fusion processes.

where $t^a = \frac{1}{2}\lambda^a$ and λ^a are the Gell-Mann matrices [85]. The amplitude of the vertex is therefore

$$\begin{aligned}
 i\mathcal{M} = & \underbrace{-}_{\text{fermion loop}} \underbrace{2}_{\text{both diag.}} \int \frac{d^4k}{(2\pi)^4} \underbrace{1}_{\text{ext. scalar}} \underbrace{(-i\lambda)}_{\text{Yukawa vertex}} \underbrace{\frac{i(\not{k} + \not{p}_1 + m)}{(k+p_1)^2 - m^2 + i\epsilon}}_{\text{fermion prop.}} \underbrace{(ig_1\gamma^\mu t^a)}_{\text{vertex}} \\
 & \underbrace{\frac{i(\not{k} + m)}{k^2 - m^2 + i\epsilon}}_{\text{fermion prop.}} \underbrace{(ig_2\gamma^\nu t^b)}_{\text{vertex}} \underbrace{\frac{i(\not{k} - \not{p}_2 + m)}{(k-p_2)^2 - m^2 + i\epsilon}}_{\text{fermion prop.}} \underbrace{\epsilon_\mu(p_1)}_{\text{ext. gluon}} \underbrace{\epsilon_\mu(p_2)}_{\text{ext. gluon}} .
 \end{aligned}$$

The fermion triangle is a closed loop with no free Dirac indices. Therefore, taking the trace of

the amplitude simplifies the calculation of the amplitude to

$$i\mathcal{M} = -2\lambda g_1 g_2 \epsilon_\mu \epsilon_\nu t^a t^b \int \frac{d^4 k}{(2\pi)^4} \text{Tr} \left\{ \underbrace{\frac{i(\not{k} + \not{p}_1 + m)}{(k + p_1)^2 - m^2 + i\epsilon}}_A \gamma^\mu \underbrace{\frac{i(\not{k} + m)}{k^2 - m^2 + i\epsilon}}_B \gamma^\nu \underbrace{\frac{i(\not{k} - \not{p}_2 + m)}{(k - p_2)^2 - m^2 + i\epsilon}}_C \right\}$$

with A , B and C being Feynman parameters for the denominator of the fractions. By using the rules for Feynman parameters according to Ref. [24], the denominator of $i\mathcal{M}$ is calculated with

$$\begin{aligned} \frac{1}{ABC} &= \int_0^1 dx dy dz \delta(x + y + z - 1) \frac{2!}{(xA + yB + zC)^3} \\ &= \int_0^1 dx dy dz \delta(x + y + z - 1) \frac{2}{D^3} \\ D &= xA + yB + zC = \\ &= x(k + p_1)^2 + yk^2 + z(k - p_2)^2 - m^2(x + y + z) + i\epsilon(x + y + z) = \\ &= k^2 - m^2 + i\epsilon + xp_1^2 + zp_2^2 + 2xkp_1 - 2zkp_2 = \\ &= k^2 + 2k(xp_1 - zp_2) - m^2 + i\epsilon = \\ &= l^2 - \Delta + i\epsilon \end{aligned}$$

where $x + y + z = 1$ and massless gluons ($p_1^2 = p_2^2 = 0$) are assumed. In the last step, the momentum k is shifted to $l = k + xp_1 - zp_2$. The substitution $\Delta = m^2 - 2xzp_1p_2 = m^2 - xzm_H^2$ can be interpreted as an effective fermion loop, where $2p_1p_2$ is the Higgs boson mass squared m_H^2 . Since there is no y dependence ($D = D(x, z)$), the initial integral can be written as

$$\int_0^1 dx dy dz \delta(x + y + z - 1) \frac{2}{D^3(x, z)} = \int_0^1 dx \int_0^{1-x} dz \frac{2}{D^3(x, z)}$$

The fact that the trace of an odd number of Dirac matrices vanishes reduces the numerator of $i\mathcal{M}$. Furthermore, the expressions $\not{k} = \not{l} - x\not{p}_1 + z\not{p}_2$ and the γ -matrix anti-commutation relation $\not{p}\gamma^\mu = 2p^\mu - \gamma^\mu\not{p}$ are inserted. In addition, the gluon polarization being transverse to the momentum ($\epsilon(p_i)p_i = 0$) is used. Since the equation now depends on the magnitude of l , it can be shown that odd powers of l vanish (see Ref. [24]).

$$\begin{aligned} \int \frac{d^4 l}{(2\pi)^4} \frac{l^\mu}{D^3} &= 0 \\ \int \frac{d^4 l}{(2\pi)^4} \frac{l^\mu l^\nu}{D^3} &= \int \frac{d^4 l}{(2\pi)^4} \frac{\frac{1}{4}g^{\mu\nu} l^2}{D^3} \end{aligned}$$

Therefore, the numerator can be written as

$$\begin{aligned}
& Tr \left\{ (\not{k} + \not{p}_1 + m)\gamma^\mu(\not{k} + m)\gamma^\nu(\not{k} - \not{p}_2 + m) \right\} = \\
& = m Tr \left\{ \gamma^\mu \not{k} \gamma^\nu \not{k} + \not{p}_1 \gamma^\mu \not{k} \gamma^\nu + \gamma^\mu \not{k} \gamma^\nu \not{p}_2 - \gamma^\mu \not{k} \gamma^\nu \not{p}_2 + \not{k} \gamma^\mu \gamma^\nu \not{k} - \right. \\
& \quad \left. - \not{k} \gamma^\mu \gamma^\nu \not{p}_2 + \not{p}_1 \gamma^\mu \gamma^\nu \not{k} - \not{p}_1 \gamma^\mu \gamma^\nu \not{p}_2 + m^2 \gamma^\mu \gamma^\nu \right\} \\
& = m Tr \left\{ \gamma^\mu (\not{l} - x\not{p}_1 + z\not{p}_2) \gamma^\nu (\not{l} - x\not{p}_1 + z\not{p}_2) + \not{p}_1 \gamma^\mu (\not{l} - x\not{p}_1 + z\not{p}_2) \gamma^\nu + \right. \\
& \quad + \gamma^\mu (\not{l} - x\not{p}_1 + z\not{p}_2) \gamma^\nu (\not{l} - x\not{p}_1 + z\not{p}_2) - \gamma^\mu (\not{l} - x\not{p}_1 + z\not{p}_2) \gamma^\nu \not{p}_2 + \\
& \quad + (\not{l} - x\not{p}_1 + z\not{p}_2) \gamma^\mu \gamma^\nu (\not{l} - x\not{p}_1 + z\not{p}_2) - (\not{l} - x\not{p}_1 + z\not{p}_2) \gamma^\mu \gamma^\nu \not{p}_2 + \\
& \quad \left. + \not{p}_1 \gamma^\mu \gamma^\nu (\not{l} - x\not{p}_1 + z\not{p}_2) - \not{p}_1 \gamma^\mu \gamma^\nu \not{p}_2 + m^2 \gamma^\mu \gamma^\nu \right\} \\
& = m Tr \left\{ l_\sigma l_\rho (\gamma^\sigma \gamma^\mu \gamma^\rho \gamma^\nu + \gamma^\sigma \gamma^\mu \gamma^\nu \gamma^\rho + \gamma^\mu \gamma^\sigma \gamma^\nu \gamma^\rho) + p_{1,\alpha} p_{2,\beta} \left(z\gamma^\alpha \gamma^\mu \gamma^\beta \gamma^\nu + \right. \right. \\
& \quad + x\gamma^\mu \gamma^\alpha \gamma^\nu \gamma^\beta - xz(\gamma^\alpha \gamma^\mu \gamma^\beta \gamma^\nu + \gamma^\beta \gamma^\mu \gamma^\alpha \gamma^\nu + \gamma^\alpha \gamma^\mu \gamma^\nu \gamma^\beta + \gamma^\beta \gamma^\mu \gamma^\nu \gamma^\alpha + \\
& \quad \left. \left. + \gamma^\mu \gamma^\alpha \gamma^\nu \gamma^\beta + \gamma^\mu \gamma^\beta \gamma^\nu \gamma^\alpha) - (1 - z - x)\gamma^\alpha \gamma^\mu \gamma^\nu \gamma^\beta \right) + m^2 \gamma^\mu \gamma^\nu \right\}
\end{aligned}$$

where the fact that the trace of any product of an odd number of γ^μ vanishes is adopted. By using the γ -matrix identities

$$\begin{aligned}
\gamma^\mu \gamma_\mu &= 4 \mathbb{1}_{4 \times 4} \\
\gamma^\mu \gamma^\nu \gamma_\mu &= -2\gamma^\nu \\
Tr(\gamma^\mu) &= Tr(\gamma^\mu \gamma^\nu \gamma^\rho) = 0 \\
Tr(\gamma^\mu \gamma^\nu \gamma^\rho \gamma^\sigma) &= 4(g^{\mu\nu} g^{\rho\sigma} - g^{\mu\rho} g^{\nu\sigma} + g^{\mu\sigma} g^{\nu\rho})
\end{aligned}$$

the numerator results in

$$4m \left[4l^\mu l^\nu - l^2 g^{\mu\nu} + (4xz - 1)p_1^\nu p_2^\mu + \left(\frac{1}{2} - xz \right) m_H^2 g^{\mu\nu} + m^2 g^{\mu\nu} \right].$$

The amplitude, with k being shifted and the integrals being separated into a term proportional to l^2/D^3 and a term proportional to $1/D^3$, can then be written as

$$\begin{aligned}
i\mathcal{M} &= -8m\lambda g_1 g_2 \epsilon_\mu \epsilon_\nu t^a t^b \int \frac{d^4 l}{(2\pi)^4} \int_0^1 dx \int_0^{1-x} dz \left[g^{\mu\nu} \int \frac{d^d l}{(2\pi)^d} \frac{l^2}{(l^2 - \Delta + i\epsilon)^3} \frac{4-d}{d} - \right. \\
& \quad \left. - \left((4xz - 1)p_1^\nu p_2^\mu + \left(\frac{1}{2} - xz \right) m_H^2 g^{\mu\nu} + m^2 g^{\mu\nu} \right) \int \frac{d^4 l}{(2\pi)^4} \frac{1}{(l^2 - \Delta + i\epsilon)^3} \right]
\end{aligned}$$

where the first integral was shifted from $\int d^4 l/(2\pi)^4$ to the more general $\int d^d l/(2\pi)^d$ with the dimension d and a diverging limit for $d \rightarrow 4$. Due to this diverging limit, no Wick rotation can be inserted here [24]. The solution to the integrals can be found in tables and leads to the result

$$\begin{aligned}
\int \frac{d^4 l}{(2\pi)^4} \frac{1}{(l^2 - \Delta + i\epsilon)^3} &= \frac{-i}{32\pi^2 \Delta} \\
\int \frac{d^d l}{(2\pi)^d} \frac{l^2}{(l^2 - \Delta)^3} &= \frac{i}{(4\pi)^{\frac{d}{2}}} \frac{d}{2} \frac{\Gamma(2 - \frac{d}{2})}{\Gamma(3)} \left(\frac{1}{\Delta} \right)^{2 - \frac{d}{2}}
\end{aligned}$$

where the latter is divergent for $d \rightarrow 4$ [41]. This divergence is avoided by using $\epsilon = 4 - d$ and expanding the Γ -function and the factor $(1/\Delta)$ to

$$\begin{aligned}\Gamma\left(\frac{\epsilon}{2}\right) &= \frac{2}{\epsilon} - \gamma + \mathcal{O}(\epsilon) \\ \left(\frac{1}{\Delta}\right)^\epsilon &= \left(\frac{1}{\Delta}\right)^0 + \left(\frac{1}{\Delta}\right)^0 \log\left(\frac{1}{\Delta}\right) \epsilon + \mathcal{O}(\epsilon^2) = 1 - \epsilon \log \Delta + \mathcal{O}(\epsilon^2)\end{aligned}$$

where the Euler-Mascheroni constant $\gamma \approx 0.577$ [86] is used. The integral then simplifies to

$$\int \frac{d^d l}{(2\pi)^d} \frac{l^2}{(l^2 - \Delta)^3} \frac{4-d}{d} = \frac{i}{(4\pi)^{\frac{d}{2}}} \frac{d}{4} \overbrace{\left(\frac{2}{\epsilon} - \gamma\right)}^{\Gamma\left(\frac{\epsilon}{2}\right)} \overbrace{\left(1 - \epsilon \log \Delta\right)}^{\left(\frac{1}{\Delta}\right)^\epsilon} \frac{\epsilon}{d} + \mathcal{O}(\epsilon) = \frac{i}{32\pi^2} + \mathcal{O}(\epsilon).$$

The term in the remaining integral with its polarization pre-factors $\epsilon_\mu \epsilon_\nu$ in the limit $\epsilon \rightarrow 0$ is then

$$\begin{aligned}\epsilon_\mu \epsilon_\nu g^{\mu\nu} &\int \frac{d^d l}{(2\pi)^d} \frac{l^2}{(l^2 - \Delta + i\epsilon)^3} \frac{4-d}{d} - \\ &- \epsilon_\mu \epsilon_\nu \left((4xz - 1) p_1^\nu p_2^\mu + \left(\frac{1}{2} - xz\right) m_H^2 g^{\mu\nu} + m^2 g^{\mu\nu} \right) \int \frac{d^4 l}{(2\pi)^4} \frac{1}{(l^2 - \Delta + i\epsilon)^3} = \\ &= \frac{i\epsilon_1 \epsilon_2}{32\pi^2} - \left((4xz - 1)(p_1 \epsilon_2)(p_2 \epsilon_1) + \left(\frac{1}{2} - xz\right) m_H^2 \epsilon_1 \epsilon_2 - m^2 \epsilon_1 \epsilon_2 \right) \frac{-i}{32\pi^2 \Delta} = \\ &= \frac{i}{32\pi^2} \left(\epsilon_1 \epsilon_2 + \frac{(4xz - 1)(p_1 \epsilon_2)(p_2 \epsilon_1) + \left(\frac{1}{2} - xz\right) m_H^2 \epsilon_1 \epsilon_2 - m^2 \epsilon_1 \epsilon_2}{m^2 - xz m_H^2} \right) = \\ &= \frac{i}{32\pi^2} \frac{(4xz - 1)(p_1 \epsilon_2)(p_2 \epsilon_1) + (m^2 - xz m_H^2) \epsilon_1 \epsilon_2 + \left(\frac{1}{2} - xz\right) m_H^2 \epsilon_1 \epsilon_2 - m^2 \epsilon_1 \epsilon_2}{m^2 - xz m_H^2} = \\ &= \frac{i}{32\pi^2} \frac{(4xz - 1)(p_1 \epsilon_2)(p_2 \epsilon_1) + (-2xz + \frac{1}{2}) m_H^2 \epsilon_1 \epsilon_2}{m^2 - xz m_H^2} = \\ &= \frac{i}{32\pi^2} \frac{4xz - 1}{m^2 - xz m_H^2} \left((p_1 \epsilon_2)(p_2 \epsilon_1) - \frac{m_H^2}{2} \epsilon_1 \epsilon_2 \right) = \\ &= \frac{i}{32\pi^2} \frac{1 - 4xz}{\tau - 4xz} \frac{\tau}{m^2} \left(\frac{m_H^2}{2} \epsilon_1 \epsilon_2 - (p_1 \epsilon_2)(p_2 \epsilon_1) \right) =\end{aligned}$$

where $\Delta = m^2 - xz m_H^2$ and $\tau = 4m^2/m_H^2$. The total amplitude is then given by

$$i\mathcal{M} = \frac{-i\lambda g_1 g_2 t^{ab} \tau}{4\pi^2} \frac{\tau}{m} \left(\frac{m_H^2}{2} \epsilon_1 \epsilon_2 - (p_1 \epsilon_2)(p_2 \epsilon_1) \right) \int_0^1 dx \int_0^{1-x} dz \frac{1 - 4xz}{\tau - 4xz}$$

For the integration of the Feynman parameters x and z , $\tau > 4xz$ is used to calculate the gluon fusion process with an on-shell top quark loop. The solution to the integrals can be found in

tables [41].

$$\begin{aligned} \int_0^{1-x} dz \frac{1-4xz}{\tau-4xz} &= \frac{\tau-1}{4x} \log \left(1 - \frac{4x(1-x)}{\tau} \right) + x - 1 \\ \frac{\tau-1}{4} \int_0^1 dx \frac{1}{x} \log \left(1 - \frac{4x(1-x)}{\tau} \right) &= \frac{\tau-1}{2} \arcsin^2 \sqrt{\frac{1}{\tau}} \\ \int_0^1 x - 1 &= -\frac{1}{2} \end{aligned}$$

This leads to the final result for the amplitude

$$i\mathcal{M} = \frac{\alpha_S \delta_{ab}}{4\pi\nu_{\text{SM}}} \left(\frac{m_H^2}{2} \epsilon_1 \epsilon_2 - (p_1 \epsilon_2)(p_2 \epsilon_1) \right) \tau \left(1 + (1-\tau) \arcsin^2 \sqrt{\frac{1}{\tau}} \right)$$

where the Yukawa coupling $\lambda = -im/\nu_{\text{SM}}$, $\nu_{\text{SM}} \approx 246$ GeV [11], equal couplings $g_1 = g_2 = g$, the strong coupling constant $\alpha_S = g^2/4\pi$ and the sum over color charges $t^a t^b \rightarrow \text{Tr}(t^a t^b) = \delta_{ab}/2$ are taken into account.

The cross section can then be retrieved from the amplitude-squared $|\mathcal{M}|^2$ using Fermi's Golden Rule. Therefore, the sum over the spin polarization for the gluon states are calculated as given in Ref. [41].

$$\sum \left(\frac{m_H^2}{2} \epsilon_{1,\mu} \epsilon_2^\mu - (p_{1,\mu} \epsilon_2^\nu)(p_{1,\rho} \epsilon_1^\rho) \right) \left(\frac{m_H^2}{2} \epsilon_{1,\sigma} \epsilon_2^\sigma - (p_{1,\eta} \epsilon_2^\eta)(p_{1,\tau} \epsilon_1^\tau) \right)^* = \frac{m_H^4}{2}$$

The average over all possible gluon polarizations (factor 2^2) and all possible color states (factor 8^2) gives an additional factor of

$$\frac{\delta_{ab} \delta_{ab}}{2^2 \cdot 8^2} = \frac{8}{256} = \frac{1}{32}.$$

The averaged amplitude-squared is therefore

$$|\overline{\mathcal{M}}|^2 = \left| \frac{\alpha_S m_H^2}{32\pi\nu_{\text{SM}}} \tau \left(1 + (1-\tau) \arcsin^2 \sqrt{\frac{1}{\tau}} \right) \right|^2.$$

The kinematics of the decay mode is considered in the phase space integral over the momentum q of the Higgs boson and its energy E_H

$$\sigma(gg \rightarrow H) = \frac{1}{4m_H^2} \int \frac{d^3q}{(2\pi)^3 E_H} (2\pi)^4 \delta^4(q - p_1 - p_2) |\overline{\mathcal{M}}|^2$$

where the amplitude-squared is independent of the momentum. Thus, the phase space integral reduces to a numerical factor.

$$\frac{1}{4m_H^2} \int \frac{d^3q}{(2\pi)^3 E_H} (2\pi)^4 \delta^4(q - p_1 - p_2) = \frac{\pi}{m_H^2} \delta((p_1 + p_2)^2 - m_H^2)$$

The cross section for an on-shell top-loop ($\tau > 1$) is given by

$$\begin{aligned} \sigma(gg \rightarrow H) &= \frac{\pi}{m_H^2} \delta((p_1 + p_2)^2 - m_H^2) |\overline{\mathcal{M}}|^2 \\ &= \frac{\alpha_S^2 m_H^2}{32^2 \pi \nu_{\text{SM}}^2} \delta((p_1 + p_2)^2 - m_H^2) \left[\tau \left(1 + (1-\tau) \arcsin^2 \left(\frac{1}{\sqrt{\tau}} \right) \right) \right]^2 \end{aligned}$$

which is the final result in this calculation according to eq. 3.2.27. The sum of the gluon momenta can be replaced by the center-of-mass energy $\sqrt{s} = p_1 + p_2$.

A.3 Minimizing the Superpotential

Soft symmetry breaking is a necessity to achieve electroweak symmetry breaking in SUSY models (see section 3.3). A detailed calculation of the minimization of the superpotential is performed according to Ref. [15]. Here and in the following, the notation $H_d = H_1$ and $H_u = H_2$ is used to be consistent with the literature. Minimizing the superpotential V_H (see eq. 3.3.1) leads to the soft symmetry breaking conditions given in eq. 3.3.5.

$$\begin{aligned}
 V_H &= V_D + V_F + V_{\text{soft}} \\
 &= \frac{g_2^2}{8} \left[4|H_1^\dagger \cdot H_2|^2 - 2|H_1|^2|H_2|^2 + (|H_1|^2)^2 + (|H_2|^2)^2 \right] + \frac{g_1^2}{8} (|H_2|^2 - |H_1|^2)^2 \\
 &\quad + \mu^2 (|H_1|^2 + |H_2|^2) \\
 &\quad + m_{H_1}^2 H_1^\dagger H_1 + m_{H_2}^2 H_2^\dagger H_2 + B\mu (H_2 \cdot H_1 + \text{h.c.}) \\
 \frac{\partial V_H}{\partial H_1^0} &= \frac{\partial V_H}{\partial H_2^0} = 0 \\
 H_1 &= \begin{pmatrix} H_1^0 \\ H_1^- \end{pmatrix} \quad H_2 = \begin{pmatrix} H_2^+ \\ H_2^0 \end{pmatrix} \quad \langle H_1 \rangle = \frac{\nu_1}{\sqrt{2}} \quad \langle H_2 \rangle = \frac{\nu_2}{\sqrt{2}}
 \end{aligned}$$

In expanding the Higgs doublets, the substitution

$$\bar{m}_1^2 = |\mu|^2 + m_{H_1}^2 \quad \bar{m}_2^2 = |\mu|^2 + m_{H_2}^2 \quad \bar{m}_3^2 = B\mu$$

is used to obtain the superpotential

$$\begin{aligned}
 V_H &= \bar{m}_1^2 (|H_1^0|^2 + |H_1^-|^2) + \bar{m}_2^2 (|H_2^0|^2 + |H_2^+|^2) - \bar{m}_3^2 (H_1^- H_2^+ + H_1^0 H_2^0 + \text{h.c.}) \\
 &\quad + \frac{g_1^2 + g_2^2}{8} (|H_1^0|^2 + |H_1^-|^2 - |H_2^0|^2 - |H_2^+|^2)^2 + \frac{g_2^2}{2} |H_1^{-*} H_1^0 + H_2^{0*} H_2^+|^2.
 \end{aligned}$$

For vacuum, the superpotential is then given by

$$(V_H)_{\text{vac}} = \bar{m}_1^2 \nu_1^2 + \bar{m}_2^2 \nu_2^2 - 2\bar{m}_3^2 \nu_1 \nu_2 + \frac{g_1^2 + g_2^2}{8} (\nu_1^2 - \nu_2^2)^2.$$

Minimizing the superpotential leads to the conditions

$$\begin{aligned}
 \frac{\partial (V_H)_{\text{vac}}}{\partial \nu_1} &= 2\bar{m}_1^2 \nu_1 - 2\bar{m}_3^2 \nu_2 + \frac{g_1^2 + g_2^2}{4} (\nu_1^2 - \nu_2^2) \nu_1 = 0 \quad \Big| \cdot \frac{1}{2\nu_1} \\
 &\rightarrow \bar{m}_1^2 - \bar{m}_3^2 \frac{\nu_2}{\nu_1} + \frac{g_1^2 + g_2^2}{8} (\nu_1^2 - \nu_2^2) = 0 \\
 \frac{\partial (V_H)_{\text{vac}}}{\partial \nu_2} &= 2\bar{m}_2^2 \nu_2 - 2\bar{m}_3^2 \nu_1 - \frac{g_1^2 + g_2^2}{4} (\nu_1^2 - \nu_2^2) \nu_2 = 0 \quad \Big| \cdot \frac{1}{2\nu_2} \\
 &\rightarrow \bar{m}_2^2 - \bar{m}_3^2 \underbrace{\frac{\nu_1}{\nu_2}}_{1/\tan\beta} - \frac{g_1^2 + g_2^2}{8} \underbrace{(\nu_1^2 - \nu_2^2)}_{\nu_{\text{SM}}^2 (\cos^2\beta - \sin^2\beta)} = 0.
 \end{aligned}$$

By using the relations

$$\tan\beta = \frac{\nu_2}{\nu_1} = \frac{\nu_{\text{SM}} \sin\beta}{\nu_{\text{SM}} \cos\beta} \quad \text{and} \quad (\nu_1^2 + \nu_2^2) = \nu_{\text{SM}}^2 = \frac{4m_Z^2}{g_1^2 + g_2^2}$$

the following two conditions are obtained

$$\begin{aligned}\bar{m}_1^2 - \bar{m}_3^2 \tan \beta + \frac{m_Z^2}{2} (\cos^2 \beta - \sin^2 \beta) &= 0 \\ \bar{m}_2^2 - \frac{\bar{m}_3^2}{\tan \beta} - \frac{m_Z^2}{2} \underbrace{(\cos^2 \beta - \sin^2 \beta)}_{\cos 2\beta} &= 0.\end{aligned}$$

The sum and the difference leads to the soft symmetry breaking conditions given in eq. 3.3.5.

$$\begin{aligned}(-): \quad \bar{m}_1^2 - \bar{m}_3^2 \tan \beta - \bar{m}_2^2 + \frac{\bar{m}_3^2}{\tan \beta} + m_Z^2 \cos 2\beta &= \\ &= \bar{m}_1^2 - \bar{m}_2^2 - \bar{m}_3^2 \underbrace{\left(\tan \beta - \frac{1}{\tan \beta} \right)}_{-2/\tan 2\beta} + m_Z^2 \cos 2\beta = 0 \\ \rightarrow -\bar{m}_3^2 &= \frac{\tan 2\beta}{2} (\bar{m}_1^2 - \bar{m}_2^2) + \frac{m_Z^2}{2} \sin 2\beta \\ &= -B\mu = \frac{\tan 2\beta}{2} (m_{H_1}^2 - m_{H_2}^2) + \frac{m_Z^2}{2} \sin 2\beta \\ (+): \quad \bar{m}_1^2 - \bar{m}_3^2 \tan \beta + \bar{m}_2^2 - \frac{\bar{m}_3^2}{\tan \beta} &= 0 \\ \rightarrow \bar{m}_1^2 + \bar{m}_2^2 &= m_{H_1}^2 + m_{H_2}^2 + 2\mu^2 = \bar{m}_3^2 \underbrace{\left(\tan \beta + \frac{1}{\tan \beta} \right)}_{\nu_{SM}^2/\nu_1\nu_2} \\ \rightarrow \mu^2 &= \frac{1}{2} \left[-m_{H_1}^2 - m_{H_2}^2 + \bar{m}_3^2 \left(\frac{\nu_{SM}^2}{\nu_1\nu_2} \right) \right] \\ &= \frac{1}{2} \left[-m_{H_1}^2 - m_{H_2}^2 - \left(\frac{\tan 2\beta}{2} (m_{H_1}^2 - m_{H_2}^2) + \frac{m_Z^2}{2} \sin 2\beta \right) \underbrace{\left(\frac{\nu_{SM}^2}{\nu_1\nu_2} \right)}_{1/\sin \beta \cos \beta = 2/\sin 2\beta} \right] \\ &= \frac{1}{2} \left[-m_{H_1}^2 - m_{H_2}^2 - \left(\frac{1}{\cos 2\beta} (m_{H_1}^2 - m_{H_2}^2) + m_Z^2 \right) \right] \\ &= -\frac{1}{2} \left[\frac{m_{H_1}^2}{\cos 2\beta} \underbrace{(\cos 2\beta + 1)}_{2 \cos^2 \beta} + \frac{m_{H_2}^2}{\cos 2\beta} \underbrace{(\cos 2\beta - 1)}_{-\sin^2 \beta} + m_Z^2 \right] \\ \mu^2 &= \frac{1}{\cos 2\beta} (m_{H_2}^2 \sin^2 \beta - m_{H_1}^2 \cos^2 \beta) - \frac{m_Z^2}{2}\end{aligned}$$

Thus, the final result is

$$\begin{aligned}B\mu &= \frac{(m_{H_1}^2 - m_{H_2}^2) \tan 2\beta + m_Z^2 \sin 2\beta}{2} \\ \mu^2 &= \frac{m_{H_2}^2 \sin^2 \beta - m_{H_1}^2 \cos^2 \beta}{\cos 2\beta} - \frac{m_Z^2}{2}.\end{aligned}$$

B Additional Results

In this section, additional results to those given in section 5 are shown. The following plots visualize the cross sections for mono- X signatures in the $\tilde{\chi}_3^0 - \tilde{\chi}_1^0$ neutralino mass planes, as well as in the relevant $m_A - \tan\beta$ parameter planes (see fig. B.1.1). The highest cross sections up to $\mathcal{O}(10 \text{ fb})$ are found for low Higgs masses, nearly independent of the soft parameter $\tan\beta$. The cross section falls smoothly as the mass of the Higgs increases.

Furthermore, additional plots of the soft parameter study are presented. Here, the cross sections for mono- X signatures are given in the soft parameter planes $M_1 - \mu$ and $M_2 - \mu$ for higgsino-like LSPs and in the soft parameter planes $M_2 - M_1$ and $\mu - M_1$ for bino-like LSPs, showing the highest cross sections for highly mixed higgsino-/gaugino-states (see fig. B.1.2).

For bino-like LSPs, the highest cross sections are found for low values of μ and thus for mixed bino- and higgsino-like states. Even though, decays to wino-/higgsino-mixed electroweakinos are preferred, the necessity of a large gaugino-higgsino mixing for heavy Higgs couplings leads to low values of μ for bino-like LSPs. The higgsino-like LSP dataset show large cross sections for highly mixed higgsino-/wino-like states, nearly independent of the signature.

Additional plots showing the bottom quark annihilation process being the dominant production channel for heavy Higgs bosons are given in the $\tilde{\chi}_3^0 - \tilde{\chi}_1^0$ neutralino mass planes and the $m_A - \tan\beta$ parameter planes for mono- X topologies (see fig. B.1.3). Up to two potentially hard b -jets in the detector give an additional handle on the search for resonant heavy Higgs bosons at the LHC.

Dijet and dilepton signatures are mostly negligible for higgsino-like and bino-like LSPs, as shown in the lightest squark-LSP ($\tilde{q} - \tilde{\chi}_1^0$), lightest slepton-LSP mass planes ($\tilde{l} - \tilde{\chi}_1^0$) and the $m_A - \tan\beta$ parameter planes (see fig. B.2.1). In these plots, the strong $\tan\beta$ dependence of the cross section is visible. As a result of the dominant entries of the H coupling matrix to light squarks $C_{H\tilde{q}\tilde{q}}$ being dependent on $\cos\beta$, the coupling is enhanced for low values of $\tan\beta$.

Additional contributions of H decaying into a chargino pair can result in the same dilepton signature and thus, the total $\sigma \times \mathcal{B}$ value is enhanced. There, the charginos decay to the LSP and an off-shell W boson each, where the leptonic decay of the latter leave each a single lepton in the detector.

A detailed description of the results is given in section 5.

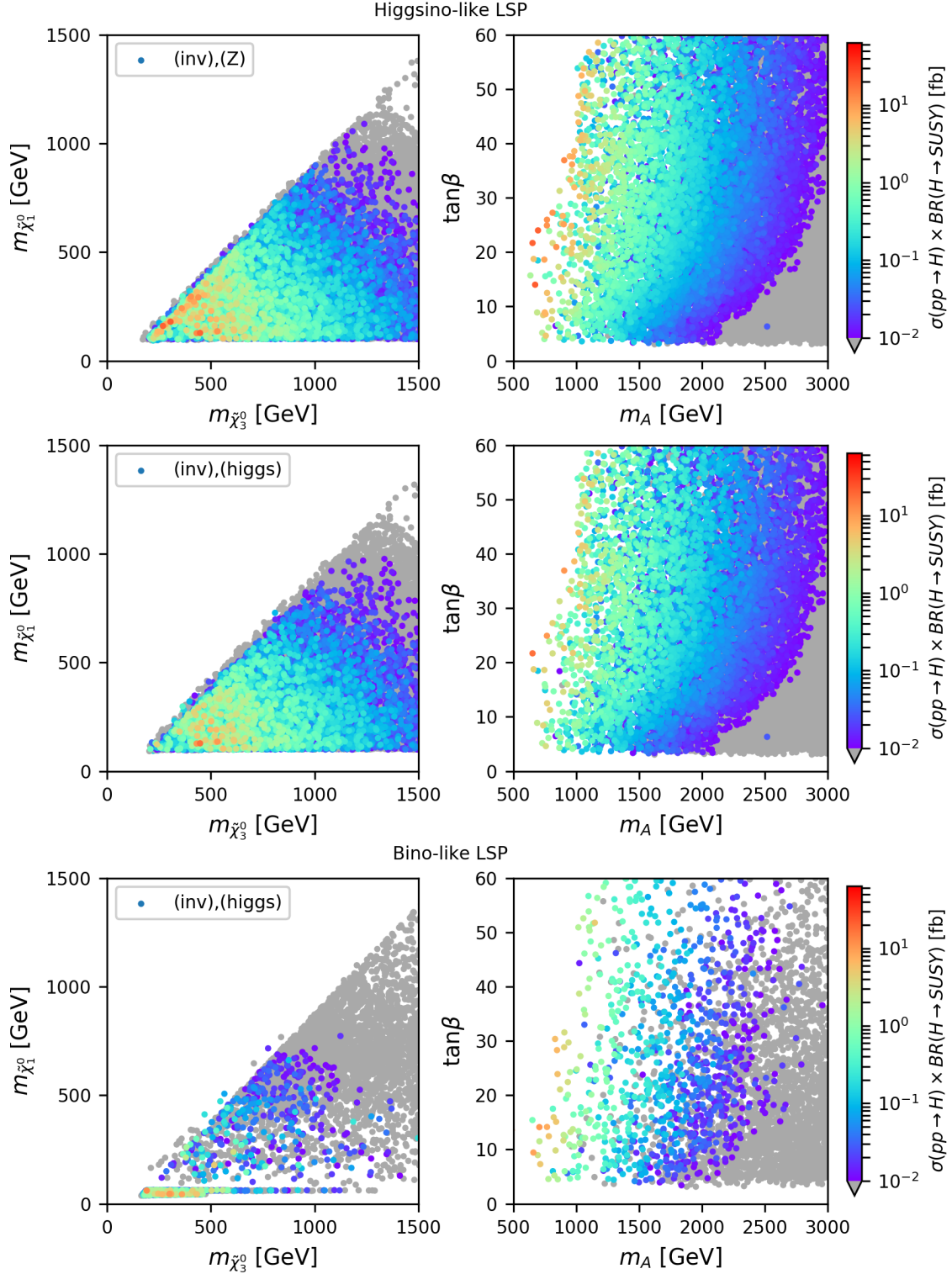
B.1 Heavy Higgs Production with Mono- X Signature


Figure B.1.1: Cross sections for heavy Higgs searches with mono- Z (upper plots) and mono- h (middle plots) signature for higgsino-like LSPs, as well as with mono- h (lower plots) signature for bino-like LSPs in the $\tilde{\chi}_3^0 - \tilde{\chi}_1^0$ mass plane (left) and the $m_A - \tan\beta$ parameter plane (right).

B.1.1 Study of the Parameter Dependence

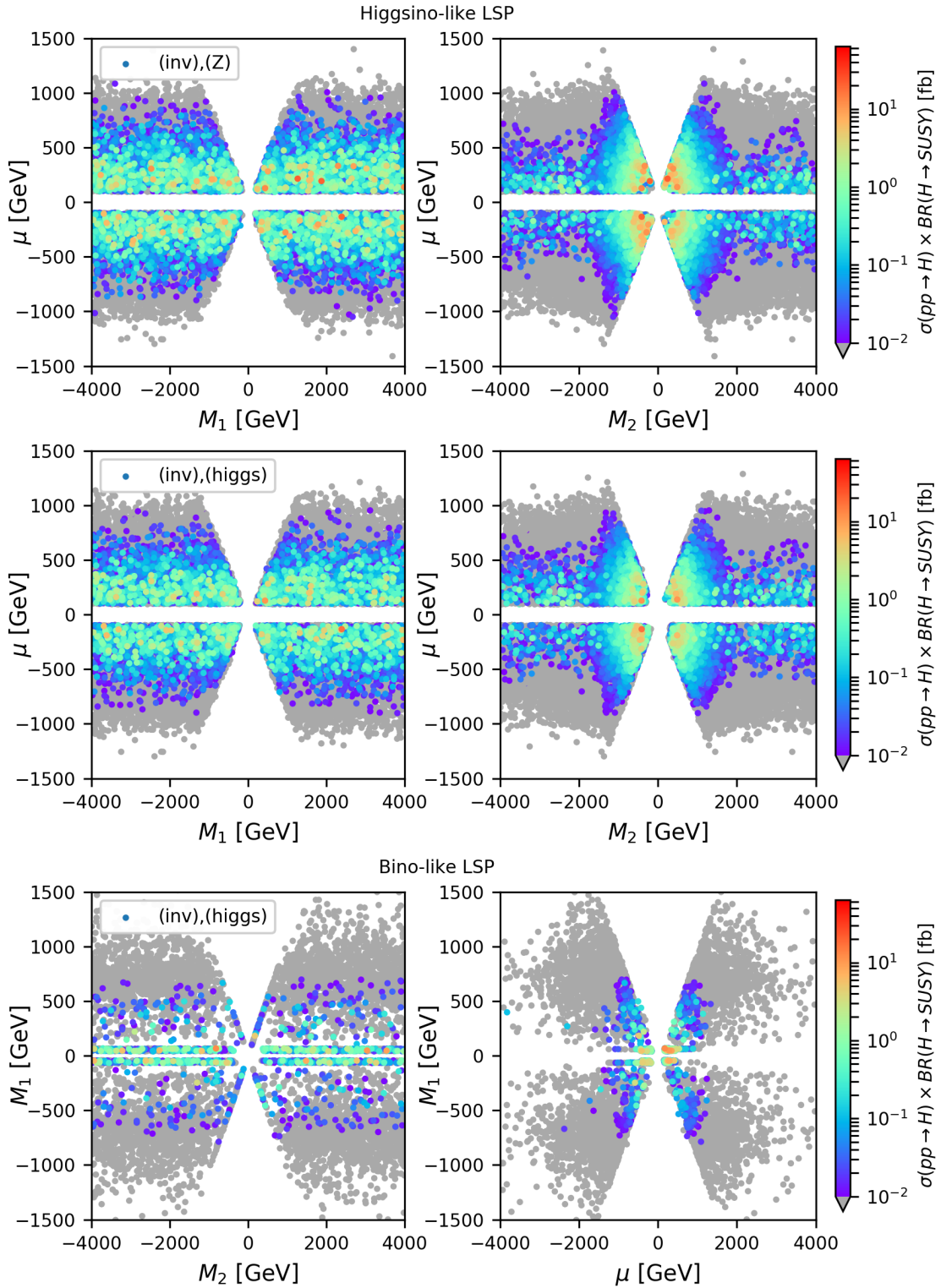


Figure B.1.2: Cross sections for heavy Higgs searches with mono- Z (upper plots) and mono- h (middle plots) signature for higgsino-like LSPs in the $M_1 - \mu$ (left) and the $M_2 - \mu$ soft parameter plane (right), as well as with mono- h (lower plots) signature for bino-like LSPs in the $M_2 - M_1$ (left) and the $\mu - M_1$ soft parameter plane (right).

B.1.2 Study of the Production Process

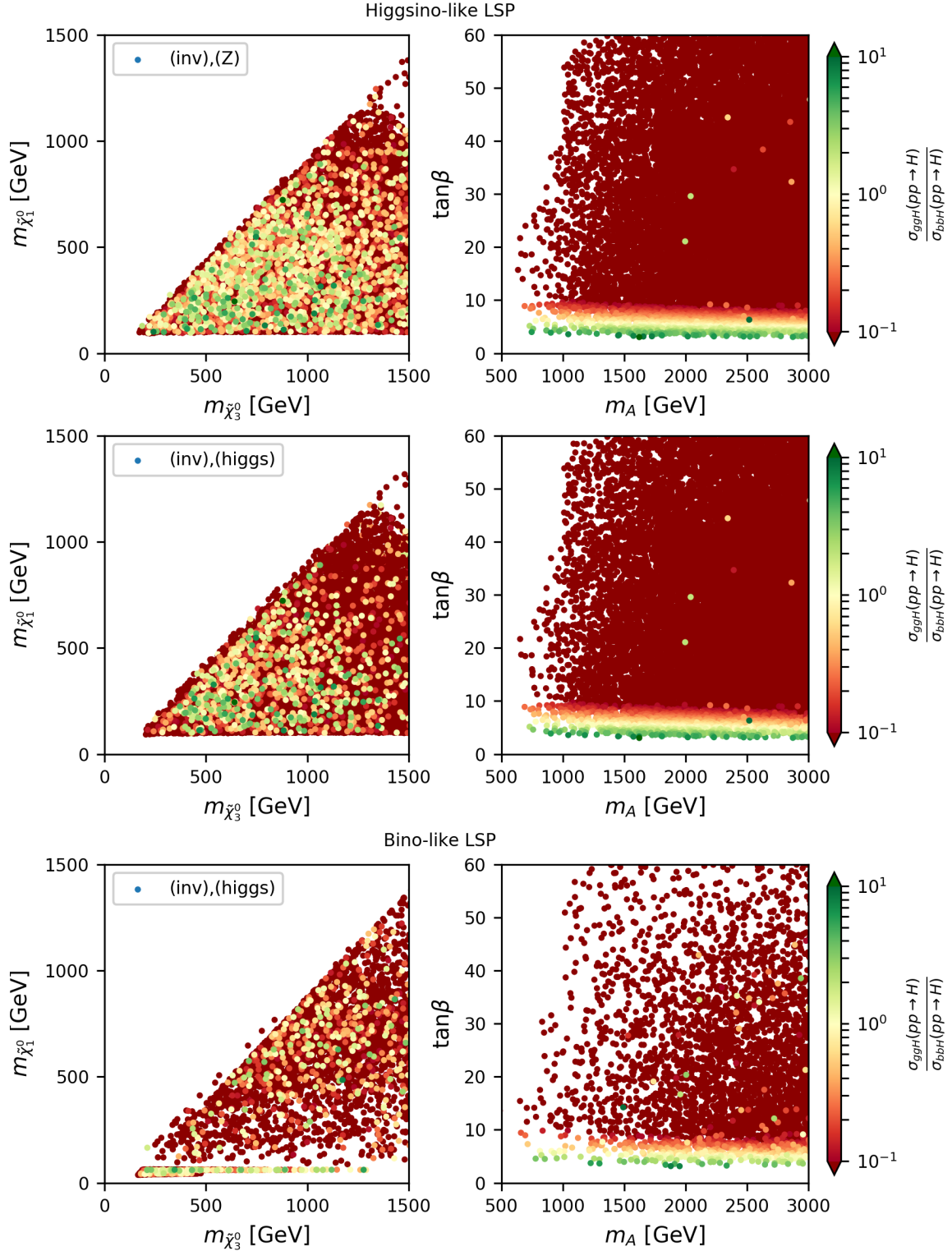


Figure B.1.3: Fraction of gluon-fusion (σ_{ggH}) to bottom quark annihilation (σ_{bbH}) cross sections for heavy Higgs production with mono- Z (upper plots) and mono- h (middle plots) signature for higgsino-like LSPs, as well as with mono- h (lower plots) signature for bino-like LSPs in the $\tilde{\chi}_3^0 - \tilde{\chi}_1^0$ mass plane (left) and the $m_A - \tan\beta$ parameter plane (right).

B.2 Heavy Higgs Decays with Dijet and Dilepton Signature

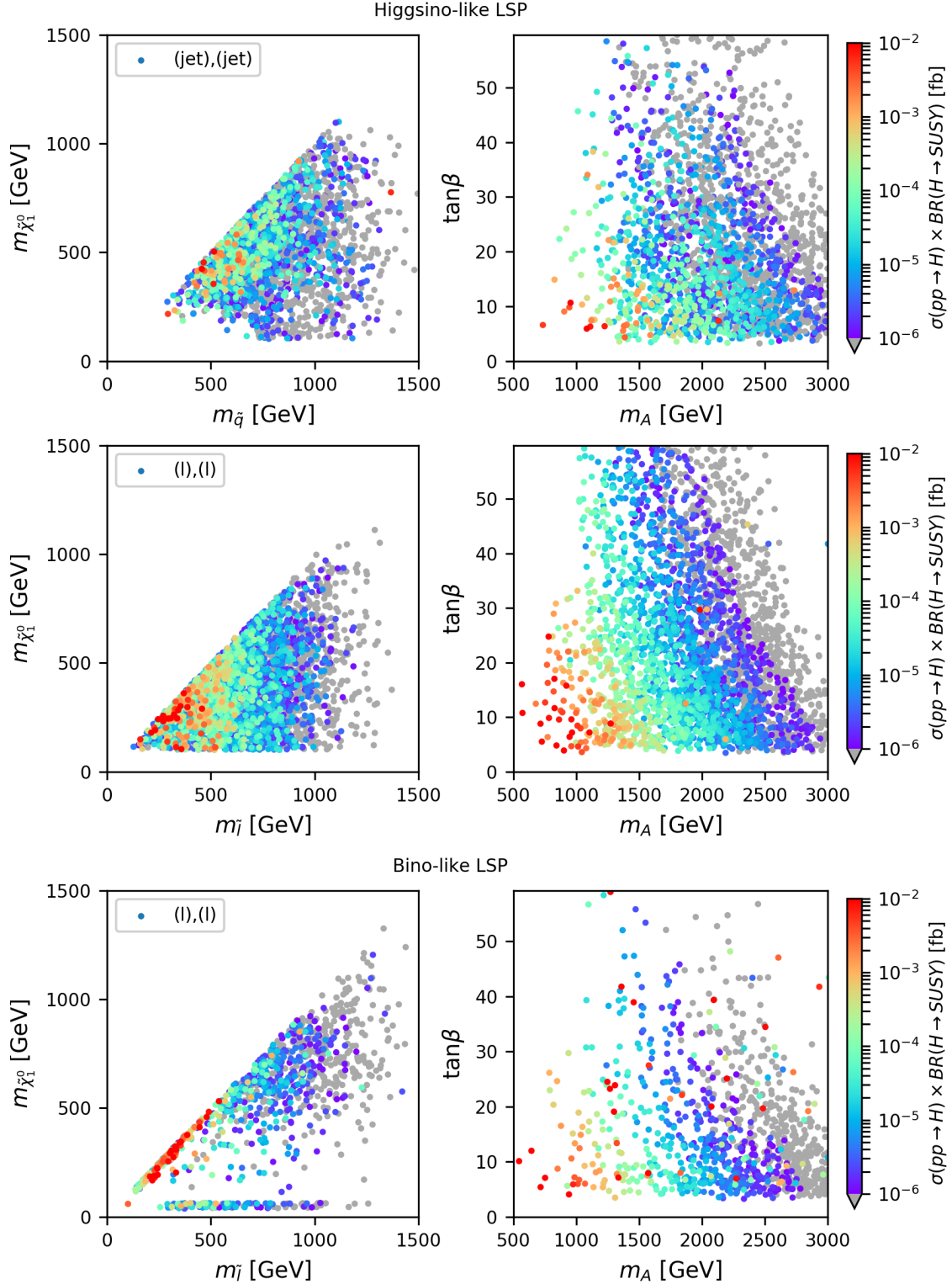


Figure B.2.1: Cross sections for heavy Higgs searches with dijet (upper plots) and dilepton (middle plots) signature for higgsino-like LSPs, as well as with dilepton (lower plots) signature for bino-like LSPs in the $\tilde{q} - \tilde{\chi}_1^0$ and $\tilde{l} - \tilde{\chi}_1^0$ mass plane (left) and the $m_A - \tan\beta$ parameter plane (right).

List of Figures

1.0.1 Simplified model for heavy Higgs decaying to SUSY particles.	1
2.2.1 The Higgs potential $V(\phi_h)$ for a complex scalar field ϕ_h	6
2.3.1 Feynman diagram for corrections to the Higgs mass.	6
2.3.2 Energy-dependence of the gauge coupling constants.	7
3.2.1 Higgs masses in m_A and $\tan\beta$ dependence.	14
3.2.2 Branching ratios of heavy CP-even Higgs bosons.	16
3.2.3 Main production channels for heavy Higgs bosons.	18
3.2.4 Higgs boson production cross sections in dependence of m_Φ , \sqrt{s} and $\tan\beta$	18
3.4.1 Feynman diagram for corrections to the Higgs mass with sfermions.	20
3.4.2 Energy-dependence of the gauge coupling constants in MSSM.	21
4.1.1 Feynman diagram for a full model and the SMS topology.	23
4.2.1 The working principle of SModelS	23
4.2.2 Decomposition procedure in SModelS	24
4.2.3 Feynman-like diagram for heavy Higgs production and its input to SModelS	25
4.2.4 Bracket notation in SModelS	25
4.2.5 Mass compression in SModelS	26
4.4.1 Lifetime of the lightest chargino.	35
4.4.2 Excluded parameter sets due to long-lived sparticles or no decay mode to sparticles.	36
4.4.3 Excluded parameter sets in the Higgs- and flavor sector.	37
5.0.1 Feynman diagrams for heavy Higgs decays with mono- X signature.	39
5.0.2 Most frequent occurring and most dominating missing topologies.	42
5.1.1 Cross sections with mono- X signature.	44
5.1.2 Parameter dependence of cross sections with mono- X signature.	46
5.1.3 Fraction of gluon-fusion to bottom quark annihilation cross sections.	47
5.2.1 Cross sections of invisible heavy Higgs decays.	49

LIST OF FIGURES

5.3.1 Cross sections with dijet signature for bino-like LSP.	50
5.4.1 Ratio of the cross section to long-cascade decays.	50
5.5.1 Parameter sets excluded by 8 TeV LHC Run 1 SUSY searches.	52
5.5.2 Parameter sets excluded by 13 TeV LHC Run 2 SUSY searches.	53
5.6.1 Branching ratio and total production cross section of heavy Higgs bosons.	54
5.7.1 Cross sections for heavy Higgs bosons decaying to charginos for wino-like LSPs.	55
A.2.1 Feynman diagrams for Higgs production in gluon fusion processes.	60
B.1.1 Cross sections with mono- X signature.	68
B.1.2 Parameter dependence of cross sections.	69
B.1.3 Fraction of gluon-fusion to bottom quark annihilation cross sections.	70
B.2.1 Cross sections with dijet and dilepton signature.	71

List of Tables

2.1.1 The particle content of the Standard Model of Particle Physics.	4
3.1.1 Standard Model particles and their superpartners.	8
3.1.2 MSSM sparticle content and their symbols.	9
3.2.1 Soft parameters in pMSSM.	10
3.2.2 Neutral MSSM Higgs couplings normalized to SM-Higgs couplings.	14
3.2.3 Main processes of neutral Higgs productions.	16
4.4.1 Parameter range for the pMSSM scan.	31
4.4.2 Standard Model input parameters for the parameter scan.	32
4.4.3 Constraints applied to the MSSM parameter scan.	33
4.4.4 Sample size and definition of the categorized parameter sets.	33
4.4.5 Breakdown of the excluded parameter sets.	34
5.0.1 Missing topologies for heavy Higgs decays and their detailed decay process. . . .	41
A.2.1 Feynman rules in gluon fusion processes.	60

Bibliography

- [1] R. K. Barman, B. Bhattacharjee, A. Chakraborty, and A. Choudhury, “Study of MSSM heavy Higgs bosons decaying into charginos and neutralinos,” *Phys. Rev.*, vol. D94, no. 7, 2016, arXiv 1607.00676.
- [2] G. Belanger, D. Ghosh, R. Godbole, and S. Kulkarni, “Light stop in the MSSM after LHC Run 1,” *JHEP*, vol. 09, p. 214, 2015, arXiv 1506.00665.
- [3] A. Arbey, M. Battaglia, and F. Mahmoudi, “Supersymmetric Heavy Higgs Bosons at the LHC,” *Phys. Rev.*, vol. D88, no. 1, 2013, arXiv 1303.7450.
- [4] D. Binosi and L. Theußl, “JaxoDraw: A graphical user interface for drawing Feynman diagrams,” *Computer Physics Communications*, vol. 161, no. 1-2, pp. 76 – 86, 2004.
- [5] G. Altarelli, “The Standard model of particle physics,” 2005, arXiv 0510281.
- [6] G. Altarelli, “Collider Physics within the Standard Model: A Primer,” 2013, arXiv 1303.2842.
- [7] A. J. Cuesta, V. Niro, and L. Verde, “Neutrino mass limits: robust information from the power spectrum of galaxy surveys,” *Phys. Dark Univ.*, vol. 13, pp. 77–86, 2016, arXiv 1511.05983.
- [8] Q. R. Ahmad *et al.*, “Measurement of the rate of $\nu_e + d \rightarrow p + p + e^-$ interactions produced by 8B solar neutrinos at the Sudbury Neutrino Observatory,” *Phys. Rev. Lett.*, vol. 87, p. 071301, 2001, arXiv 0106015.
- [9] Y. Fukuda *et al.*, “Evidence for oscillation of atmospheric neutrinos,” *Phys. Rev. Lett.*, vol. 81, pp. 1562–1567, 1998, arXiv 9807003.
- [10] R. W. Rasmussen, L. Lechner, M. Ackermann, M. Kowalski, and W. Winter, “Astrophysical neutrinos flavored with Beyond the Standard Model physics,” 2017, arXiv 1707.07684.
- [11] K. A. Olive *et al.*, “Review of Particle Physics,” *Chin. Phys.*, vol. C38, 2014.
- [12] S. Glashow, “The renormalizability of vector meson interactions,” *Nuclear Phys.*, vol. 10, 1959.
- [13] A. Salam and J. C. Ward, “Weak and electromagnetic interactions,” *Il Nuovo Cimento (1955-1965)*, vol. 11, no. 4, pp. 568–577, 1959.
- [14] J. F. Gunion, H. E. Haber, G. L. Kane, and S. Dawson, “The Higgs Hunter’s Guide,” *Front. Phys.*, vol. 80, pp. 1–404, 2000.
- [15] A. Djouadi, “The Anatomy of electro-weak symmetry breaking. II. The Higgs bosons in the minimal supersymmetric model,” *Phys. Rept.*, vol. 459, pp. 1–241, 2008, arXiv 0503173.
- [16] K. Kohri and H. Matsui, “Higgs vacuum metastability in primordial inflation, preheating, and reheating,” *Phys. Rev.*, vol. D94, no. 10, 2016, arXiv 1602.02100.

- [17] L. M. Krauss and A. J. Long, “Metastability of the False Vacuum in a Higgs-Seesaw Model of Dark Energy,” *Phys. Rev.*, vol. D89, no. 8, 2014, arXiv 1310.5361.
- [18] V. A. Bednyakov, N. D. Giokaris, and A. V. Bednyakov, “On Higgs mass generation mechanism in the Standard Model,” *Phys. Part. Nucl.*, vol. 39, pp. 13–36, 2008, arXiv 0703280.
- [19] G. L. Kane, “Modern Elementary Particle Physics,” *Cambridge University Press*, 2017.
- [20] P. W. Higgs, “Broken symmetries, massless particles and gauge fields,” *Phys. Lett.*, vol. 12, pp. 132–133, 1964.
- [21] F. Englert and R. Brout, “Broken Symmetry and the Mass of Gauge Vector Mesons,” *Phys. Rev. Lett.*, vol. 13, pp. 321–323, 1964.
- [22] S. Chatrchyan *et al.*, “Observation of a new boson at a mass of 125 GeV with the CMS experiment at the LHC,” *Phys. Lett.*, vol. B716, pp. 30–61, 2012, arXiv 1207.7235.
- [23] G. Aad *et al.*, “Observation of a new particle in the search for the Standard Model Higgs boson with the ATLAS detector at the LHC,” *Phys. Lett.*, vol. B716, pp. 1–29, 2012, arXiv 1207.7214.
- [24] M. E. Peskin and D. V. Schroeder, “An Introduction to Quantum Field Theory,” *Westview*, 1995.
- [25] A. Djouadi, “The Anatomy of electro-weak symmetry breaking. I: The Higgs boson in the standard model,” *Phys. Rept.*, vol. 457, pp. 1–216, 2008, arXiv 0503172.
- [26] “Running coupling constants for SM and MSSM.” https://www.nobelprize.org/nobel_prizes/physics/laureates/2004/popular.html. (accessed on Oct 15th, 2017).
- [27] P. A. R. Ade *et al.*, “Planck 2015 results. XIII. Cosmological parameters,” 2015, arXiv 1502.01589.
- [28] M. Bersanelli *et al.*, “Planck pre-launch status: Design and description of the Low Frequency Instrument,” *AAP*, vol. 520, 2010, arXiv 1001.3321.
- [29] F. Zwicky, “Die Rotverschiebung von extragalaktischen Nebeln,” *Helvetica Physica Acta*, vol. 6, pp. 110–127, 1933.
- [30] V. Springel *et al.*, “Simulating the joint evolution of quasars, galaxies and their large-scale distribution,” *Nature*, vol. 435, pp. 629–636, 2005, arXiv 0504097.
- [31] D. J. Eisenstein *et al.*, “Detection of the baryon acoustic peak in the large-scale correlation function of SDSS luminous red galaxies,” *Astrophys. J.*, vol. 633, pp. 560–574, 2005, arXiv 0501171.
- [32] J. Kovac *et al.*, “Detection of polarization in the cosmic microwave background using DASI,” *Nature*, vol. 420, pp. 772–787, 2002, arXiv 0209478.
- [33] D. N. Spergel *et al.*, “Wilkinson Microwave Anisotropy Probe (WMAP) three year results: implications for cosmology,” *Astrophys. J. Suppl.*, vol. 170, p. 377, 2007, arXiv 0603449.
- [34] R. Scarpa, “Modified newtonian dynamics, an introductory review,” *AIP Conf. Proc.*, vol. 822, pp. 253–265, 2006, arXiv 0601478.
- [35] M. Drees, R. Godbole, and P. Roy, “Theory and phenomenology of Sparticles: an account of four-dimensional N=1 supersymmetry in high-energy physics,” *World Scientific*, 2004.
- [36] S. P. Martin, “A Supersymmetry primer,” 1997, arXiv 9709356.

-
- [37] R. V. Harlander, S. Liebler, and H. Mantler, “SusHi: A program for the calculation of Higgs production in gluon fusion and bottom-quark annihilation in the Standard Model and the MSSM,” *Comput. Phys. Commun.*, vol. 184, pp. 1605–1617, 2013, arXiv 1212.3249.
- [38] R. V. Harlander, S. Liebler, and H. Mantler, “SusHi Bento: Beyond NNLO and the heavy-top limit,” *Comput. Phys. Commun.*, vol. 212, pp. 239–257, 2017, arXiv 1605.03190.
- [39] S. Heinemeyer, W. Hollik, and G. Weiglein, “FeynHiggs: A Program for the calculation of the masses of the neutral CP even Higgs bosons in the MSSM,” *Comput. Phys. Commun.*, vol. 124, pp. 76–89, 2000, arXiv 9812320.
- [40] A. Djouadi, “Decays of the Higgs bosons,” pp. 197–222, 1997, arXiv 9712334.
- [41] “Gluon fusion production cross section calculations.” https://www.hep.ucl.ac.uk/twiki/pub/Main/StefanRichter/Gluon_fusion_to_Higgs_at_NLO.pdf. (accessed on Oct 15th, 2017).
- [42] G. Apollinari *et al.*, “High-Luminosity Large Hadron Collider (HL-LHC): Preliminary Design Report,” *CERN*, 2015.
- [43] I. Bejar Alonso and L. Rossi, “HiLumi LHC Technical Design Report,” *CERN-ACC-2015-0140*, 2015.
- [44] M. Benedikt and F. Zimmermann, “Future Circular Colliders,” *PoS*, 2016.
- [45] S. Raby, M. Ratz, and K. Schmidt-Hoberg, “Precision gauge unification in the MSSM,” *Phys. Lett.*, vol. B687, pp. 342–348, 2010, arXiv 0911.4249.
- [46] K. Garrett and G. Duda, “Dark Matter: A Primer,” *Adv. Astron.*, 2011, arXiv 1006.2483.
- [47] C. Munoz, “Models of Supersymmetry for Dark Matter,” 2017, arXiv 1701.05259.
- [48] S. Chatrchyan *et al.*, “Interpretation of Searches for Supersymmetry with Simplified Models,” *Phys. Rev.*, vol. D88, no. 5, 2013, arXiv 1301.2175.
- [49] S. Kraml *et al.*, “SModelS: a tool for interpreting simplified-model results from the LHC and its application to supersymmetry,” *Eur. Phys. J.*, vol. C74, 2014, arXiv 1312.4175.
- [50] F. Ambrogio *et al.*, “SModelS v1.1 user manual,” 2017, arXiv 1701.06586.
- [51] “The SModelS Homepage.” <http://smodels.hephy.at>. (accessed on Oct 15th, 2017).
- [52] A. Buckley, “PySLHA: a Pythonic interface to SUSY Les Houches Accord data,” *Eur. Phys. J.*, vol. C75, no. 10, p. 467, 2015, arXiv 1305.4194.
- [53] F. Mahmoudi, “SuperIso v2.3: A Program for calculating flavor physics observables in Supersymmetry,” *Comput. Phys. Commun.*, vol. 180, pp. 1579–1613, 2009, arXiv 0808.3144.
- [54] F. Mahmoudi, “SuperIso: A Program for calculating the isospin asymmetry of $B \rightarrow K^* \gamma$ in the MSSM,” *Comput. Phys. Commun.*, vol. 178, pp. 745–754, 2008, arXiv 0710.2067.
- [55] M. Knecht, “The Anomalous Magnetic Moment of the Muon: A Theoretical Introduction,” *Lect. Notes Phys.*, vol. 629, pp. 37–84, 2004, arXiv 0307239.
- [56] P. Bechtle *et al.*, “HiggsBounds-4: Improved Tests of Extended Higgs Sectors against Exclusion Bounds from LEP, the Tevatron and the LHC,” *Eur. Phys. J.*, vol. C74, no. 3, p. 2693, 2014, arXiv 1311.0055.

-
- [57] P. Bechtle *et al.*, “Recent Developments in HiggsBounds and a Preview of HiggsSignals,” *PoS*, p. 024, 2012, arXiv 1301.2345.
- [58] W. Porod and F. Staub, “SPHeno 3.1: Extensions including flavour, CP-phases and models beyond the MSSM,” *Comput. Phys. Commun.*, vol. 183, pp. 2458–2469, 2012, arXiv 1104.1573.
- [59] W. Porod, “SPHeno, a program for calculating supersymmetric spectra, SUSY particle decays and SUSY particle production at $e^+ e^-$ colliders,” *Comput. Phys. Commun.*, vol. 153, pp. 275–315, 2003, arXiv 0301101.
- [60] P. Bechtle *et al.*, “HiggsSignals: Confronting arbitrary Higgs sectors with measurements at the Tevatron and the LHC,” *Eur. Phys. J.*, vol. C74, no. 2, p. 2711, 2014, arXiv 1305.1933.
- [61] C. Anastasiou *et al.*, “High precision determination of the gluon fusion Higgs boson cross-section at the LHC,” *JHEP*, vol. 05, p. 058, 2016, arXiv 1602.00695.
- [62] M. R. Whalley, D. Bourilkov, and R. C. Group, “The Les Houches accord PDFs (LHAPDF) and LHAGLUE,” pp. 575–581, 2005, arXiv 0508110.
- [63] C. F. Berger, J. S. Gainer, J. L. Hewett, and T. G. Rizzo, “Supersymmetry Without Prejudice,” *JHEP*, vol. 02, p. 023, 2009, arXiv 0812.0980.
- [64] Cahill-Rowley *et al.*, “The New Look pMSSM with Neutralino and Gravitino LSPs,” *Eur. Phys. J.*, vol. C72, p. 2156, 2012, arXiv 1206.4321.
- [65] M. W. Cahill-Rowley, J. L. Hewett, A. Ismail, and T. G. Rizzo, “More energy, more searches, but the phenomenological MSSM lives on,” *Phys. Rev.*, vol. D88, no. 3, 2013, arXiv 1211.1981.
- [66] M. Cahill-Rowley, J. L. Hewett, A. Ismail, and T. G. Rizzo, “Lessons and prospects from the pMSSM after LHC Run I,” *Phys. Rev.*, vol. D91, no. 5, 2015, arXiv 1407.4130.
- [67] G. Aad *et al.*, “Summary of the ATLAS experiment’s sensitivity to supersymmetry after LHC Run 1 — interpreted in the phenomenological MSSM,” *JHEP*, vol. 10, p. 134, 2015, arXiv 1508.06608.
- [68] B. C. Allanach, “SOFTSUSY: a program for calculating supersymmetric spectra,” *Comput. Phys. Commun.*, vol. 143, pp. 305–331, 2002, arXiv 0104145.
- [69] B. C. Allanach *et al.*, “Next-to-Minimal SOFTSUSY,” *Comput. Phys. Commun.*, vol. 185, pp. 2322–2339, 2014, arXiv 1311.7659.
- [70] B. C. Allanach and M. A. Bernhardt, “Including R-parity violation in the numerical computation of the spectrum of the minimal supersymmetric standard model: SOFTSUSY,” *Comput. Phys. Commun.*, vol. 181, pp. 232–245, 2010, arXiv 0903.1805.
- [71] A. Djouadi, J.-L. Kneur, and G. Moultaka, “SuSpect: A Fortran code for the supersymmetric and Higgs particle spectrum in the MSSM,” *Comput. Phys. Commun.*, vol. 176, pp. 426–455, 2007, arXiv 0211331.
- [72] A. Djouadi, M. M. Muhlleitner, and M. Spira, “Decays of supersymmetric particles: The Program SUSY-HIT (SUSpect-SdecaY-Hdecay-Interface),” *Acta Phys. Polon.*, vol. B38, pp. 635–644, 2007, arXiv 0609292.

- [73] A. Djouadi, J. Kalinowski, and M. Spira, “HDECAY: A Program for Higgs boson decays in the standard model and its supersymmetric extension,” *Comput. Phys. Commun.*, vol. 108, pp. 56–74, 1998, arXiv 9704448.
- [74] J. Alwall *et al.*, “The automated computation of tree-level and next-to-leading order differential cross sections, and their matching to parton shower simulations,” *JHEP*, vol. 07, p. 079, 2014, arXiv 1405.0301.
- [75] G. Belanger, F. Boudjema, A. Pukhov, and A. Semenov, “micrOMEGAs₃: A program for calculating dark matter observables,” *Comput. Phys. Commun.*, vol. 185, pp. 960–985, 2014, arXiv 1305.0237.
- [76] K. De Bruyn *et al.*, “Probing New Physics via the $B_s^0 \rightarrow \mu^+ \mu^-$ Effective Lifetime,” *Phys. Rev. Lett.*, vol. 109, p. 041801, 2012, arXiv 1204.1737.
- [77] O. Stål and T. Stefaniak, “Constraining extended Higgs sectors with HiggsSignals,” *PoS*, vol. EPS-HEP2013, p. 314, 2013, arXiv 1310.4039.
- [78] T. Sjostrand, S. Mrenna, and P. Z. Skands, “PYTHIA 6.4 Physics and Manual,” *JHEP*, vol. 05, p. 026, 2006, arXiv 0603175.
- [79] T. Sjöstrand *et al.*, “An Introduction to PYTHIA 8.2,” *Comput. Phys. Commun.*, vol. 191, pp. 159–177, 2015, arXiv 1410.3012.
- [80] S. S. AbdusSalam *et al.*, “Benchmark Models, Planes, Lines and Points for Future SUSY Searches at the LHC,” *Eur. Phys. J.*, vol. C71, p. 1835, 2011, arXiv 1109.3859.
- [81] V. Khachatryan *et al.*, “Searches for Supersymmetry using the M_{T2} Variable in Hadronic Events Produced in pp Collisions at 8 TeV,” *JHEP*, vol. 05, p. 078, 2015, arXiv 1502.04358.
- [82] ATLAS Collaboration, “Search for squarks and gluinos with the ATLAS detector in final states with jets and missing transverse momentum and 20.3 fb^{-1} of $\sqrt{s} = 8 \text{ TeV}$ proton-proton collision data,” Tech. Rep. ATLAS-CONF-2013-047, CERN, Geneva, 2013.
- [83] A. Barr and J. Liu, “First interpretation of 13 TeV supersymmetry searches in the pMSSM,” 2016, arXiv 1605.09502.
- [84] A. Barr and J. Liu, “Analysing parameter space correlations of recent 13 TeV gluino and squark searches in the pMSSM,” *Eur. Phys. J.*, vol. C77, no. 3, p. 202, 2017, arXiv 1608.05379.
- [85] M. Gell-Mann, “Symmetries of baryons and mesons,” *Phys. Rev.*, vol. 125, pp. 1067–1084, 1962.
- [86] N. J. A. Sloane, “The On-Line Encyclopedia of Integer Sequences,” *Sequence A001970*. <http://oeis.org>.